New Bio-Based Polymers

Synthesis and Polymerization of Cystine-Based Macrocycles

Felix Nicolas Behrendt

zur Erlangung des akademischen Grades
„doctor rerum naturalium“
(Dr. rer. nat.)
in der Wissenschaftsdisziplin „Polymerchemie“

eingereicht an der
Mathematisch-Naturwissenschaftlichen Fakultät
der Universität Potsdam

Potsdam, Mai 2018

"Some who have read the book, or at any rate have reviewed it, have found it boring, absurd, or contemptible, and I have no cause to complain, since I have similar opinions of their works, or of the kinds of writing that they evidently prefer."

- J. R. R. Tolkien, The Lord of the Rings

Published online at the
Institutional Repository of the University of Potsdam:
URN urn:nbn:de:kobv:517-opus4-418316
http://nbn-resolving.de/urn:nbn:de:kobv:517-opus4-418316

1 Eidesstattliche Erklärung

Diese Arbeit wurde in der Zeit von Januar 2014 bis Mai 2018 am Max-Planck-Institut für Kolloid- und Grenzflächenforschung und der Universität Potsdam unter der Leitung von Prof. Dr. Helmut Schlaad angefertigt.

Ich versichere, diese Arbeit selbständig und lediglich unter Benutzung der angegebenen Quellen und Hilfsmittel verfasst zu haben.

Ich erkläre weiterhin, dass die vorliegende Arbeit noch nicht im Rahmen eines anderen Prüfungsverfahrens eingereicht wurde.

Potsdam, den _____ **_____**

(Felix Nicolas Behrendt)

2 Abstract

Redox-responsive polymers, such as poly(disulfide)s, are a versatile class of polymers with potential applications including gene- and drug-carrier systems. Their degradability under reductive conditions allows for a controlled response to the different redox states that are present throughout the body. Poly(disulfide)s are typically synthesized by step growth polymerizations. Step growth polymerizations, however, may suffer from low conversions and therefore low molar masses, limiting potential applications. The purpose of this thesis was therefore to find and investigate new synthetic routes towards the synthesis of amino acid-based poly(disulfide)s.

The different routes in this thesis include entropy-driven ring opening polymerizations of novel macrocyclic monomers, derived from cystine derivatives. These monomers were obtained with overall yields of up to 77% and were analyzed by mass spectrometry as well as by 1D and 2D NMR spectroscopy. The kinetics of the entropy-driven ring-opening metathesis polymerization (ED-ROMP) were thoroughly investigated in dependence of temperature, monomer concentration, and catalyst concentration. The polymerization was optimized to yield poly(disulfide)s with weight average molar masses of up to 80 kDa and conversions of ~80%, at the thermodynamic equilibrium. Additionally, an alternative metal free polymerization, namely the entropy-driven ring-opening disulfide metathesis polymerization (ED-RODiMP) was established for the polymerization of the macrocyclic monomers. The effect of different solvents, concentrations and catalyst loadings on the polymerization process and its kinetics were studied. Polymers with very high weight average molar masses of up to 177 kDa were obtained. Moreover, various post-polymerization reactions were successfully performed.

This work provides the first example of the homopolymerization of endo-cyclic disulfides by ED-ROMP and the first substantial study into the kinetics of the ED-RODiMP process.

3 Kurzzusammenfassung

Redoxresponsive Polymere, wie etwa Polydisulfide, sind eine vielseitige Klasse von Polymeren, die unter anderem als Gen- und Wirkstoffträgersysteme eingesetzt werden können. Ihre Abbaubarkeit unter reduktiven Bedingungen ermöglicht eine kontrollierte Reaktion auf die verschiedenen Redoxzustände im Körper. Polydisulfide werden jedoch häufig durch Stufenwachstums-polymerisationen synthetisiert. Diese führen oft zu niedrigen Umsätzen und daher zu niedrigen molaren Massen. Das Ziel dieser Arbeit war daher neue Synthesewege für aminosäurebasierte Polydisulfide zu finden und zu untersuchen.

Diese Wege beinhalteten entropiegetriebene ringöffnende Polymerisationen von neuen makrozyklischen Monomeren, auf der Basis von Cystin-Derivaten. Diese Monomere konnten mit einer Gesamtausbeute von bis zu 77% synthetisiert werden und wurden mit Massenspektrometrie sowie mit 1D- und 2D-NMR-Spektroskopie analysiert. Die Kinetik der entropiegetriebenen ringöffnenden Metathese Polymerisation (ED-ROMP) wurde im Hinblick auf Temperatur, Monomerkonzentration und Katalysatormenge sorgfältig untersucht. Durch Optimierungen konnten Polydisulfide mit gewichtsmittleren Molmassen von bis zu 80 kDa und Umsätzen von ~80%, im thermodynamischen Gleichgewicht synthetisiert werden. Zusätzlich wurde eine alternative metallfreie Polymerisation, die entropiegetriebene ringöffnende Disulfidmetathese Polymerisation (ED-RODiMP), für die Polymerisation der makrozyklischen Monomere etabliert. Die Auswirkungen verschiedener Lösungsmittel, Konzentrationen und Katalysatorkonzentrationen auf die Kinetik dieses Polymerisationsprozesses wurden untersucht. Hierdurch wurden Polymere mit sehr hohen gewichtsmittleren Molmassen von bis zu 177 kDa erhalten. Darüber hinaus wurden verschiedene Postpolymerisationsreaktionen erfolgreich durchgeführt.

Diese Arbeit liefert das erste Beispiel für die Homopolymerisation endo-zyklischer Disulfide durch ROMP und eine erste substanzielle Studie der Kinetik des ED-RODiMP-Prozesses.

4 Table of Content

5 Introduction

5.1 Theoretical Background

Fossil fuels, such as natural gas, petroleum and coal, are the carbon-rich products of the degradation and decomposition of organic matter over millions of years. As a result of the progressive burial of this organic matter and its degradation products over geological timescale, fossil fuels are generally stored deep underground. Early uses of fossil fuels date back thousands of years, but remained limited. Since the beginning of the industrial revolution in the late 18th century, large amounts of fossil fuels were incinerated, in order to power the contemporary machines.

Not only did this fuel craze lead to rising carbon dioxide levels in the atmosphere and the resulting global warming, but it also contributed to the global depletion of fossil fuels, thereby limiting and complicating their extraction in the near future. As a result, oil companies have begun to harvest fossil fuels from deposits that are less accessible, with a high risk for the environment and public health. As an example, shale gas fracking is a relatively new method used for the extraction of natural gas from porous rock. Its long term effect, which is for now hard to predict, might include an increased greenhouse effect caused by higher energy consumption, methane gas pollution due to well leaks, and environmental contamination by toxic fracking additives from leakage of flowback water.[1,2] Deepwater drilling represents another type of hazardous fossil fuel extraction technique, aiming to extract the remaining oil deposits. In 2010 the explosion of the Deepwater Horizon drilling rig resulted in the death of eleven workers and an unprecedented environmental disaster.[3] The oil spill that emerged under the sunken rig into the Gulf of Mexico was estimated to contain around 4.9 million barrels of

oil (*i.e.,* 800 million liters), with severe long term effects on the local environment.[4] These examples illustrate the need to globally limit the use of fossil fuel.

This applies not only to the energy production sector, but also to the chemical industry which heavily relies on oil-based raw materials. Notably, the plastic industry is particularly oil-thirsty, which justifies the need for new bio-sourced plastics. However, bio-based polymers are still limited to niche applications. Examples of such polymers include polylactic acid used for bio-degradable garbage bags, agricultural foils and packaging, or nitrocellulose used in pregnancy test probes or as a binding agent in lacquers (Figure 1). They only play a minor role in the overall polymer production, which amounts to over 322 mega tons per year.[5]

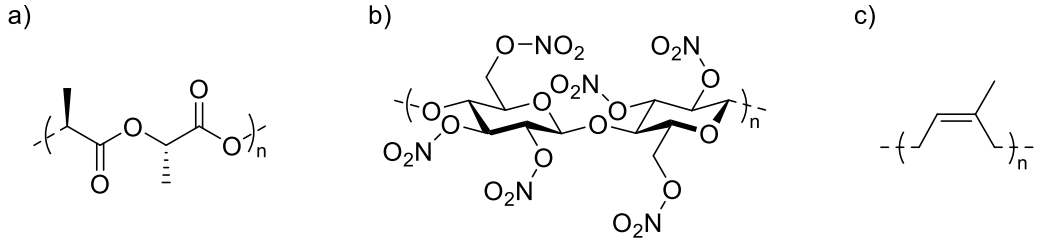

Figure 1: Examples of bio-based polymers with industrial applications; a) Poly-L-lactic acid, b) nitrocellulose and c) natural rubber.

Nature provides us with a variety of renewable resources such as carbohydrates, terpenes, and amino acids, which are suitable as feedstock for the production of polymers and plastics. Substituting crude oil for these bio-sourced raw materials in the production of polymers can offer many advantages. Amino acids for example are a diverse group of highly functional building blocks. They are used by nature as repeating units of proteins and enzymes. Their functions range from catalysis and transport, to structural stabilization. Amino acids consist of an amino- and a carboxylic group, as well as a side-chain that can bear a variety of functionalities. Although these properties are not essential to artificial poly(amino acid)s such as polypeptides, they often are bio-degradable, bio-mimetic as well as bio-compatible.

5.1.1 Poly(amino acid)s

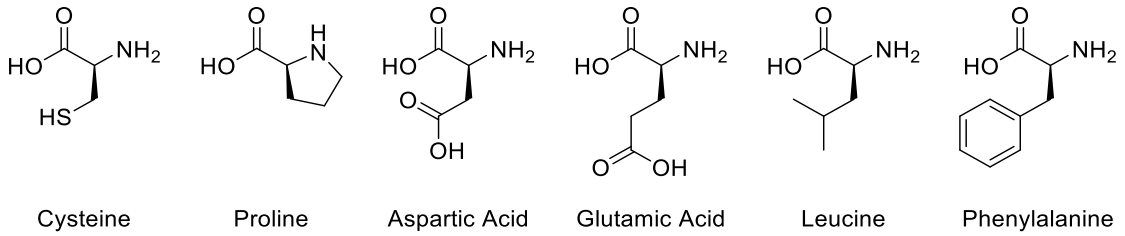

Figure 2: Selection of proteinogenic L-amino acids.

Naturally occurring amino acids are usually L-α-amino acids. Over twenty different amino acids are used as building blocks for polypeptides and proteins (Figure 2). In these biopolymers, the amino acids are ordered in a specific sequence, also known as primary structure. These sequences are key to the assembly of the proteins on different hierarchical levels. In addition, even large proteins often have a precise molecular weight, instead of a molar mass distribution that is common in artificial polymers. A naturally occurring polypeptide that is of great commercial interest is poly-(γ-glutamic acid) (γ-PGA). Large scale synthesis of γ-PGA can be achieved through a fermentation process. γ-PGA differs from other natural polypeptides on several levels. Unlike the latter, γ-PGA is formed by L- as well as D-amino acids. The polymer does not have a defined sequence, but is composed of only one amino acid. And finally α- as well as unusual γ-linkages are connecting the amino acids along the polymer chain. It is a biodegradable and edible polymer that can be used for a variety of potential applications in food industry, personal healthcare, and agriculture.[6]

Most commonly, synthetic polypeptides are polymerized by solid phase synthesis or by the ring opening polymerization of amino acid *N*-carboxyanhydrides (NCA). Solid phase synthesis gives rise to polypeptides with well-defined amino acid sequences, thereby generating biomimetic polypeptides. However, the overall yields are low and high molecular weights cannot be achieved with this method, limiting their range of applications. NCAs, on the other hand, can be polymerized by a controlled living polymerization, which allows for the synthesis of complex

polymers, such as block, gradient and star polymers.[7] However, NCAs are quite unstable and degrade in presents of moisture. Their synthesis usually requires highly toxic reagents, such as phosgene or phosphorous pentachloride.

The incorporation of amino acids into polymers can also be achieved through the functionalization of side-chains, which typically generates non-polypeptide-like structures.[8] Side-chain functionalizations have been used extensively for various systems. In general, the aim is to mimic some of the properties of natural poly(amino acid)s. A particular focus was placed on the influence of the amino acid side-chains to the polymerization behavior and properties of methacrylamide based polymers. Interestingly, *N*-methacryloyl-L-leucine methyl ester showed higher reactivity than methyl methacrylate in a free radical polymerization.[9] The higher reactivity might be caused by the interaction of L-leucine units with the propagating chain ends. In addition, the resulting polymer exhibited an increased and inversed specific optical rotation. Bulk polymerization of a methionine-based methacrylamide with azobisisobutyronitrile (AIBN) produced high molar mass polymer (number average apparent molar mass (M_n^{app}) = 509 kDa). The thioester group of the latter can be selectively oxidized by hydrogen peroxide to yield either the corresponding sulfone or sulfoxide, depending on the amount of oxidizing agent.[10]

In addition, controlled radical polymerizations have been used for the polymerization of functionalized acrylates, providing the opportunity to produce α- and ω- functionalized polymers as well as block-copolymers.[11] Reversible addition-fragmentation chain transfer (RAFT) polymerization of *tert*-butyl acrylate followed by a chain extension with an L-phenylalanine-based monomers afforded a block copolymer.[12] The *tert*-butyl ester unit can be cleaved by a treatment with trifluoroacetic acid (TFA) to generate an amphiphilic block copolymer, able to self-assemble in water to give micelles with a chiral core. RAFT polymerization was also used for the synthesis of block copolymers with a polystyrene block and a short vinylbenzoic acid L-hydroxyproline ester block.[13] The resulting polymers were tested for catalytic activity in selective aldol reactions and were found to be as effective as unsupported L-proline organo catalysts. The authors showed that the catalytic

activity and selectivity of the polymer-supported system did not decrease after three reaction cycles.

Ring opening metathesis polymerizations (ROMP) of norbornene derivatives with amino acid and peptide side-chains have also been studied. The group of Grubbs copolymerized a norbornene with an elastine-inspired peptide side-chain, with a poly(ethylene glycol) (PEG) functionalized norbornene. The resulting polymer showed a thermo-responsive behavior.[14] Other norbornenes with short peptide sequences as side-chains have been explored, to verify the compatibility of the different amino acids with the ROMP. While most of the amino acids do not have a negative effect, when they are incorporated in the peptide side-chains, the sulfhydryl groups of cysteine must be protected for instances with an acetamidomethyl group to enable the polymerization.[15] Norbornene provides the possibility of two side-chain functionalizations per monomer unit (Figure 3). It has been shown that *endo,exo* and *exo,exo* amino acid functionalized norbornenes can be polymerized using a second generation Grubbs catalyst, while the *endo,endo* derivative does not polymerize.[16]

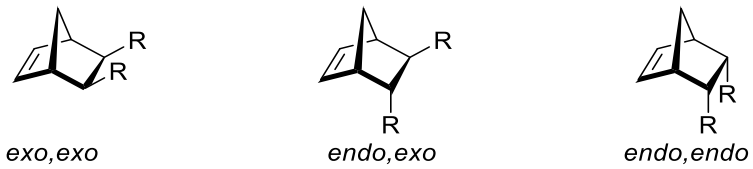

Figure 3: Side-chain functionalized norbornenes.

A drawback of side-chain functionalized polymers is the non-degradable hydrocarbon backbone. To circumvent this, it is possible to incorporate amino acids and their functional groups into the polymer backbone of a polymer, for instance by step growth polymerizations. This is especially useful, when complex architecture and controlled polymerization are not required. Regarding applications, one of the most promising poly(amino acid)s prepared by step growth polymerization is poly(aspartic acid) (PASA).[17] There are several different synthetic routes leading to PASA. The simplest one is the polycondensation of aspartic acid to a polysuccinimide, which yields PASA upon the hydrolysis of the imide. Similar to γ-

PGA, the resulting PASA is non-enantiomerically pure and is not only connected by α-linkages. Other synthetic amino acid based polymers and copolymers have been synthesized with polycondensation as well as other polymerization techniques. Their properties include self-assembly stimuli responsiveness, biodegradability, and biocompatibility. Potential applications are, among others, biomedical applications, as well as, food and agricultural packaging.[8,18]

A trigger based on redox-responsive properties can be introduced by cystine, the natural occurring dimer of cysteine, linked by a disulfide bridge. Compared to carbon-carbon or carbon-hydrogen bonds, the sulfur-sulfur bond is a relatively weak link and thus can be easily and reversibly cleaved by reduction. Cystine is used in polymers mostly as a cross-linker between the individual polymer chains, for instance for micelle stabilization purposes.[19,20] Polymers with the disulfide linkage of the cystine along the backbone are uncommon. Recently, Jayakannan et al. polymerized tert-butyloxycarbonyl (Boc) protected dimethyl cystine with aliphatic diols via melt polycondensation.[21] The resulting polymers had a weight average apparent molar mass M_w^{app} of up to 32 kDa. However, shortening the diols from a C12 to a C8 led to significantly lower M_w^{app} of 8 kDa. Deprotection of the Boc-groups was performed using TFA in dry dichloromethane (DCM). Despite the likeliness of a main chain cleavage under such conditions, the final molar masses were not reported.

5.1.2 Olefin Metathesis Reactions

The word metathesis is derived from ancient Greek and can be translated as 'exchange'. In chemistry it usually refers to reactions, were one group is exchanged with a similar one. Two examples for this are the olefin metathesis and the disulfide metathesis. The olefin metathesis was discovered in the 1950th, but the underlying mechanism remained unclear until 1971, when it was confirmed by Yves Chauvin (Scheme 1).[22] The reaction is a redistribution of alkylidene groups and is catalyzed by a metal alkylidene complex.[23] It involves a [2+2]-cycloaddition of the complex with an olefin to form a metalla-cyclobutane, followed by a retro [2+2] cycloaddition leading to either the starting reactants or a new olefin and a metal alkylidene complex.

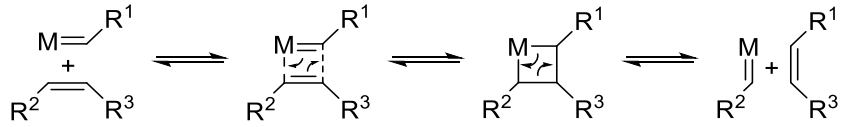

Scheme 1: Mechanism of the olefin metathesis.

With the discovery of a highly active molybdenum-based catalyst by Richard R. Schrock in 1990s, the olefin metathesis, which until then was a niche topic, became the focus of many studies by the organic and polymer chemistry community. While highly reactive, Schrock catalysts are also sensitive to oxygen, moisture and a variety of functional groups. This limitation was overcome by the ruthenium complexes first discovered by Robert H. Grubbs in 1992.[24] Extensive research in this field produced a wealth of highly reactive metathesis catalysts (Figure 4). The impact on the scientific community was such that Yves Chauvin, Richard R. Schrock, and Robert H. Grubbs were awarded with the Nobel Prize in chemistry in 2005 "for the development of the metathesis method in organic synthesis".[25]

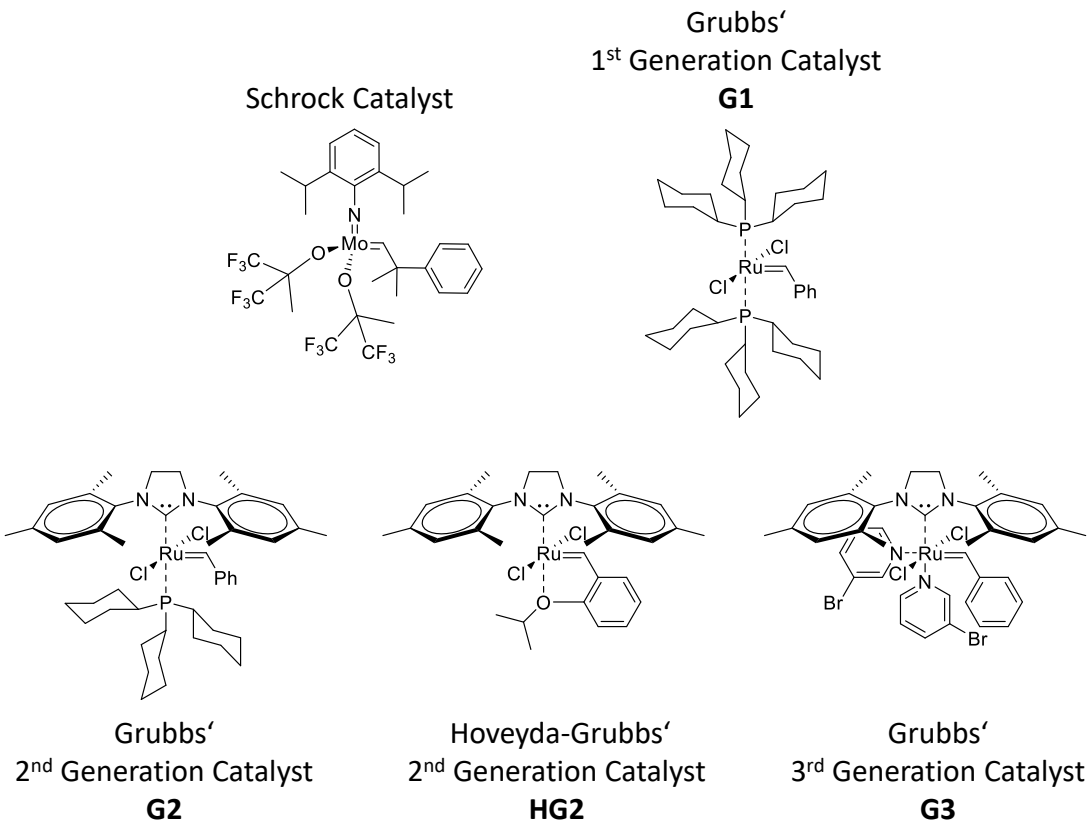

Figure 4: Standard catalysts for olefin metathesis reactions.

Since then, the olefin metathesis reaction emerged to be one of the most ubiquitous C-C bond forming reactions. Development of new catalysts include, Z-selective catalysts, catalysts for sterically demanding double bonds, polymer supported catalysts for easier removal and water soluble catalysts for olefin metathesis reactions in aqueous media.[26–29]

5.1.2.1 Olefin Metathesis Polymerization

Olefin metathesis polymerizations typically fall in two categories, which are the ring opening metathesis polymerization (ROMP) and the acyclic diene metathesis (ADMET) polymerization (Scheme 2).

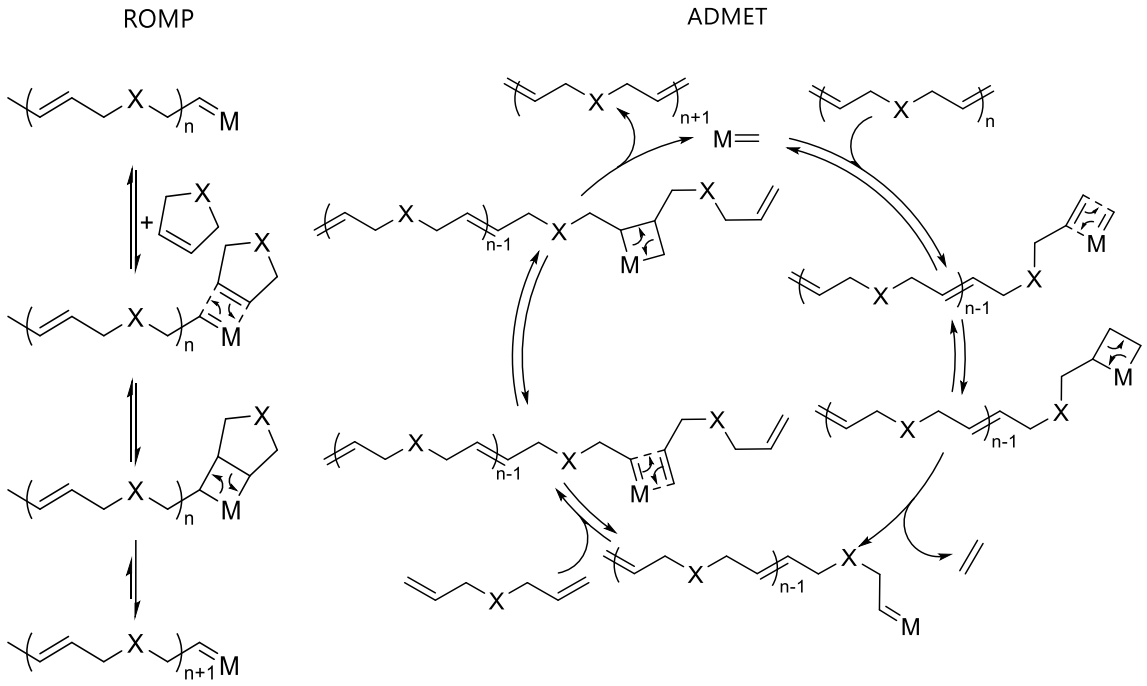

Scheme 2: Mechanisms of polymer growth during olefin metathesis polymerizations. (Right) ROMP, (Left) ADMET polymerization.

The ROMP is a chain growth polymerization, applied mostly on strained ring monomers, *e.g.,* norbornene and cyclooctene derivatives, and is generally controlled. However, the use of this polymerization technique for bio-derived monomers is limited. Side-chain functionalization of norbornenes is often used to introduce functional groups or bio-derived building blocks into polymers. For instance, amino acids and short peptide chains have been used as side-chain functionalization for functional polynorbornenes.[15,30]Another way to introduce bio-derived moieties in polymers is to use a cyclopentadiene derivative and a dienophile to synthesize a norbornene-like bio-based monomer.[31,32]

The ADMET polymerization, on the other hand, is a step growth polymerization that follows a polycondensation pathway, with ethylene as the most common side product. The α,ω-dienes used for the reaction are easily synthesized and therefore bio-derived building blocks can be incorporated without the need for a tedious monomer synthesis.

Fatty acids for instance can be converted into ADMET monomers in a simple synthesis by creating acid anhydrides or diesters. The resulting α,ω-dienes can be polymerized with a ruthenium based catalyst to hydrolyzable polymers with apparent molar masses of up to 18.5 kDa.[33] Similarly itaconic acid can be converted into a diester with 10-undecenol and subsequently polymerized with **G1**. The resulting polymers could be further functionalized by Michael addition reactions.[34] Amino acid derived amino alcohols were first incorporated into ADMET polymers by Wagener et al.[35] The synthesized polyesteramides showed semi-crystalline behaviors and apparent molar masses of up to M_n^{app} = 33 kDa. α,ω-Alkenyl esters of L-glutamic acid diketopiperazine were polymerized by Masuda et al.[36] Tertiary amides of glycine derived diketopiperazine were homo and copolymerized by the group of Schlaad, leading to low molar mass polymers.[37] More recently, an L-lysine-based diacryl amide was copolymerized with a phosphate diene for drug delivery purposes.[38] However, certain functional groups, such as carbonyl groups, can have a negative neighboring group effect (NNGE) on the polymerizations conducted with ruthenium catalysts. The most pronounced effect is observed when a six-membered chelating complex can be formed during the reaction, leading to the complete deactivation of the catalyst (Figure 5). Therefore, long aliphatic chains are usually used as linkers between the double bonds and the carbonyl groups, to prevent the complexation.[35,37,39,40]

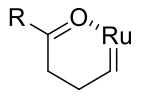

Figure 5: Chelation during olefin metathesis reactions.

5.1.3 Disulfide Metathesis Reaction

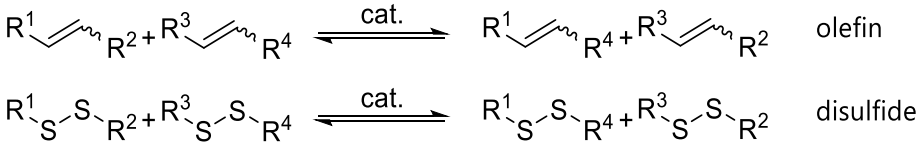

Scheme 3: Schematic comparison between the olefin metathesis (top) and the disulfide metathesis (bottom).

The thiol-disulfide exchange reaction or disulfide metathesis reaction shows several similarities to the olefin metathesis reaction. First of all, they fall into the category of exchange reactions. In the olefin metathesis, the alkylidene groups of a double bond are exchanged, whereas the disulfide metathesis can be seen as an exchange of thiyl residues of a disulfide bond. Both reactions involve the cleavage and formation of a covalent bond, are reversible and can take place at room temperature. However, the underlying mechanisms of both reactions are significantly different. While the olefin metathesis is transition metal-catalyzed and involves a [2+2]-cycloaddition (as described above), the mechanism of the disulfide exchange is a simple S_N2 mechanism.

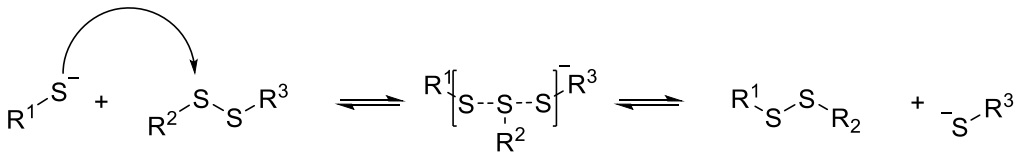

Scheme 4: Mechanism of the disulfide metathesis.

The reaction is base-catalyzed with a thiolate being the nucleophile as well as the leaving group. The transition state has long been debated but seems to have a linear trisulfide like configuration.[41–43] In the transition state, the charge is distributed over all three sulfur atoms, with a higher density on the attacking and the leaving sulfur groups. The reaction takes place under very mild conditions (*e.g.,* aqueous solutions, room temperature, and neutral pH). The disulfide metathesis reaction plays an important role in diverse enzymatic processes and is crucial for protein folding and stabilization. Furthermore, important biological redox processes

are based on disulfide metathesis reactions.[44,45] Since the thiolate and not the thiol is the reacting nucleophile, the reaction kinetics depend on the dissociation of the thiols and hence on the pH of the reaction media.[46] In polar protic solvents, the thiolate anion is stabilized by solvation, which leads to a decrease of the reaction rate of the disulfide metathesis by about three orders of magnitude.

5.1.4 Disulfide metathesis polymerization

The presence of disulfide groups within polymer backbones gives rise to interesting properties. For instance, the disulfide bridge can be cleaved under mild reductive conditions, which make poly(disulfide)s degradable under these conditions. Glutathione is a natural tripeptide, which is abundant in cells of various kinds of animals and plants. Due to its free thiol group it is a reducing agent and can thus cleave disulfide bonds. The higher concentrations of glutathione in certain types of tumor make these polymers promising candidates for biomedical applications.[47] Furthermore, poly(disulfide)s may exhibit an enhanced cellular uptake and could therefore be used in the context of gene delivery.[48,49] In addition, the dynamic nature of the disulfide bond fulfills the main condition for self-healing materials.

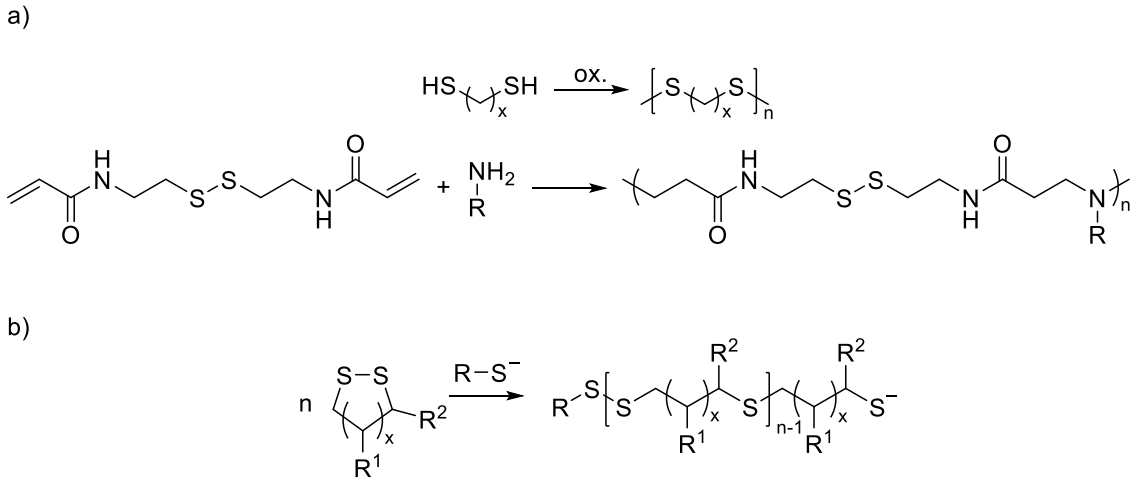

Scheme 5: a) Common pathway towards functional poly(disulfide)s. b) Ring opening disulfide metathesis polymerization.

Usually poly(disulfide)s are synthesized by the direct oxidations of dithiols or by polyaddition reactions. The first has been shown to produce high molar mass polymers.[50–52] For instance, the oxidative polymerization of 2-[2-(2-sulfanylethoxy)ethoxy]ethanethiol (DODT) proceeded via a radical pathway involving cyclic intermediates, resulting in polymers with M_n^{app} of up to 350 kDa and dispersities as low as 1.15.[53] It remains, however, unclear why such low dispersities were achieved, since there is neither simultaneous initiation, nor any ring strain in the intermediately formed macrocycles. The synthesis of poly(disulfide)s via polyaddition reactions is usually performed by a Michael addition of a bis(acryl amide), such as *N,N′*-bis(acryloyl)cystamine, and a primary amine.[54,55] This synthetic pathway allows for the synthesis of a variety of poly(disulfide)s. Unfortunately, the corresponding molar masses are usually low, since a high conversion and an 1:1 stiochiometric ratio of the two functional groups are necessary for the achievement of high molar masses. Poly(disulfide)s are, despite this, promising candidates for being the next generation of gene delivery agents.[56–58]

Thiolate-initiated ring opening disulfide metathesis polymerizations have been rarely reported in the literature. Almost exclusively, five and six-membered disulfide rings (*i.e.,* 1,2-dithiane and 1,2-dithiolane derivatives) have been polymerized under mild conditions (Figure 6). For instance, Matile et al. polymerized lipoic and asparagusic acid esters for self-organizing surface-initiated polymerizations and copolymerizations. Oriented structures on surfaces with suitable properties for organic solar cells and photosystems were obtained.[59–61] The same building blocks (*i.e.,* lipoic acid ester and asparagusic acid ester derivatives) were also used for the synthesis of cell-penetrating poly(disulfide)s.[49] Fluorescence-labeled polymers prepared via the same technique facilitate the monitoring of fast transport into the cytosol of HeLa cells and their rapid depolymerization.

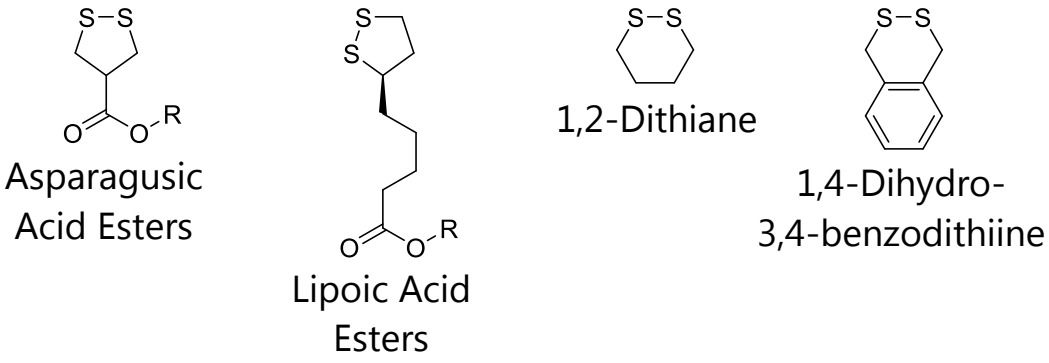

Figure 6: Selection of disulfides used in thiolate-initiated ring opening disulfide metathesis.

The group of Endo polymerized 1,2-dithiane and 1,4-dihydro-2,3-benzodithiine.[62,63] They used benzyl mercaptan as well as α,α'-mercapto-*o*-xylene as the initiators to yield polymers with M_n^{app} of up to 92 kDa. Thiolate initiated polymerizations were also used by the Regen and coworkers.[64,65] In their work they explored the stabilization of micelles and liposomes using lipoic acid derivatives. The polymerization could be initiated by the reduction of some of the disulfides to the corresponding dithiols. The polymerizations were performed under mild conditions in aqueous media. The group showed that the permeability of the liposomes can be tuned by the ratio of polymerizable lipids to non-polymerizable lipids.

5.1.5 Polymerization of Unstrained Macrocycles

The polymerization of unstrained macrocycles (ring size > 14)[66,67] is a ring opening and chain growth polymerization. Like most of the ring opening polymerizations, it is a polyaddition. However, the resulting polymers usually exhibit a Schulz-Flory molar mass distribution (*i.e.,* dispersities ($Đ$) ≈ 2), which is common for step growth polymerizations. For polycondensations, the theory of the ground lying equilibrium between oligomeric macrocycles and polymer chains was first described by Jacobson and Stockmayer in 1950, but can also by applied for the polymerization of unstrained macrocycles.[68]

The lack of ring strain in macrocyclic monomers leads to polymerizations where the change in enthalpy (ΔH) during the polymerization is zero.[69] For a polymerization reaction to take place the change in Gibbs energy (ΔG) has to be negative. Which would imply in this case, that the change in entropy (ΔS) has to be positive (equation 1).

$$\Delta G = \Delta H - T\Delta S \qquad (1)$$

In other words, these polymerizations are entropy-driven ring opening polymerizations (ED-ROP). In general, translational entropy decreases during all polymerization reactions, making polymerization reactions entropically unfavorable. This effect becomes less pronounced with increasing molar masses of the monomers and at high concentrations. On the other hand, a macrocycle can be seen as a linear chain restricted to a conformation with a small end-to-end distance, similar to a bond distance.[68] By turning a macrocycle into a linear chain the number of possible conformations increases leading to a concentration-independent increase of conformational entropy. At high concentrations the conformational part of the entropy takes over, leading to a negative ΔG. Overall the ED-ROP mechanism is a chain growth polymerization with extensive chain transfer "backbiting". The ED-ROP leads to two different unrelated size distributions, one for the linear polymers and one for the macrocycles. If the reaction reaches the equilibrium, all macrocycles result from backbiting reactions. In order for the active chain end to attack a functional group, along the polymer backbone, it has to be in close vicinity. Figure 7 illustrates that the probability for a backbiting to take place is highest for short distances along the polymer chain. Hence, the resulting macrocycles contain only a few repeating units and their size distribution usually shows an exponential decline. The average molar mass of the polymer, on the other hand, is derived by the amount of chain ends per monomer unit in the linear fraction.

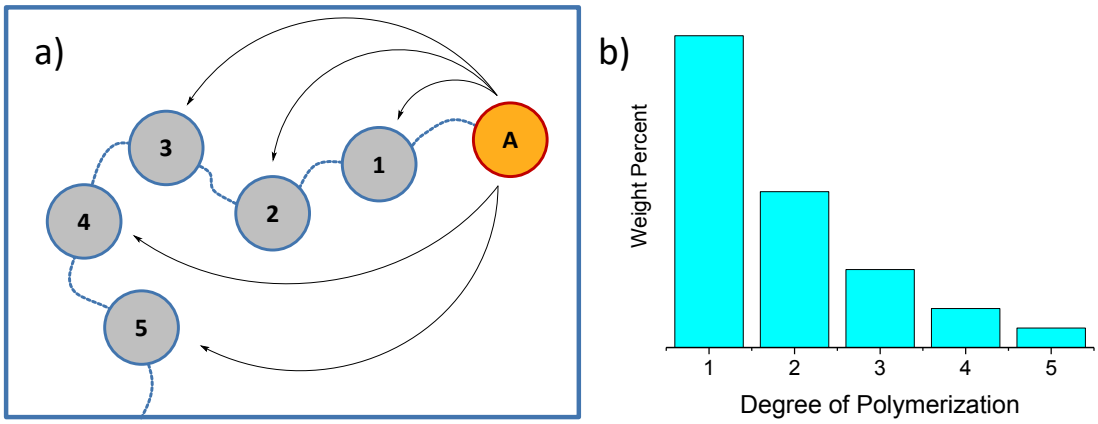

Figure 7: a) Schematic illustration of the backbiting reaction during an ED-ROP. b) Exemplary simplified description of the size distribution of the cyclic fraction.

The required macrocyclic monomers for ED-ROP are often derived from monomers for classic polycondensations. For this, oligomeric rings are formed in a condensation reaction under high dilution conditions. For the ED-ROP, the pure oligomeric rings are submitted to polymerization conditions in high concentration. The end groups are usually provided by impurities or initiators. A general drawback of step growth polycondensations is that a 1:1 stoichiometric match and high conversion are essential in order to reach high molar masses. The expected average degree of polymerization $\bar{X}_n$ of AA-BB step growth polymerizations can be calculated by the Carothers equation (equation 2).

$$\bar{X}_n = \frac{1+r}{1+r-2pr} \qquad (2)$$

With

$$r = \frac{N_B}{N_A} \leq 1 \qquad (3)$$

Where r is the stoichiometric ratio, p is the conversion and N_B and N_A are the corresponding amounts of the monomers A and B. In contrast to that, the ED-ROP follows a chain growth mechanism and high conversions are not necessary. Hence, the ED-ROP can be a good alternative to step growth polymerizations. For instance, polyesters like poly(ethylene terephthalate) (PET) can be synthesized by an ED-ROP, by polymerizing macrocycles that typically form (as side products) during

the classic polycondensation of PET or result from its depolymerization during recycling.[70,71] Also, pentadecalactone (PDL) can be polymerized to high molar masses by enzymatic polymerizations or aluminum-salen complex. The resulting polymers were shown to be promising candidates as a low density polyethylene alternative.[72,73] Even polyaramides can be obtained by an ED-ROP. N,N'-Di-sec-butyl-*p*-terephthalamide cyclic oligomers can be polymerized by the highly nucleophilic L-methyl-3-*n*-butylimidazole-2-thione as the initiator and phenylphosphonic acid as the cocatalyst at 275 °C, to yield semicrystalline polyaramide.[74]

The olefin metathesis is an ideal reaction for ED-ROP because the equilibration of the reaction is fast and the required reaction temperatures are usually low. A wide range of polymers have been synthesized by entropy-driven ring opening metathesis polymerization (ED-ROMP) resulting in unique polymers, including sequence-encoded polylactides, polyamides and polypseudorotaxenes.[75–78] Grubbs and coworkers demonstrated the advantage of an ED-ROP compared to a step growth reaction. They polymerized a 14-membered crown ether analog by ED-ROMP and compared it with the polymer obtained by ADMET polymerization. While the former yielded polymers of molecular weights of up to 200 kDa, the latter only led to molecular weights smaller than 11 kDa.[79,80] The same was observed for the polymerization of monomers based on natural occurring bile acid.[81] The polymerization of the macrocyclic derivatives via ED-ROMP led to significantly higher molar masses than the polymerization of the corresponding dienes via ADMET polymerization. The resulting polymers showed promising properties as shape memory effect polymers. Similarly, bio-derived sophorolipids can also be polymerized by ED-ROMP. The macrocyclic monomer is accessible by yeast fermentation. The fermentation process results in a mixture of macrocyclic lactones and an open derivative, with the macrocycle as the main product. The macrocycles can be isolated and subsequently polymerized by ED-ROMP to yield semi-crystalline bio-based polymers.[82] One of the characteristics of ED-ROPs is the broad size distribution that is usually obtained. Gutekunst and Hawker were able to circumvent this by using a sophisticated enyne trigger system. Incorporating this

into sequence-encoded lactide based macrocycles facilitated the ED-ROMP with $Đ$ as low as 1.15.[83]

Macrocyclic disulfides are another class of monomers that can be polymerized by an ED-ROP, for instance by a heat-induced radical pathway. Macrocyclic aryl disulfides can be polymerized at high temperatures.[84] The polymerization proceeds under normal as well as inert atmosphere. The polymers obtained in the presence of air had a higher glass transition (T_g) as well as a lower decomposition temperature. It was suggested that this was the result of a partial oxidation of the disulfides into the corresponding thiosulfonates.

Regen et al. also investigated the thiolate initiated ring opening polymerization of phosphatidylcholine and quarternized ammonium macrocyclic disulfides for vesicle stabilization.[85] Analysis of the thiol end-groups indicate number average molar masses up to M_n = 28 kDa. Apart from that, the thiolate-initiated entropy driven ring opening polymerization of macrocyclic disulfides remains largely unexplored.

5.2 Analytical Methods

5.2.1 Nuclear Magnetic Resonance spectroscopy

The nuclear magnetic resonance (NMR) spectroscopy is a powerful tool for structural and chemical elucidation of small molecules as well as polymers. The solid state NMR will not be discussed in this paragraph. The NMR technique is based on a magnetic resonance of the spin state of a nucleus inside of a strong magnetic field. Therefore, it is only applicable to isotopes that exhibit a magnetic spin, such as ^{1}H, ^{13}C, ^{15}N, ^{19}F and ^{31}P. Atom nuclei that have a nuclear spin also exhibit a magnetic moment. This magnetic moment is restricted to a defined set of spin states. For example, the hydrogen atom (^{1}H) has a spin (*I)* of ½. The number of spin states can be calculated by the formula $2I+1$. Hence, hydrogen ^{1}H has two different magnetic quantum numbers $m_1 = +½$ and $m_2 = -½$, referred to as up and down spin. The energy of the spin states, and by extension the frequency to induce spin transitions, is directly proportional to the external magnetic field B_0 and the nuclear magnetic moment μ. In an NMR measurement, a sample is typically placed in a magnetic field and a radio wave source is used to cause transitions between the spin states. In a Fourier transform spectrometer, a radio magnetic pulse is used to induce all transitions of the analyzed isotope at same time. This leads to the emission of energy while the system returns to the ground state. A Fourier transformation of the so called free induction decay (FID) signal produces the NMR spectrum (Figure 8).

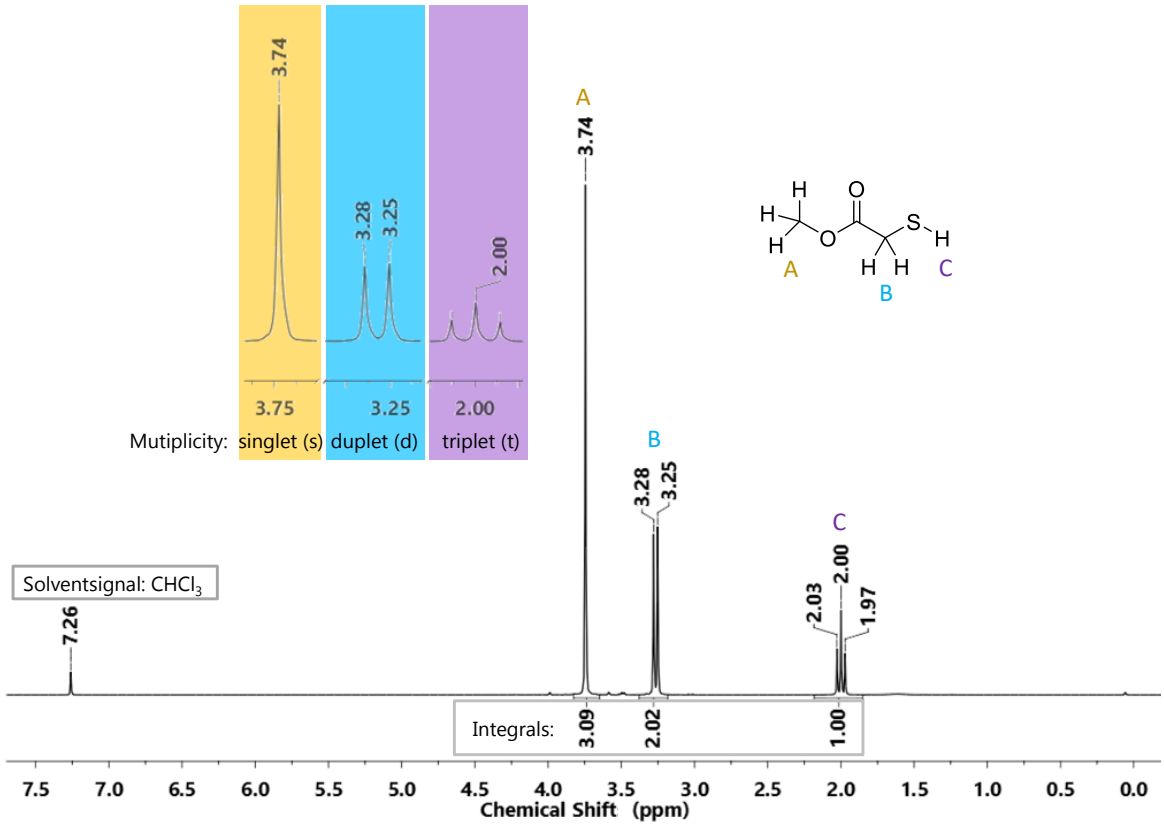

Figure 8: Example of a ^{1}H NMR spectrum. ^{1}H NMR (300 MHz, $CDCl_3$) of methyl thioglycolate (MTG).

Different isotopes exhibit different resonance wavelengths and can therefore be analyzed individually from one another in the NMR spectrum. Furthermore, the electron density on a given nucleus results in a shielding effect from the external magnetic field. Thus, a shift of the NMR signals occurs in the spectra. Since the electron density is influenced by the neighboring atoms in a molecule, the so called chemical shift allows distinguishing functional groups by NMR analysis. The chemical shift δ is reported in ppm, in comparison to a certain reference compound, which is set to be 0. For ^{1}H and ^{13}C NMR experiments, tetramethylsilane (TMS) is used as the reference. Additionally to the chemical shift, a spin-spin coupling of neighboring nuclei with $I \neq 0$ takes place, resulting in a splitting of energy levels In practice, this effect causes the proton signals to be split into so-called multiplets. In a simple ^{1}H NMR, the integration of these peaks can be used to quantify the abundance of the corresponding hydrogen atoms. 2D NMR experiments measure the intensity as a function of two frequencies. These experiments can be used to

gather additional information about a molecular structure. Examples of common 2D NMR experiments are correlation spectroscopy (COSY), heteronuclear single-quantum correlation (HSQC), and heteronuclear multiple-band correlation (HMBC). In polymer science the NMR experiments are used to determine not only the chemical composition, but also the absolute molar mass as well as the stereochemistry of a polymer.

5.2.2 Electrospray Ionization Time-of-Flight Mass Spectrometry

Time-of-flight mass spectrometry (ToF MS) is an analytical method that can be used for molecule identification, structural elucidation and determination of the elemental composition. An ionized molecule can be accelerated inside an electric field. The acceleration of this molecule is proportional to the charge to mass ratio. In other words, for an identical charge, a heavy molecule accelerates less and therefore needs a longer time to reach a detector than a light molecule.

Different ionization technique, such as, electron ionization (EI), matrix assisted laser desorption/ionization (MALDI) and electronspray ionization (ESI) can be used to produce the ions that are needed for time-of-flight measurements. MALDI, and ESI are considered to be soft ionization methods leading to only minimal fragmentation of the analyte. This makes them ideal for the analysis of macromolecules. EI on the other hand usually leads to fragmentation of the molecules. Fragmentation needs to be avoided for macromolecules, as the resulting spectra would not be representative of the actual molar mass and the spectrum might get to complex to resolve. For small molecules the fragmentation pattern can help to identify functional groups and determine the structure of the molecule.

For the electronspray ionization, a dilute solution of the analyte is passed through a thin tube with a high electric field applied at the tip. The electric field forces charged ions to the tip and subsequently small droplets are emitted in to the surrounding gas. After that the highly charged droplets are further reduced in size,

by solvent evaporation. As a result of this, additional shear forces and deformation of the droplets takes place. As the droplet size decreases, the density of likewise-charged ions at the surface of the droplet and their repulsion increase. When the repulsion of the charges becomes greater than the surface tension, the Rayleigh stability limit is reached. The droplet explodes into even smaller droplets. These undergo further solvent evaporation followed by another explosion. From these droplets, ions become airborne and are further analyzed by mass spectrometry (Figure 9).

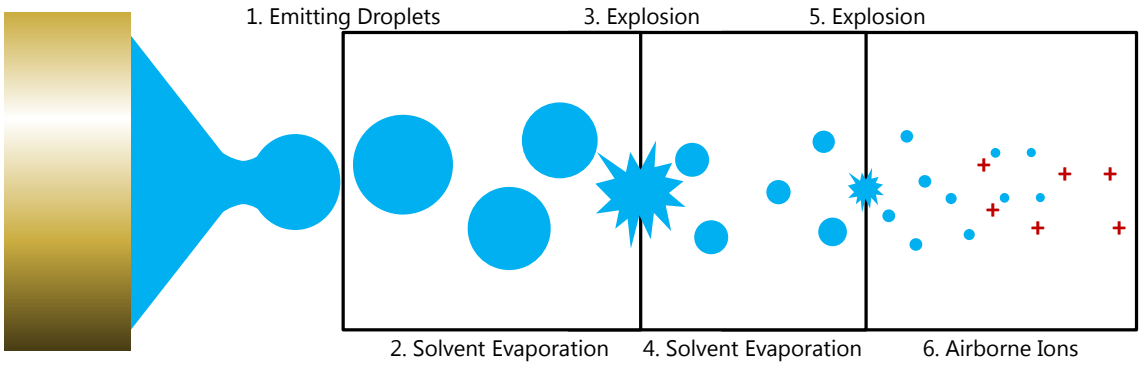

Figure 9: Schematic illustration of the ESI process, from the ejection of charged droplets to airborne ions.

5.2.3 Size Exclusion Chromatography

Size exclusion chromatography (SEC), also known as gel permeation chromatography (GPC), is an analytical method that is used to determine the average molar mass and molar mass distribution of polymers. Like other chromatography techniques, SEC consists of a stationary and mobile phase. While the stationary phase consists of porous gel beads, the mobile phase is the solvent that dissolves and carries the polymer sample through the stationary phase. The aim of the SEC is to separate the individual polymer chains according to their hydrodynamic size in solution. Important prerequisites for a successful separation include: a solubility of the polymer in the mobile phase, no interactions of the stationary phase and the polymer sample, as well as a good swellability of the stationary phase in the mobile phase. When a dilute solution of the sample is

injected into the SEC column, the sample molecules diffuse together with the mobile phase through and around the porous gel beads. The bigger the hydrodynamic volume of a molecule the faster it will pass the column. Small molecules can diffuse in most of the pores, while larger molecules cannot enter the smallest pores. Notably, the largest polymers will not be able to enter any of the pores and thus elute very fast through the SEC column, whereas the smaller polymers will diffuse through the porous gels and thus elute slowly (Figure 10). The molecules that elute from the column are typically detected by a change of the refractive index of the solution or by an ultraviolet–visible (UV-Vis) detector. The detector response is plotted against the elution volume of the mobile phase. Polymer standards are used to calibrate the SEC and calculate molar masses. As such the molar masses determined by SEC are relative (to the standards used) and thus not absolute. Additionally, the hydrodynamic volumes of two polymers that are different in molar mass and chemical composition might still be identical, thus elute from the column at the same time. Hence, the SEC is most precise when polymer standards and analytes are chemically identical. For the same reason, apparent molar masses for polymers that are chemically different from the standards used might be significantly different from the absolute values.

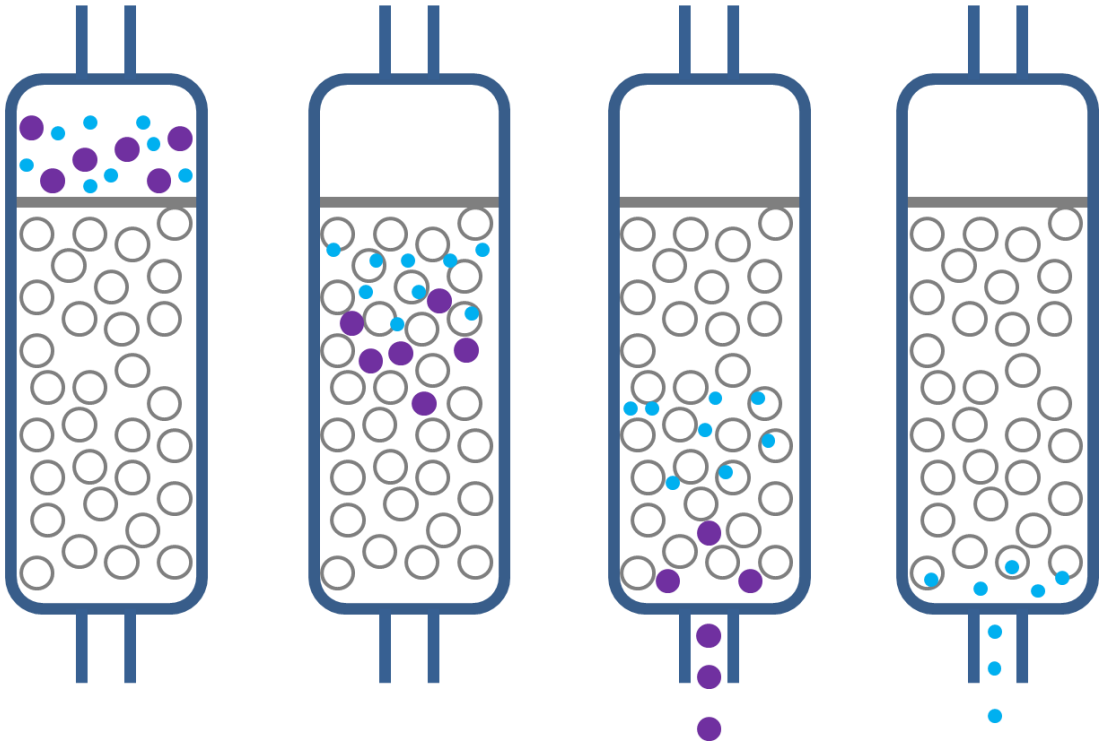

Figure 10: Schematic illustration of the separation of molecules with different hydrodynamic volumes with the SEC.

5.2.4 Thermal Analysis

The analysis of the thermal properties of polymers provides information on the phase transitions, such as melting temperature and enthalpy, crystallinity and glass transition, as well as thermal decomposition under different conditions. Such properties are useful for targeting and narrowing down the types of applications that the analyzed polymer can be aimed at.

5.2.4.1 Thermogravimetric Analysis

Thermogravimetric Analysis (TGA) is used to follow the thermal decomposition of a given sample. The temperature range is usually between ambient temperature and 1000 °C. For this measurement a sample is placed in a sample holder and positioned on a balance. The sample is then heated at a chosen heating

rate under controlled atmosphere (*e.g.*, nitrogen). During the experiment the weight of the sample is measured as a function of temperature. The TGA curve can be used to determine the onset temperature of the thermal decomposition of the sample. This can be useful for other measurements (*e.g.*, DSC) or can provide information about the operating temperature in which a material can be used. Thermal decomposition might take place in several individual steps, corresponding to a stepwise decomposition of individual parts (*e.g.*, functional groups) of the sample. The TGA can also be coupled with other analytical instruments, such as mass spectrometry (TGA/MS) to analyze the gases that are released during the sample decomposition. Finally, the residual mass can be measured after decomposition.

5.2.4.2 Differential Scanning Calorimetry (DSC)

DSC is an analytical method used to investigate the thermal behavior of a sample. Two crucibles are heated under inert atmosphere and their relative heat flow is measured. One of these crucibles contains the analyte, while the other, the reference crucible, is empty. Sample and reference are heated and cooled at a continuous rate and maintained at nearly the same temperature throughout the experiment. The difference in heat flow between sample and reference is measured and plotted as a function of temperature (Figure 11). With this, it is possible to measure the required temperatures as well as the specific heat for different phase transitions or reactions that a sample may undergo. For instance, the glass transition (T_g) of an amorphous polymer, a second-order transition, will appear as an endothermic shift of the DSC curve, indicative of a change in heat capacity (C_p). In the glassy state, below the T_g, the polymer is rigid and brittle. Above the T_g, in the rubbery state, the polymer backbone gains a degree of freedom, which means the polymer becomes softer and flexible and results in a higher heat capacity of the polymer. Additionally to the T_g a polymer might also exhibit a crystallization (T_c) and a melting temperature (T_m). These first order phase transitions are observed at higher temperatures than the T_g. At T_c, the polymer chains align into ordered,

crystalline domains, and heat is released. Hence, an exothermic peak is observed in the thermogram. For a melting to take place heat is required and the thermogram shows an endothermic peak. The heat that is released or absorbed by the polymer can be quantified by measuring the corresponding peak areas.

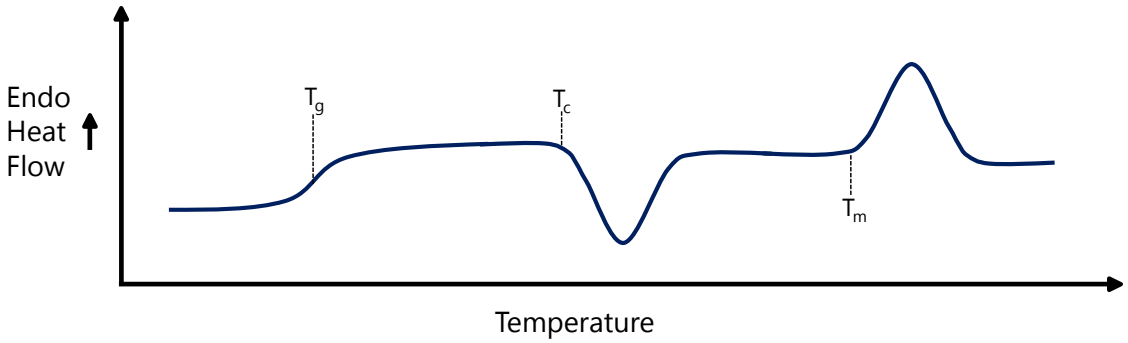

Figure 11: Schematic illustration of a DSC thermogram.

6 Results and Discussion

The aim of this work was to explore new routes towards bio-based main-chain poly(disulfide)s. L-Cystine is a natural occurring disulfide, that is ubiquitous throughout nature. Together with its monomer L-cysteine it plays an important role in protein stabilization and for the redox system inside cells. Therefore, cystine and cystine derivatives are ideal platform chemicals for new main-chain poly(disulfide)s. ADMET polymerization was thought to be a viable polymerization technique for the polymerization of cystine-based monomers.

6.1 Synthesis of N,N'-diboc dibutenyl cystinate

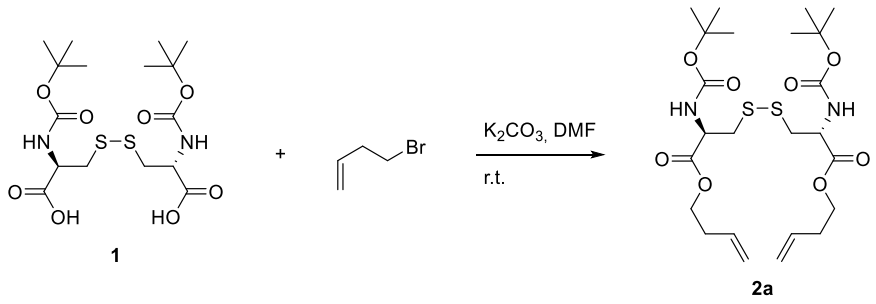

Scheme 6: Synthesis of the L-cystine based α,ω-diene **2a.**

Commercially available N,N'-di-Boc-L-cystine was chosen as a model component to investigate synthetic routes and polymerization techniques towards new poly(disulfide)s. The synthesis of the required α,ω-unsaturated monomer was done by esterification with 4-bromo-1-butene. The usefulness of 4-bromo-1-butene for the synthesis of amino acid-based monomers has been shown before.[37]

2a was synthesized by an S_N2 reaction with N,N'-diboc-L-cystine and an excess of 4-bromo-1-butene. The reactions were performed in N,N-dimethylformamide (DMF) and an excess of potassium carbonate was used to neutralize the formed hydrobromic acid. Different reaction times were explored. The isolated yield increased significantly, by increasing the reaction times from 1 to 4 days (Table 1). The long reaction times were necessary due the weak nucleophilicity of the carboxylate. Fortunately, no tedious workup strategies, such as distillation, column chromatography, or recrystallization, were necessary to give the pure product (Figure 12). Inorganic byproducts and the high boiling solvent DMF could be removed by a filtration with subsequent liquid extractions. The excessive 4-bromo-1-butene could be removed by freeze-drying of the crude product with 1,4-dioxane.

Table 1: Isolated yield of **2a**

Entry	Reaction Time	Isolated Yield
1	1 d	34 %
2	2 d	63%
3	3 d	71%
4	4 d	90%

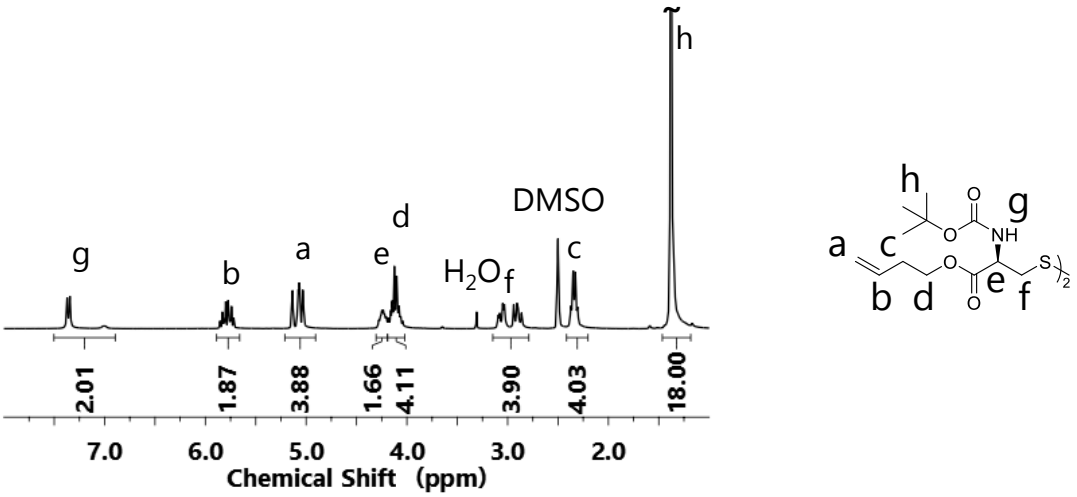

Figure 12: ^{1}H NMR (300 MHz, DMSO-d_6) spectrum of the L-cystine based α,ω-diene **2a**

In some cases the formation of several byproducts and a decrease of the isolated yield from 90 % to just 30 % (after column chromatography) were observed. It was hypothesized that the formation of side products is caused by moisture. When potassium carbonate reacts with water it forms hydroxide ions. These might be able to deprotonate the α-carbon of the amino acid, followed by an elimination of the disulfide. The resulting amino acrylate **A** could be identified by HSQC NMR to be the major side products of the reaction and was isolated with a

yield of 23%. The two different terminal double bonds can be assigned in the ^{1}H NMR spectrum (Figure 13). A second fraction is presumable a mixture of the disubstituted cysteine derivatives **B** and **C**, with about 70% being the disulfide derivative **C** (Scheme 7). Hence, using dry reagents and keeping the reaction in dry conditions throughout the whole reaction time is crucial for a successful synthesis of **2a**.

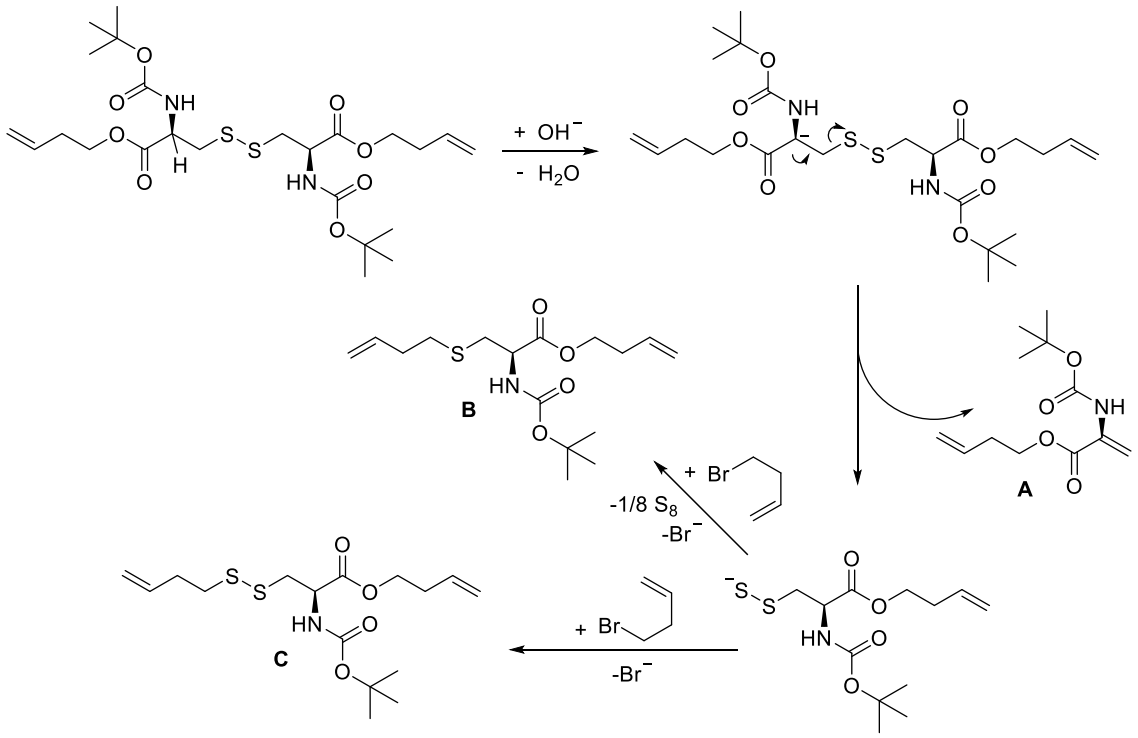

Scheme 7: Proposed mechanism for the formation of the side products **A**, **B** and **C**.

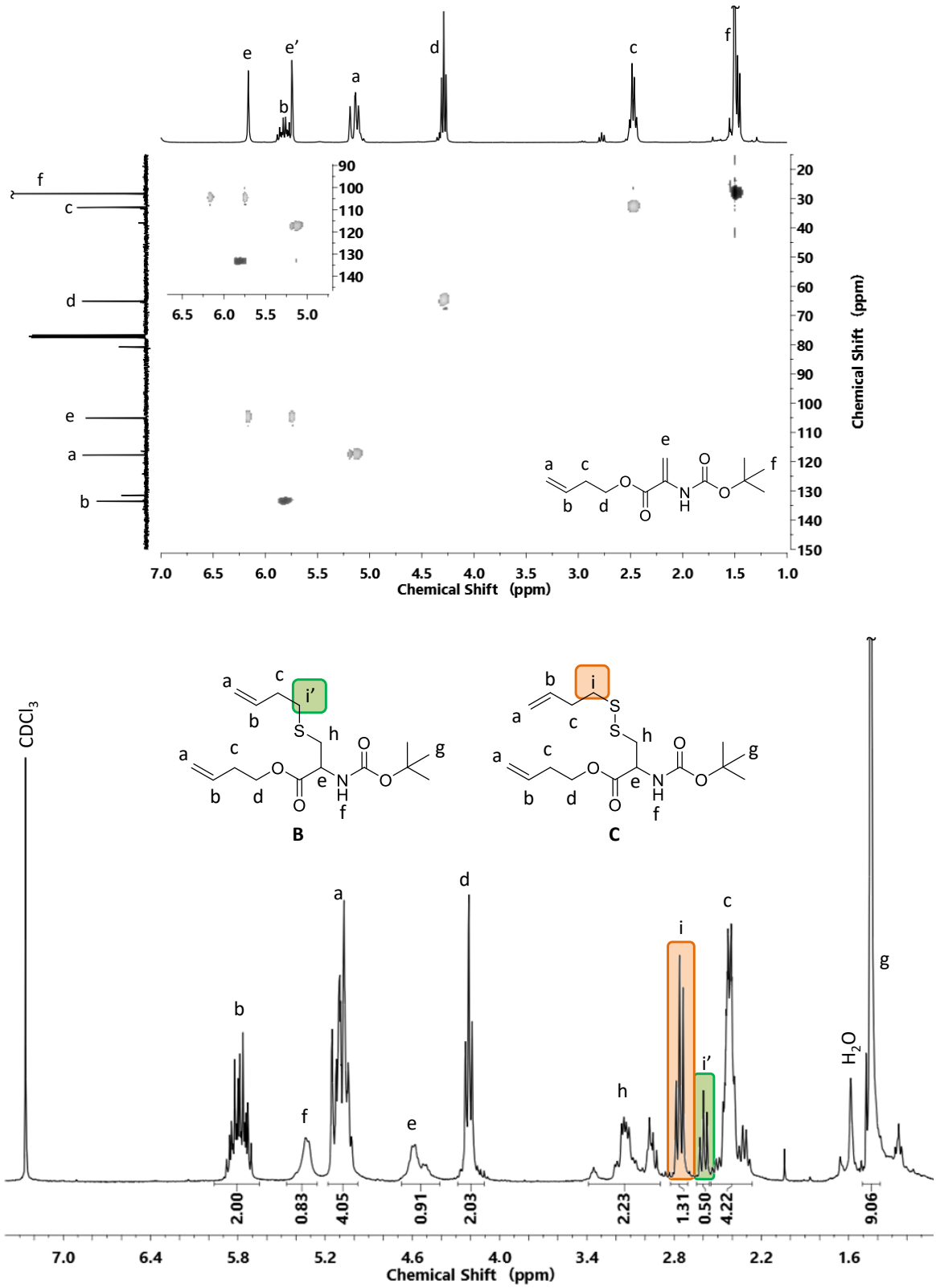

Figure 13: (Top) HSQC NMR (300 MHz, $CDCl_3$) of the side product **A**, with assigned CH_x-groups. (Bottom) ^1H NMR (300 MHz, $CDCl_3$) of the mixture of **B** and **C**.

6.2 ADMET Polymerization

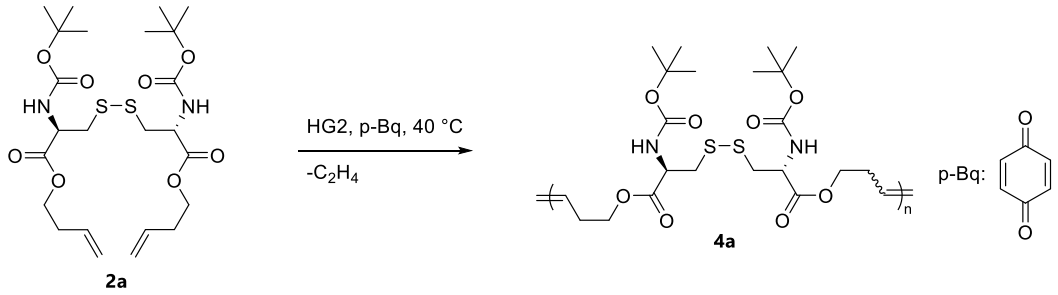

Scheme 8: ADMET polymerization of **2a**

The ADMET polymerization is a polycondensation reaction, which can be carried out under mild reaction conditions. Since synthetic procedures toward α,ω-unsaturated monomers are usually easily accessible, the ADMET polymerization is a useful tool for the polymerization of bio-derived functional monomers. A first experiment with **2a** in 0.2 M solution in dichloromethane (DCM) with the HG2 catalyst (catalyst loading: $[\mathbf{2a}]_0/[HG2]_0 = 100:5$) led to a full conversion of the vinyl double bonds (Figure 15). However, the SEC trace showed only oligomers and no evidence for a high molar mass fraction (Figure 14). The assumption was that the dilute conditions led to a high amount of intramolecular reactions (ring closing) and suppressed the intermolecular polymerization reaction. A second experiment was therefore done in a 1.2 M concentration. The higher boiling solvent chloroform was used instead of DCM. The use of DCM as solvent for ADMET polymerizations is critical because co-evaporation of DCM together with the released ethylene might take place, especially at high monomer concentrations. The evaporation of DCM leads to a further concentration of the polymerization mixture and sometimes to solidification. Hence, higher boiling solvents are recommended for these experiments. ^{1}H-NMR analysis of the second polymerization attempt revealed a conversion of terminal double bonds of only 60 % (Figure 15). In polycondensations high conversions are needed to obtain polymers. Consequently, only oligomers were detected in the SEC (Figure 14).

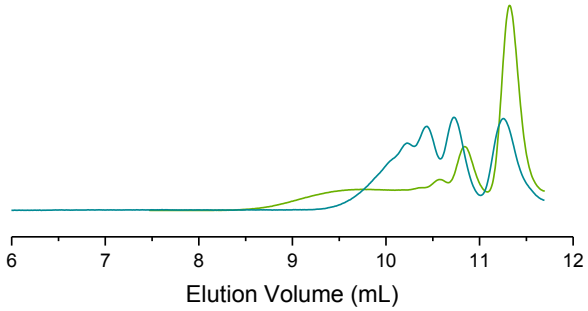

Figure 14: SEC-RI traces of ADMET attempts (areas under RI signals are normalized). (Green) 0.2 M DCM, 42 h, [**2a**]$_0$/[HG2]$_0$ = 100:5. (Blue) 1.2 M $CHCl_3$, 24 h, [**2a**]$_0$/[HG2]$_0$ = 100:5.

Further attempts to polymerize **2a** included bulk polymerization as well as the use of small amounts of high boiling solvents (o-xylene and DMF) but failed (Appendix I). Since pronounced ring closing of **2a** was observed during the first ADMET attempt, a RCM under dilute conditions should lead to a high yield of the corresponding macrocycle **3a** (see Chapter 6.3).

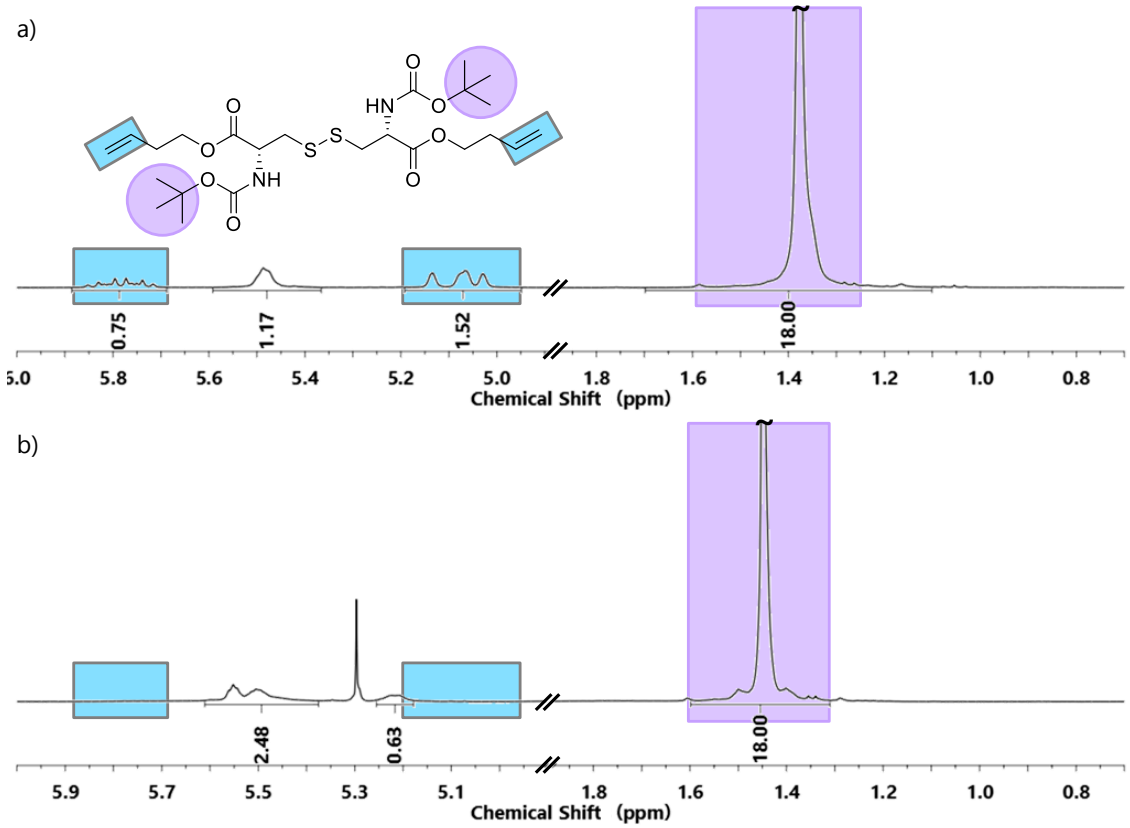

Figure 15: ^{1}H NMR spectra of the crude ADMET polymerization attempts. Terminal double bonds highlighted in blue. a) 1.2 M $CHCl_3$, 24 h, 40 °C, [**2a**]$_0$/[HG2]$_0$ = 100:5. b) 0.2 M DCM, 48 h, 40 °C, [**2a**]$_0$/[HG2]$_0$ = 100:5.

6.3 Ring Closing Metathesis

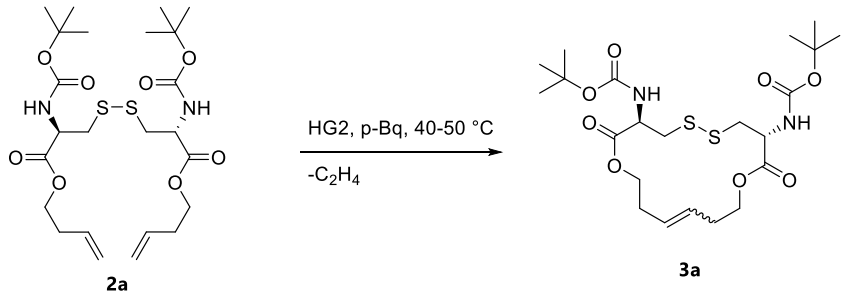

Scheme 9: RCM of **2a**.

Since the ADMET polymerization of **2a** failed, we envisioned to polymerize the corresponding macrocycles **3a** via ED-ROMP. In general, ED-ROMP has been shown to be a powerful alternative to ADMET polymerizations.[79–81] The synthesis of suitable macrocycles is often done by a ring closing metathesis (RCM). The olefin metathesis offers a toolbox of different reactions, such as the ADMET polymerization, ROMP, ring opening metathesis (ROM), cross metathesis (CM) and the RCM. The RCM, nowadays, is an important reaction to create heterocyclic rings in various kinds of sizes.[86,87] According to the Ziegler-Ruggli-dilution-principle an intramolecular reaction, such as a ring closing, is favored over intermolecular reactions in high dilution. Additionally, the closed cycles may be in equilibrium with open chains (*i.e.* ring chain equilibrium).[88] Therefore, the products have to be kept under dilute condition until the reaction is terminated. The synthesized α,ω-unsaturated monomer, was therefore converted, by a ring closing metathesis (RCM) into the corresponding macrocycle **3a**.

3a was synthesized by a RCM, carried out with 0.01 equivalence (equiv) HG2 catalyst. The cyclization reaction was done in a dilute solution of 0.01 M (according to **2a**) in DCM at 40°C. 0.02 equiv of *para*-benzoquinone (*p*-Bq), a hydride scavenger, was used as an additive to prevent olefin isomerization.[89,90] Olefin isomerization is a known side reaction when using *N*-heterocyclic carbene-based ruthenium catalysts, such as HG2. The side reaction is catalyzed by ruthenium

hydrides, which occur especially at longer reaction times and higher temperatures. Benzoquinone derivatives are usually used to suppress the isomerization.

The reaction was refluxed for 6 h and the conversion was monitored by TLC. The reaction was terminated with ethyl vinyl ether to deactivate the catalyst. Dimethyl sulfoxide (DMSO) was added to the terminated reaction mixture to improve the ruthenium removal by column chromatography.[91] The macrocycle **3a** could be isolated in 86% yield.

Instead of chlorinated solvents such as DCM, ethyl acetate was reported to be a good, greener alternative in olefin metathesis reactions.[92] RCM of **2a** in ethyl acetate at 50 °C resulted in a slightly lower but good yield of 74%. Olefin isomerization was not observed.

6.3.1 Monomer Characterization

3a was characterized by ESI-ToF MS analysis, elemental analysis and ^{1}H and ^{13}C NMR spectroscopy. The elemental composition was confirmed to be $C_{36}H_{65}N_2O_8S_2$ by MS and elemental analysis. The ^{1}H NMR spectrum of **3a** (Figure 16) shows two separated signals for the H-N of the carbamate (urethane). This is a known characteristic of carbamates. Like amides, carbamates exhibit a rotational barrier around the C-N-bond, even though it is less pronounced, with a strong preference towards the *anti*-conformer.[93,94] Furthermore, the double bond exhibits a cis/trans ration of 0.15-0.2, which is within the expected range for standard ruthenium-based metathesis catalysts.[95]

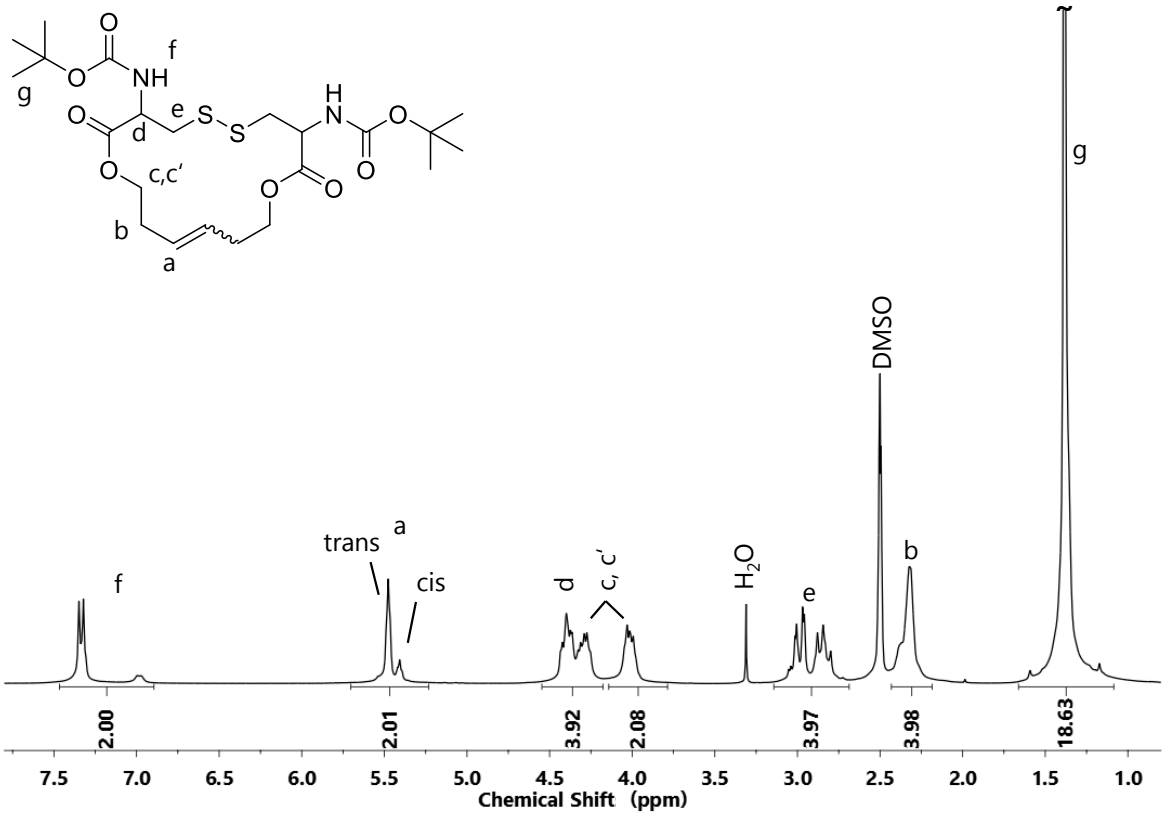

Figure 16: ^{1}H NMR (600 MHz, DMSO-d_6) spectrum of the macrocycle **3a**.

Interestingly, the methylene units adjacent to the ester groups (c, c') show a geminal coupling in the ^{1}H-NMR spectra. A geminal coupling usually occurs if the two hydrogen atoms on one methylene unit are chemically not identical. This leads to two different sets of signals in the ^{1}H-NMR spectrum. In the case of **3a**, one of the hydrogens of the methylene unit is in close proximity to the Boc-group, while the other hydrogen is on the opposite side of the ring. In the acyclic precursor **2a** rotation is less restricted and therefore the two hydrogen atoms are indistinguishable in the ^{1}H NMR spectrum.

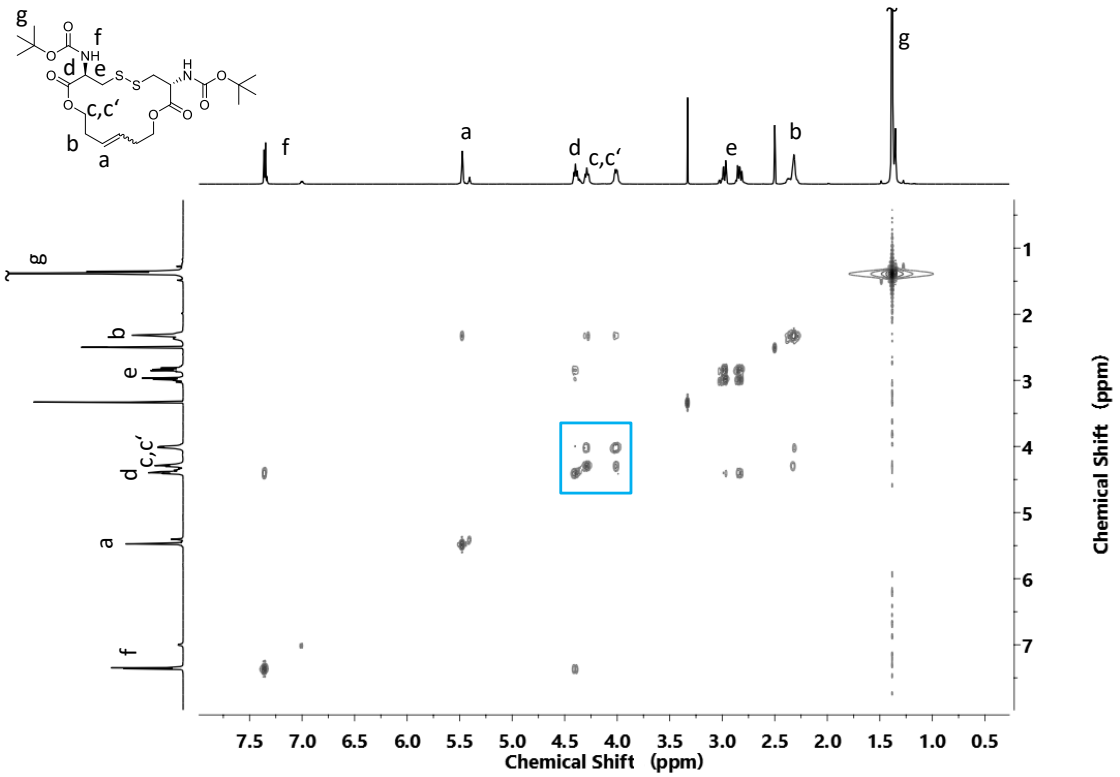

Figure 17: 2D [^{1}H,^{1}H] COSY NMR spectrum (600 MHz, DMSO-d_6) of **3a**; the box shows the region between 3.8 and 4.6 ppm showing the geminal coupling of -OCH_2- groups.

The geminal coupling can also be verified with 2D NMR experiments. Figure 17 shows the ^{1}H,^{1}H COSY NMR of **3a**. The boxed area can be assigned to the geminal coupling of the methylene unit next to the ester group.

6.4 Entropy-Driven Polymerization of Cystine-Based Alkene-Disulfide Macrocycles

6.4.1 Reaction Monitoring

The conversion of entropy driven polymerizations were monitored by two different means during this work.

Method 1: The first was to make use of the geminal coupling that is present in the macrocycle. Since the polymers are not cyclic, no geminal coupling is expected to be observed in the ^{1}H NMR spectra. Samples for ^{1}H NMR analysis of the crude polymerization mixtures were taken after the termination with ethyl vinyl ether. The molar mass (M_n^{app}) was determined by SEC after purification of the samples.

Method 2: The second method was to analyze the trace of the refractive index detector of the SEC (SEC-RI trace) of the crude polymerization mixtures after termination. With the assumption that the refractive index increment is the same for polymer and monomer, the monomer conversion can be determined by dividing the peak integral of the monomer signal by the overall integral.

Conversions measured with NMR and by SEC are in good agreement with each other. The same applies for the M_n^{app} of the high molar mass fraction of the crude polymerization mixtures and the polymer after precipitation. However, conversions determined by NMR and M_n^{app} determined by SEC on the crude polymers are on average ~5% higher (Appendix I).

6.4.2 Olefin Metathesis Polymerization (ED-ROMP)

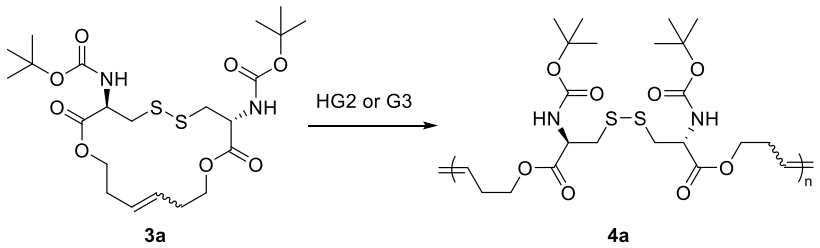

Scheme 10: ED-ROMP of the macrocycle **3a**.

The first attempt to polymerize **3a** by ED-ROMP was done with a catalyst loading of $[\mathbf{3a}]_0/[HG2]_0 = 100{:}1$ in 1 M solution of chloroform. The polymerization was quenched with ethyl vinyl ether after 6 h at 50 °C. After precipitation, a polymer was obtained with M_n^{app} = 38 kDa. With this first positive result, the next step was to investigate the kinetics of this polymerization in more detail. For entropy-driven polymerizations it is crucial to polymerize at high monomer concentrations.

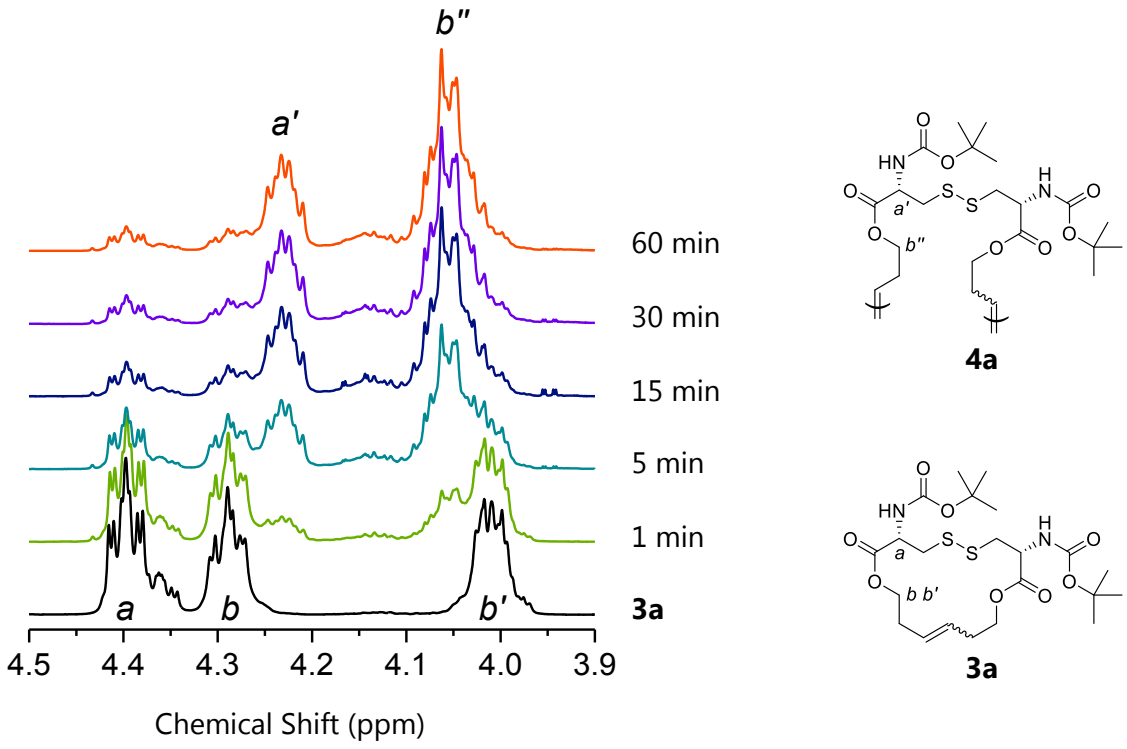

Figure 18: ^{1}H NMR (600 MHz) spectra (region from 4.5 to 3.9 ppm) of the crude polymerization mixtures measured in DMSO-d_6, following the disappearance of the geminal coupling of the monomer.

Therefore, 1.2 M concentration was chosen for further polymerizations, since it appears to be upper solubility limit of **3a** in chloroform. The catalyst HG2 is a slow initiating catalyst and therefore not recommended for kinetic studies. The G3 catalyst, on the other hand, shows comparable reactivity to HG2 while initiation is much faster.[96,97] The polymerization was monitored by ^{1}H NMR spectroscopy. The NMR spectra show the disappearance of the signals *b* and *b'* assigned to the -OCH_2- geminal coupling and the appearance of a new peak *b''* similar to the signal observed for **2a** (Figure 18). Integration of the peak areas led to the time conversion curve in Figure 19.

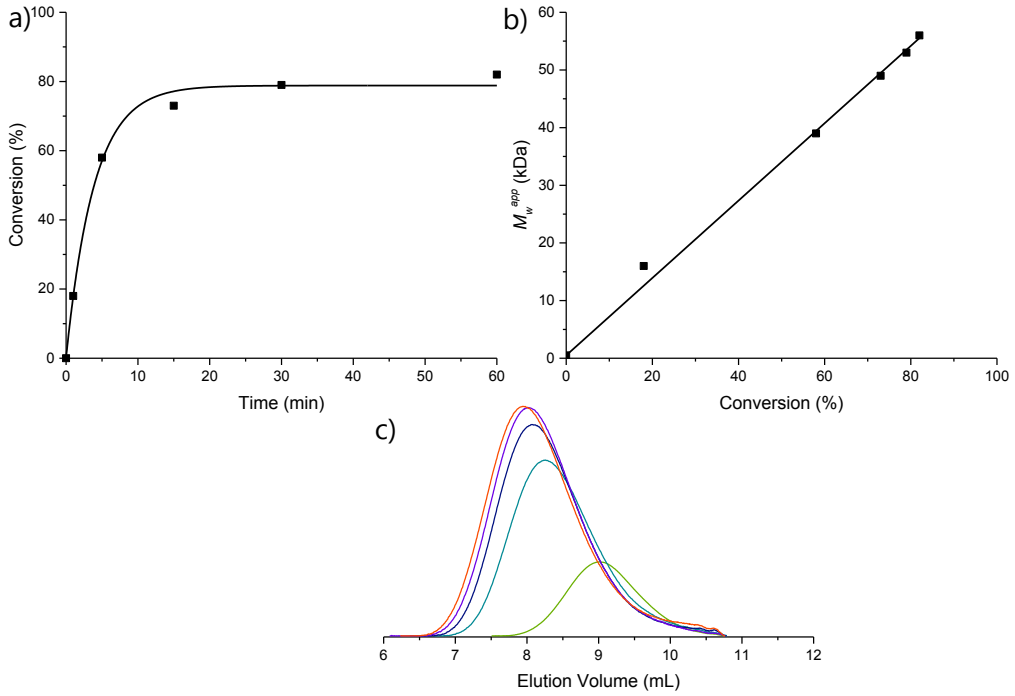

Figure 19: ED-ROMP of macrocycle **3a** (conversion and M_n^{app} determined by method 1) ([**3a**]$_0$/[G3]$_0$ = 100:1), 1.2 M in chloroform at 40 °C: a) Evolution of M_n^{app} of the polymer **4a** with conversion of monomer. b) Time-conversion plot, c) SEC-RI traces (eluent tetrahydrofuran (THF)) of the purified polymer, showing the evolution of molar mass during the ED-ROMP (areas under RI signals are normalized to monomer conversion). Polymer purification was done by dialysis.

The evolution of molar masses was monitored according to method 1. The polymer samples were purified by dialysis with a molecular weight cut off (MWCO) of 3.5 kDa. The molar mass of the polymer increased linearly with conversion, with a maximum conversion of 80% and M_n^{app} = 59 kDa. This conversion corresponds to the thermodynamic equilibrium at the given concentration of 1.2 M, as will be

shown later (Page 51). The maximum conversion is already achieved after 30 minutes, which is by far faster than it would be expected for ADMET polymerizations. An asymptotic behavior could be observed in the time-conversion plot, when the reaction reached equilibrium. In the ED-ROMP the maximum conversion should be virtually independent from the reaction temperature, while the equilibration should be faster when the temperature is increased. To validate this, another set of experiments were conducted at 60 °C and 30 °C under otherwise identical conditions. The polymerization kinetics were monitored according to method 2. As expected, the polymerization at 60 °C led to a faster equilibration, within 15 min, compared to the polymerization at lower temperatures (Figure 20), while the maximum conversion or equilibrium monomer concentration was the same.

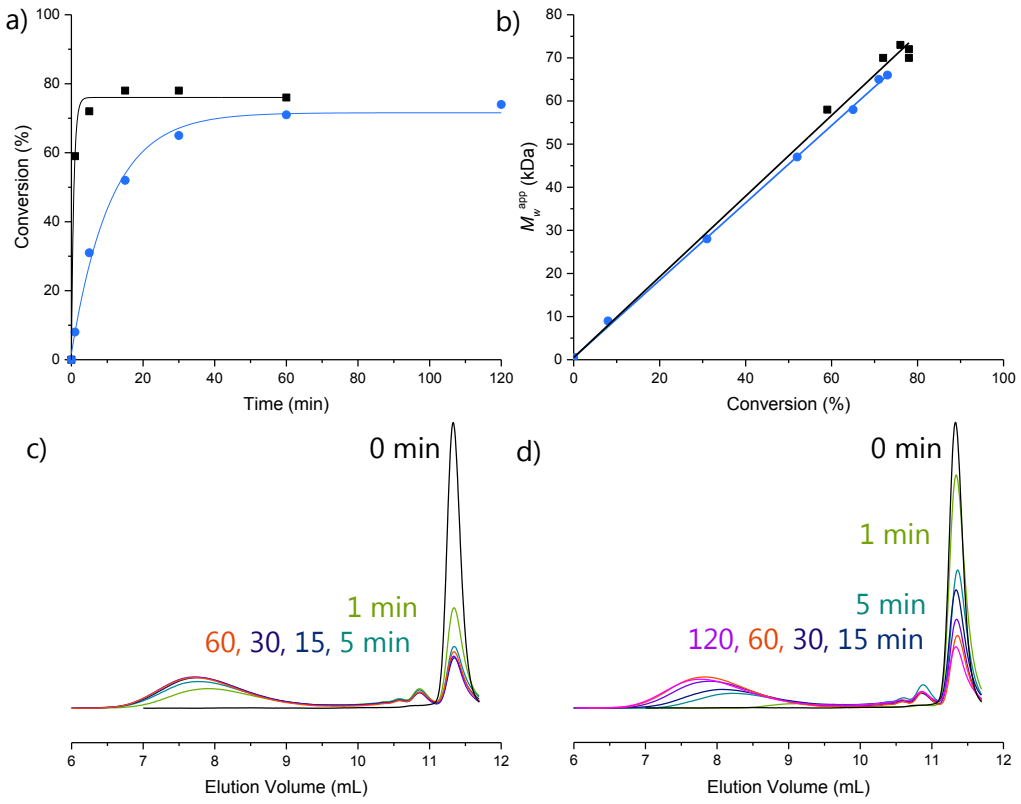

Figure 20: ED-ROMP of macrocycle **3a** at different temperatures (conversion and M_n^{app} determined by method 2); (a) time-conversion plots of the polymerizations at 30 °C (blue) and 60 °C (black), (b) evolution of apparent weight-average molar mass M_w^{app} of polymer **4a** with monomer conversion at 30 °C (blue) and 60 °C (black), and SEC-RI traces (eluent: THF) of the crude polymer **4a** obtained at different reaction times (areas under RI signals are normalized) at (c) 60 °C and at (d) 30 °C.

Furthermore, the thermodynamic equilibrium of the reaction was investigated by lowering the concentration of the polymerization. This should shift the equilibrium further to the lower molar mass ring fraction of the polymerization, leading to lower monomer conversion at the thermodynamic equilibrium. As expected the maximum conversion of **3a** decreased to 48% and 24% when using 0.6 M and 0.3 M concentrations, respectively (Figure 21). Additionally, the required time to reach the thermodynamic equilibrium is very similar, for all three polymerizations.

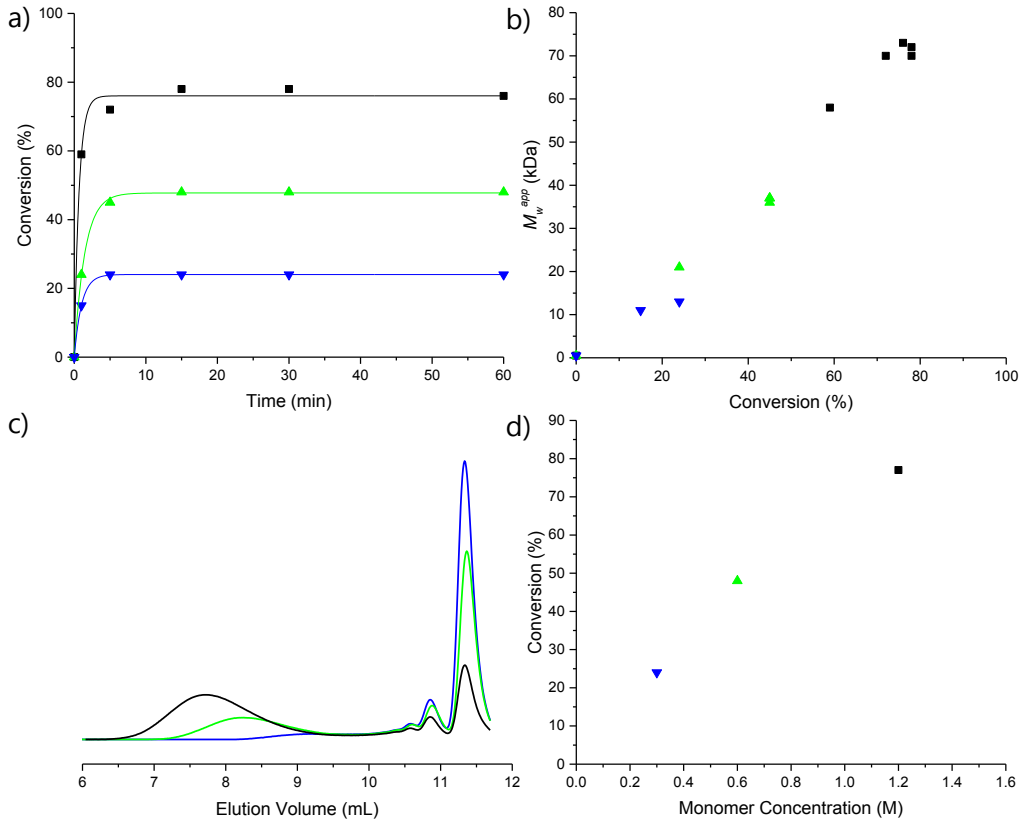

Figure 21: ED-ROMP of macrocycle **3a** at different concentrations with 1.2 M (black), 0.6 M (green) and 0.3 M (blue) monomer concentration in $CHCl_3$; (a) time-conversion plots of the polymerizations (conversion determined by method 2), (b) evolution of apparent weight-average molar mass M_w^{app} of polymer **4a** with monomer conversion, (c) SEC-RI traces of the crude polymerization mixtures (areas under RI signals are normalized), (d) Maximum conversion plotted against initial monomer concentration.

The end groups of polymers prepared by ED-ROMP are introduced by the catalyst (α-end) and the terminating agent (ω-end) ethyl vinyl ether. Because the catalyst acts as an initiator lower catalyst loadings should lead to fewer but longer

polymer chains. In an attempt to achieve control over the molar mass, three polymerizations with different catalyst loadings at 1.2 M in $CHCl_3$ at 30 °C, were performed (Figure 22).

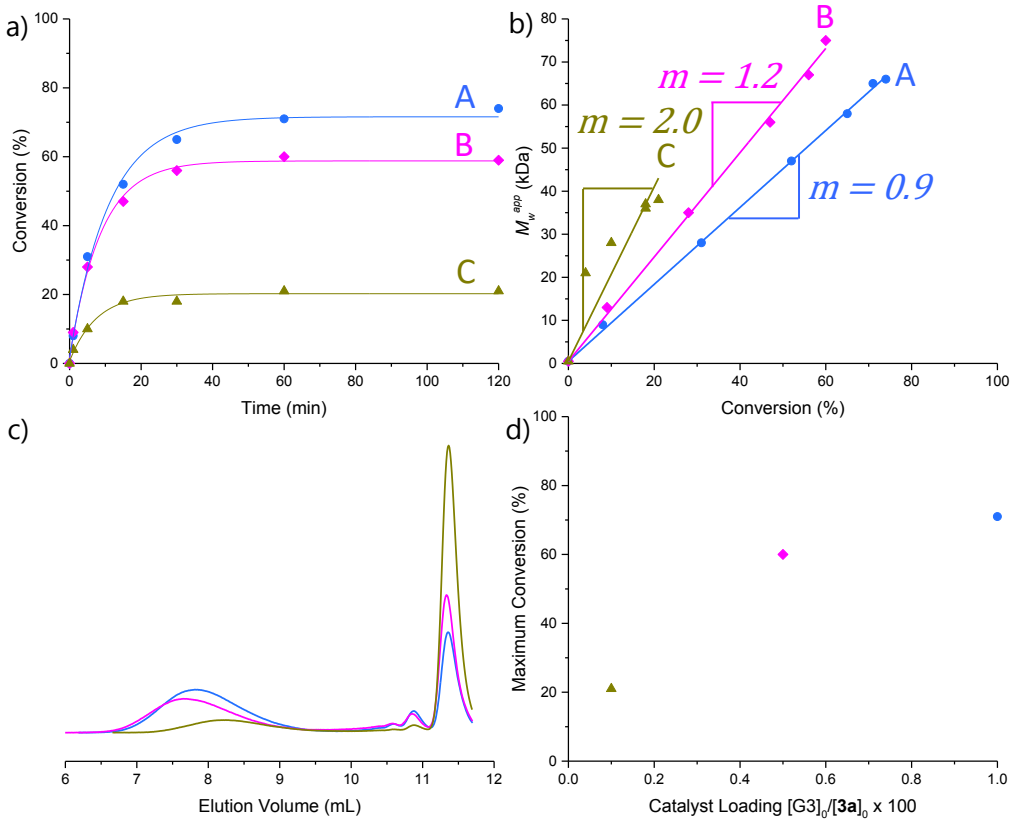

Figure 22: ED-ROMP of macrocycle **3a** with different catalyst loadings $[\mathbf{3a}]_0/[G3]_0$ (A, light blue; 100:1), (B, magenta; 100:0.5) and (C, gold; 100:0.1); (conversion and M_n^{app} determined by method 2); (a) time-conversion plots of the polymerizations, (b) evolution of apparent weight-average molar mass M_w^{app} of polymer **4a** with monomer conversion, (c) SEC-RI traces of the crude polymerization mixtures (areas under RI signals are normalized), (d) maximum conversion plotted as a function of catalyst loading.

The degree of polymerization *DP* of these polymerizations should follow

$$DP = \frac{[M]_o}{[I]_0} \cdot p \qquad (4)$$

where $[M]_0$ is the initial monomer concentration, $[I]_0$ is the initiator concentration and p is the monomer conversion. Form this it follows that

$$M_w \propto \frac{[M]_o}{[I]_0} \cdot p \qquad (5)$$

The observed slopes of the molar mass-conversion plots of the performed polymerizations are, as expected from equation 5, steeper for lower catalyst loadings (Figure 22, b). The slopes of the linear fits are 0.9, 1.2, and 2.0, for A, B and C respectively. Theoretically, the ratios of these slopes to each other should be 1:2:5, but actually are 1:1.3:2.2. Another unexpected observation, that deviates from the theory, is that lower catalyst loadings led to lower conversions of the monomers (*i.e.,* 74, 64 and 21%, for A, B and C, respectively) (Figure 22, c). In entropy-driven polymerizations, the conversion is dependent on the thermodynamic equilibrium between ring and chains and should not be affected by the catalyst loading. A reasonable explanation for the unexpected mass-conversion plots and the low conversions is a deactivation of the catalyst during the reaction. Emrick et. al. observed an NNGE during the polymerization of a disulfide based cyclooctene derivative.[98] They assigned this to a five membered chelate structure that formed during their polymerization, which in their case prevented a homopolymerization of the disulfide based monomer. However, in the monomer **3a** the distance between the double bond and the disulfide group is by four bonds longer. The smallest chelate ring structure that can be formed between the ruthenium and the disulfide is therefore a nine membered ring, which should be less stable (Figure 23). The hypothesis of a deactivation during the olefin metathesis can be tested by a dilution experiment.[99] For this, **3a** was polymerized under the same condition as entry 3 (Table 2). After 1 h a sample was taken and the remaining polymerization mixture was diluted with chloroform and further reacted for 1 h. If the chain-ends of the polymer where still active, the polymer should depolymerize upon dilution. But instead, the SEC traces of the polymer before and after the dilution are identical (Figure 24). This further supports the assumption that a deactivation of the catalyst takes place during the reaction.

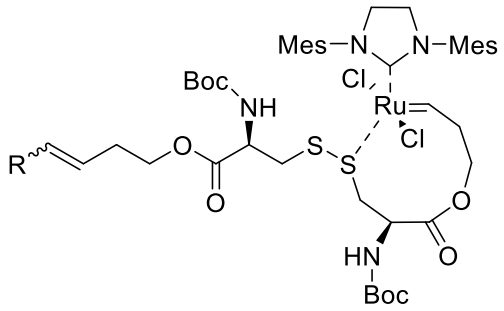

Figure 23: Proposed deactivation of the macrocycle **3a**.

Since ADMET polymerizations usually need long reaction times, the deactivation might also contribute to the low conversion of the ADMET polymerization in high concentrations, by a deactivation of the catalyst before high conversions can be obtained.

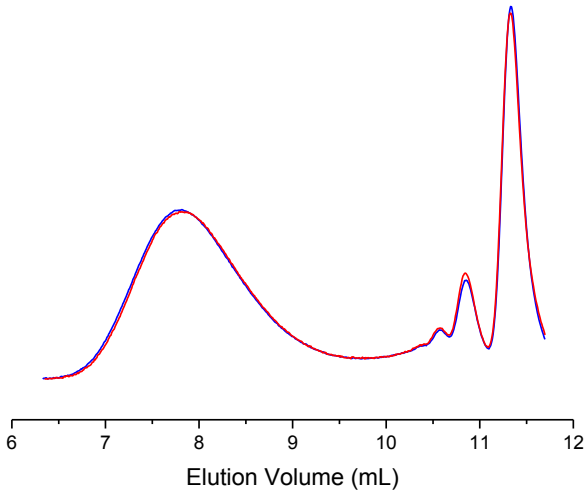

Figure 24: Crude polymerization mixtures of **3a**; (blue) before dilution, (red) after dilution.

As mentioned earlier, ethyl acetate is considered a green replacement for chlorinated solvents in olefin metathesis reactions. Therefore, a polymerization of **3a** in ethyl acetate was attempted. Due to the lower solubility of **3a** in this solvent, the polymerization was conducted at a concentration of 0.7 M ($[\mathbf{3a}]_0/[G3]_0$= 100:1, 40°C, 30 min). As expected, the low concentration leads to a conversion of only 60 % and an M_n^{app} of 38 kDa.

Table 2: Results of the ED-ROMP of the macrocycles **3a**.

Entry	Conc. in $CHCl_3$ [M]	$[\mathbf{3a}]_0/[G3]_0$	Temp [°C]	Conv. [%]	Equilibration Time [min]	M_n^{app} [kDa]	$Đ$
1	1.0	100:1[a]	50	n.d.	n.d.	36[b]	1.8[b]
2	1.2	100:1	40	80[b]	30	59[b]	1.9[b]
3	1.2	100:1	60	78[c]	15	73[c]	1.8[c]
4	1.2	100:1	30	74[c]	120	66[c]	1.8[c]
5	0.6	100:1	60	48[c]	15	37[c]	1.7[c]
6	0.3	100:1	60	24[c]	5	13[c]	1.3[c]
7	1.2	100:0.5	30	64[c]	30[d]	75[c]	1.8[c]
8	1.2	100:0.1	30	21[c]	15[d]	38[c]	1.6[c]
9	0.7[e]	100:1	40	60[b]	n.d.	42[b]	2.3[b]

(a) HG2 was used instead of G3, (b) analysis was done according to method 1, (c) analysis was done according to method 2, (d) the value corresponds to the maximum conversion, (e) polymerization in ethyl acetate, not determined (n.d.).

6.4.3 Disulfide Metathesis Polymerization (ED-RODiMP)

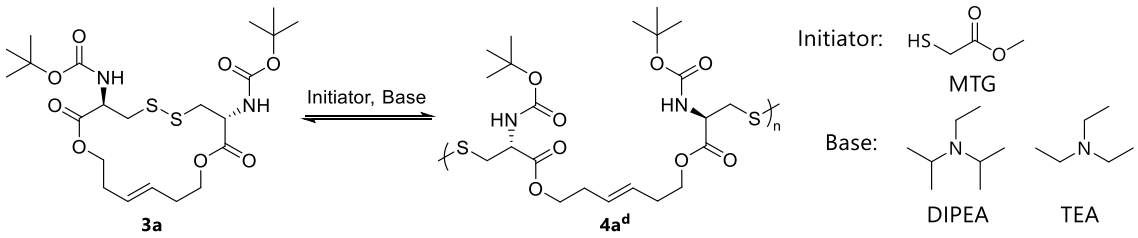

Scheme 11: ED-RODiMP of the macrocycle **3a** and the used initiator and bases.

The olefin metathesis was successfully used to polymerize the endo-cyclic disulfide macrocycle **3a**. Unfortunately, the olefin metathesis has several draw backs. First of all, it is restricted to rather unpolar solvents, limiting the choice of monomers to either low melting or unpolar molecules for bulk and solution polymerizations, respectively. Additionally, disulfides seem to have a negative effect on the ruthenium catalysts, resulting in poisoning of the catalysts after a certain reaction time. Furthermore, due to the toxicity of ruthenium, the levels in medicinal products have to be low. Several protocols for the removal of ruthenium catalysts exist, but none of them are universally applicable.[100] This makes the removal especially from polymers a very challenging and sometimes a not viable task. The disulfide metathesis on the other hand does not require any toxic transition-metal based catalyst and the most recommended solvents are polar aprotic solvents, which expands the scope of polymerizable monomers.

Since the monomer **3a** contains two ester groups and the propagating species of the disulfide polymerization is a thiolate nucleophile, a test experiment was conducted to rule out the possibility of a nucleophilic attack of the thiolate to the ester. Butyl acetate was heated to 85 °C for 1 h with 0.1 equiv diisopropylethylamine (DIPEA) and 0.1 equiv methyl thioglycolate (MTG).

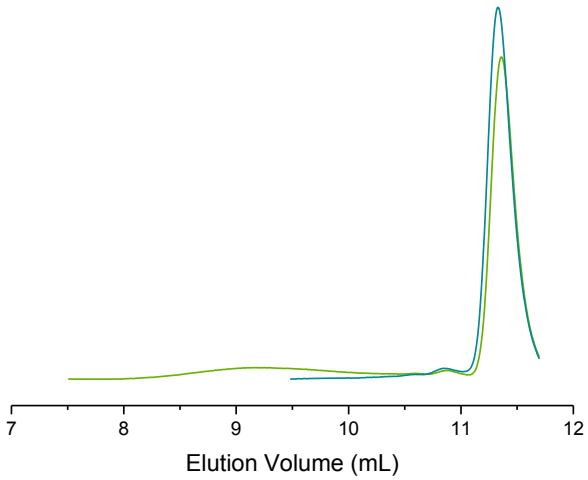

Figure 25: SEC-RI traces of the ED-RODiMP of **3a** in 1.2 M solution in $CHCl_3$ at (olive) 30 °C, and (green) 60 °C (areas under RI signals are normalized).

No sign of a nucleophilic attack of was observed in the ^1H NMR spectrum (Appendix I). A first polymerization of **3a** was conducted at 30 °C with (triethyl)amine (TEA) as the base in $CHCl_3$ (1.2 M, $[\mathbf{3a}]_0/[MTG]_0/[TEA]_0$= 100:1:1). Samples were quenched with acetic acid and analyzed by method 2. No polymerization took place after 2 h. A second polymerization was therefore carried out at 60 °C under otherwise identical conditions. After 2 h a high molar mass fraction was detected in the SEC elugram (Figure 25), but the conversion of the monomer as well as the molar mass of the obtained polymer were considerably lower as compared to the results of the olefin metathesis (M_w^{app} = 11 kDa, conv. = 21%).

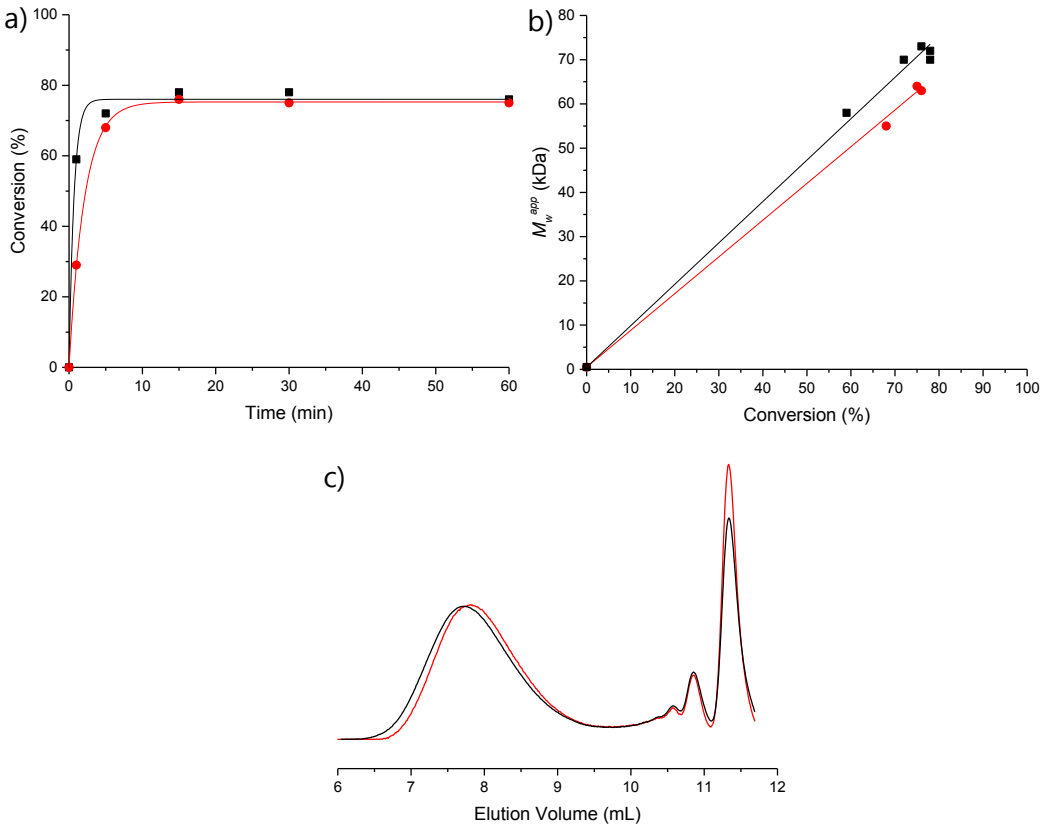

Figure 26: Comparison of the ED-ROMP (black) and ED-RODiMP (red) under similar reaction conditions, regarding temperature and initiator/catalyst loadings (conversion and M_w^{app} determined by method 2); (a) time-conversion plots of the polymerizations, (b) evolution of apparent weight-average molar mass M_w^{app} with monomer conversion, (c) SEC-RI traces (eluent: THF) of crude polymers **4a** and **4a^d** obtained after 30 minutes (areas under RI signals are normalized).

Since the polymerization is dependent on the concentration of thiolates as active chain ends, polar solvents should improve the polymerization. Another experiment was therefore conducted in dimethylacetamide (DMAc) a particularly good solvent for **3a** (1.2 M at 60°C, [**3a**]$_0$/[MTG]$_0$/[DIPEA]$_0$= 100:1:1). And indeed, the polymerization reached a maximum conversion of 74% within 15 min, with similar results compared to the ED-ROMP of **3a** (1.2 M at 60°C in $CHCl_3$, [**3a**]$_0$/[G3]$_0$= 100:1)(Figure 26).

Increasing the reaction temperature form 60 °C to 85 °C led to even faster polymerization and equilibration of the system (Figure 27) and reached maximum conversion after 5 min. DMAc offers the possibility to conduct the polymerization at even higher concentrations. A polymerization with a monomer concentration of 1.9 M ([**3a**]$_0$/[MTG]$_0$/[DIPEA]$_0$= 100:1:1, at 85 °C) led to an expected higher conversion of up to 85%.

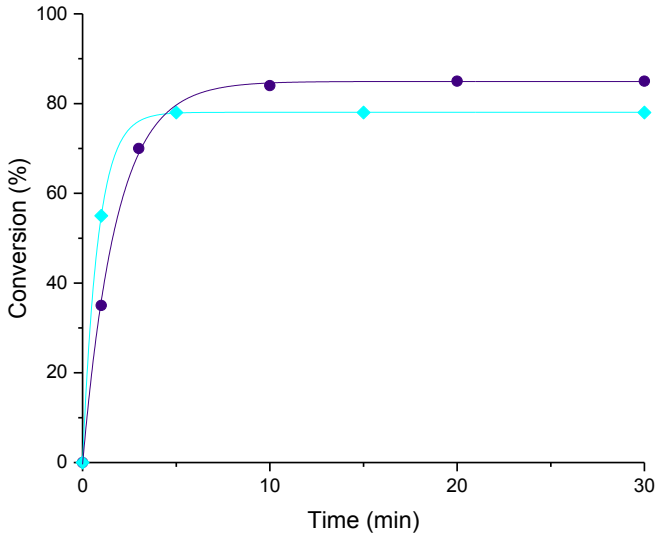

Figure 27: Time-conversion plots of the ED-RODiMP of macrocycle **3a** at different concentrations with 1.2 M (cyan), and 1.9 M (purple) monomer concentration in DMAc at 85 °C (conversion determined by method 2).

Other solvents were also tested as polymerization media. Polymerization of **3a** in DMSO at 85 °C was even faster than that in DMAc with a full equilibration within less than 1 min. Maximum conversion was, within the experimental error, virtually the same in both solvents (Table 3). γ-Valerolactone (GVL) is considered a greener replacement to common aprotic polar solvents, such DMSO or DMF.[101] The polymerization in GVL showed similar reaction kinetics to the one in DMAc (Figure 28).

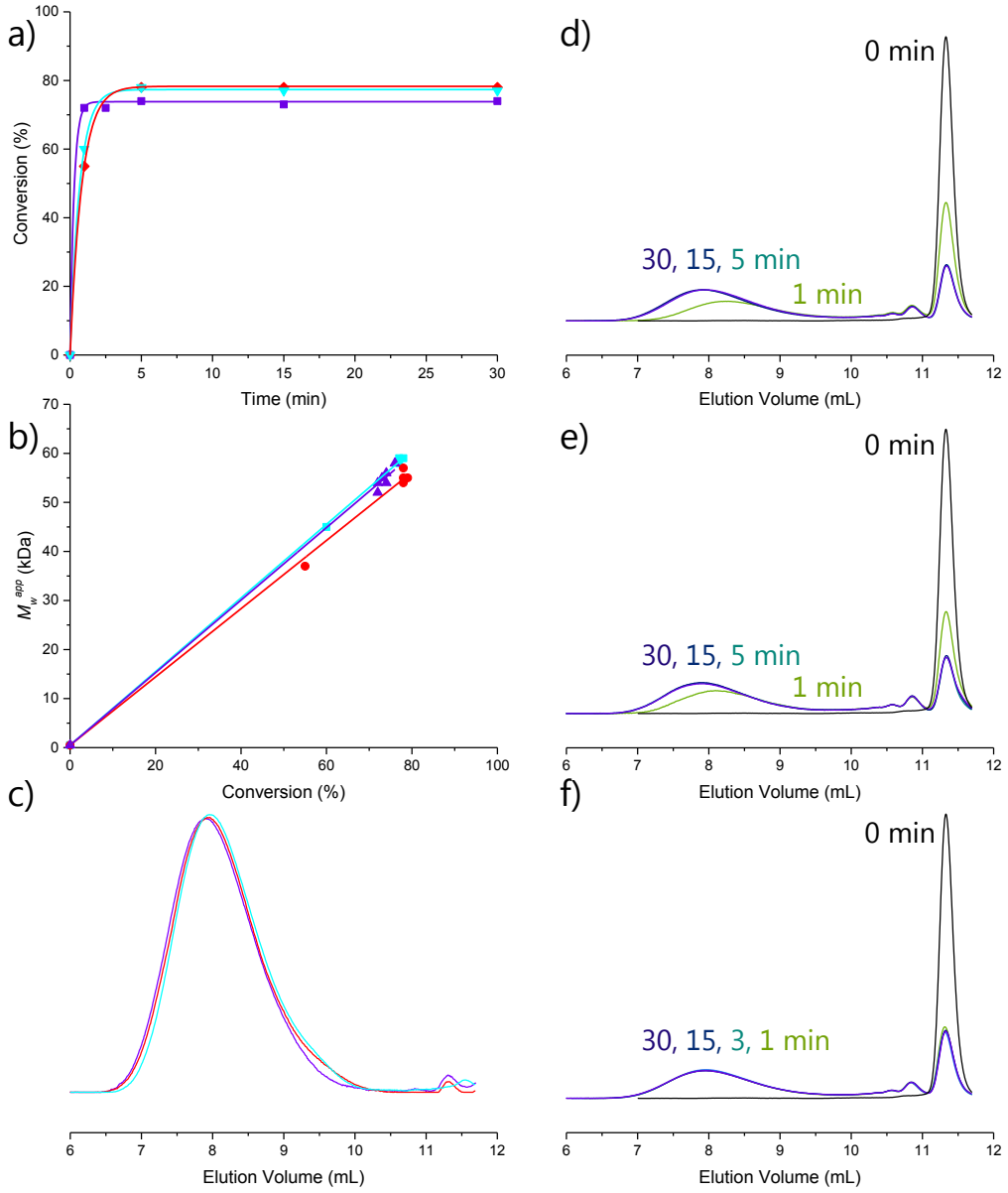

Figure 28: ED-RODiMP of macrocycle **3a** in varying solvents (conversion and M_w^{app} determined by method 2); a) Time-conversion plots of polymerizations in DMAc (red), GVL (cyan), and DMSO (purple), b) Evolution of M_w^{app} of the polymers **4a**$^{\mathbf{d}}$ with monomer conversion, c) SEC-RI traces (eluent THF) of the purified polymers; purification by precipitation in cyclohexane, and SEC-RI traces (eluent: THF) of crude polymer **4a**$^{\mathbf{d}}$ obtained at different reaction times of the polymerizations in d) DMAc, e) GVL, and f) DMSO (areas under RI signals are normalized).

Since no metal-centered catalysts are required for the ED-RODiMP, no termination during the reaction should occur and the thiolate chain-ends should stay active even after an extended reaction time. Dilution of a polymerization reaction after 1 h (1.2 M in DMAc at 85°C, [**3a**]$_0$/[MTG]$_0$/[DIPEA]$_0$= 100:1:1) led to a shift of the equilibrium towards the ring fraction, equivalent to a depolymerization of the

polymer (Figure 29, a). This shows, that in contrast to the olefin metathesis polymerization, the chain ends remain active during the polymerization. This should also enable a certain control over the obtained molar masses by varying the monomer-to-initiator ratio. Lowering the monomer/initiator ratio (1.2 M in DMSO at 85 °C, 10 min, [**3a**]$_0$/[MTG]$_0$/[DIPEA]$_0$ = 100:2:2) led to a polymer with decreased molar mass of M_n^{app} = 35 kDa (Figure 29, b). By increasing the monomer-initiator ratio drastically ([**3a**]$_0$/[MTG]$_0$/[DIPEA]$_0$ = 100:0.05:0.05) a very high molar mass polymer (M_n^{app} = 177 kDa) could be obtained. The theoretical molar mass (*i.e.*, M_n^{theo} = 1.6 MDa) would be even higher, but even small amounts of impurities in the polymerization mixture, such as remaining precursor **2a**, can serve as additional chain ends. Nevertheless, the polymerization proceeded to the equilibrium of 82% conversion after 24 h. The slightly higher conversion might be an effect caused by evaporation of the solvent. The ED-RODiMP at a monomer concentration of 1.2 M generally leads to conversions 73-82%. Since no deactivation of the polymerization takes place it can be concluded that this value indeed corresponds to the thermodynamical equilibrium. The obtained value is similar to the value obtained by ED-ROMP. Therefore, it can be concluded that ED-ROMP of **3a** using a catalyst loading of [**3a**]$_0$/[G3]$_0$= 100:1 is sufficient to reach a full equilibration, before the catalyst deactivation.

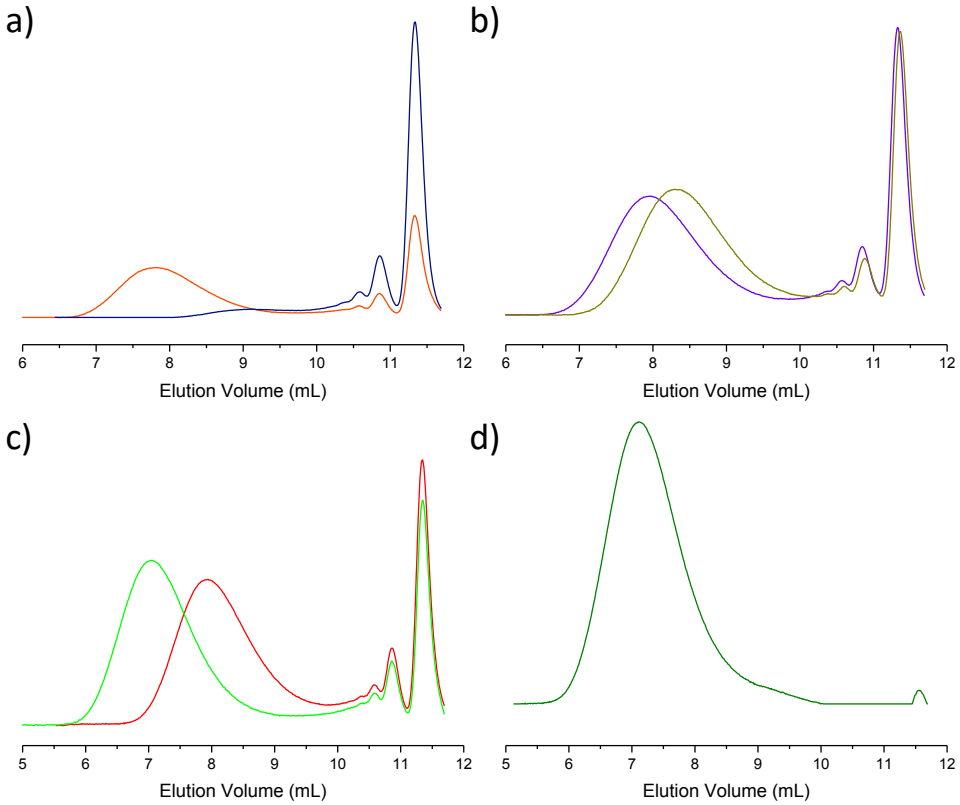

Figure 29: ED-RODiMP of macrocycle **3a**; a) SEC-RI traces of the crude polymerization with 1.2 M solution of **3a** at 60 °C, $[\mathbf{3a}]_0/[MTG]_0/[DIPEA]_0$= 100:1:1, before (orange) and after dilution (blue), b) SEC-RI traces of the crude polymerization with 1.2 M solution of **3a** in DMSO at 85 °C, with $[\mathbf{3a}]_0/[MTG]_0/[DIPEA]_0$= 100:1:1 (purple), and $[\mathbf{3a}]_0/[MTG]_0/[DIPEA]_0$= 100:2:2 (gold), c) SEC-RI traces of the crude polymerization with 1.2 M solution of **3a** in DMAc at 85 °C, with $[\mathbf{3a}]_0/[MTG]_0/[DIPEA]_0$= 100:1:1 (red), and $[\mathbf{3a}]_0/[MTG]_0/[DIPEA]_0$= 100:0.05:0.05 (olive), d) SEC-RI traces of the purified polymer (1.2 M solution of **3a** at 85 °C, with $[\mathbf{3a}]_0/[MTG]_0/[DIPEA]_0$ = 100:0.05:0.05; (areas under RI signals are normalized).

Table 3: Results of the ED-RODiMP of the macrocycles **3a**.

Entry	Conc. [M]	[**3a**]$_0$/ [MTG]$_0$/ [DIPEA]$_0$	Temp [°C]	Conv. [%]	Equilibration Time [min]	M_n^{app} [kDa]	$Đ$
1	1.2 M $CHCl_3$	100:1:1	30	-	-	-	-
2	1.2 M $CHCl_3$	100:1:1	60	21	-	11	1.6
3	1.2 M DMAc	100:1:1	60	75	15	63	1.7
4	1.2 M DMAc	100:1:1	85	78	5	55	1.8
5	1.9 M DMAc	100:1:1	85	85	10	81	1.8
6	1.2 M DMSO	100:1:1	85	73	1	56	1.8
7	1.2 M GVL	100:1:1	85	77	5	59	1.7
8	1.2 M DMSO	100:2:2	85	74	n.d.	35	1.8
9	1.2 M DMAc	100:0.05:0.05	85	82	n.d.	177	1.9

All entries are analyzed according to method 2.

6.4.4 Polymerization by Homolytic Cleavage of the Disulfide Bond

The disulfide metathesis can also be conducted via a radical pathway. It has been shown that homolytic cleavage and subsequent disulfide metathesis can be induced by heat or ultra-sonication.[102] Heat-induced polymerization of disulfides seems only to occur above the melting point of the monomers.[62] Due to the high melting point of the macrocycle **3a** (*i.e.*, 176–178 °C), a heat-induced disulfide metathesis polymerization is not possible. Ultra-sonication was also ineffective as after 16 h of ultra-sonication of **3a** with an ultrasonic frequency of 35 Hz and an ultrasonic output of 80 W at 40 °C no reaction took place (Appendix I).

6.5 Expanding the Macrocyclic Toolbox

Synthesis and polymerization of the macrocycle **3a** was shown to be an excellent synthetic strategy towards high molar mass functional poly(disulfide)s. The following chapter is dedicated to the exploration of the synthetic pathway as well as the investigation of the impact of molecular structure to the polymerization kinetics and polymer properties. Besides **3a**, four additional L-cystine-based macrocycles were synthesized, each of them deriving from a different cystine derivative (Figure 30). Like **1a**, **1b** is an L-cystine derivative with a carbamate-based amine protecting group (*i.e.*, Carboxybenzyl (Cbz)). **1c** is the deaminized derivative of cystine, while **1d** is a dimethyl ester of L-cystine.

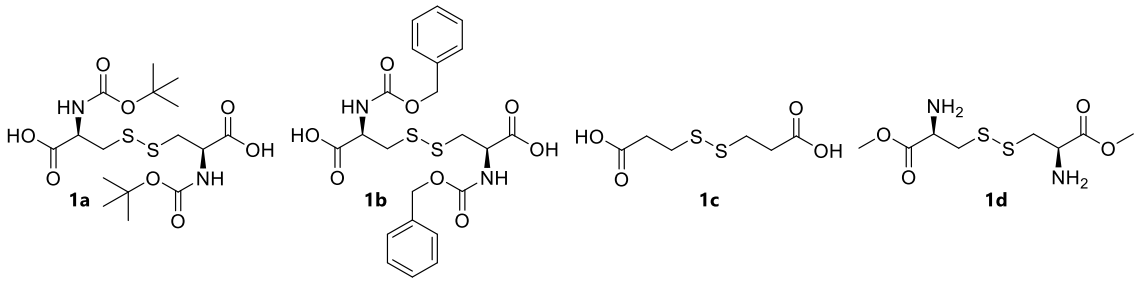

Figure 30: The four different cystine derivatives **1a**-**1d**.

6.5.1 Further Monomer Synthesis

6.5.1.1 Synthesis of α,ω-Dienes

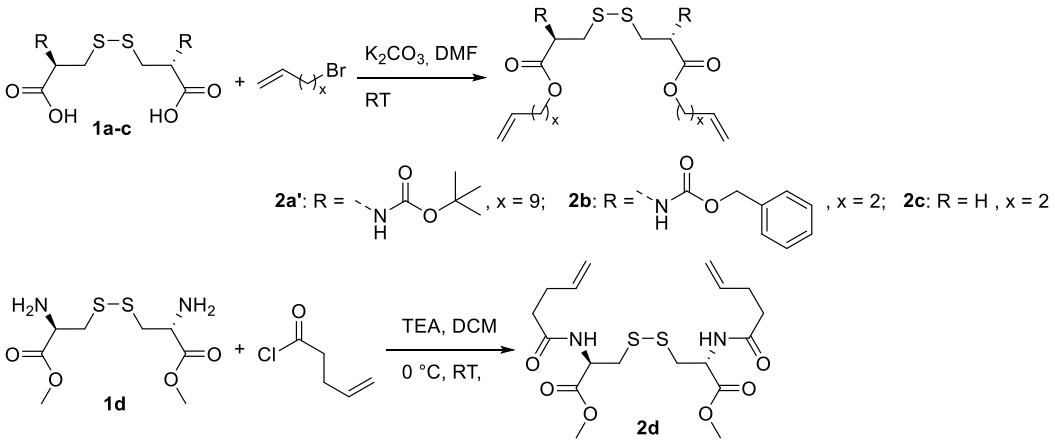

Scheme 12: Synthesis of α,ω-unsaturated cystine derivatives **2a'**-**2d**.

The cystine derivatives **1a**-**1c** are diacids that can be functionalized by an esterification reaction to form the α,ω-unsaturated molecules **2a**-**2c** (Scheme 12). The α,ω-unsaturated cystine derivatives **2a'** and **2b** were synthesized using the same synthetic procedure as for **2a** with yields of 50% and 60%, respectively (Table 4). The significantly lower yields for the products **2a'** and **2b** compared to **2a** are somewhat surprising due to the similarity of the reactions. The difference might be explained by the long alkyl chain that was used for the synthesis of **2a'**, which might reduce the reactivity. In addition, the likewise steric hindrance of the Cbz-group in the synthesis of **2b** might affect the yield.

2a' failed to crystallize under the conditions tested (*e.g.*, -20 °C in n-pentane). Instead, an organogel was obtained, which was stable at low temperatures, but redissolved when brought back to room temperature. Cystine derivatives are known to be highly effective gelators.[103] Presumably, long range ordering of the low molecular weight gelator **2a'** occured via hydrogen bonding of the Boc-protecting group. However, the organogel was not further analyzed.

The synthesis of **2c** was performed at an elevated temperature of 80 °C for 26 h. The isolated yield was 89%. Elevated temperatures were avoided in the former reactions to reduce the probability of side-reactions involving the R-group. Since the

deaminized derivative does not have an acidic CH-group occurrence of side reactions are less likely.

The cystine derivative **1d** is an acid-protected diamine (Scheme 12). The corresponding α,ω-unsaturated molecule **2d** was synthesized by an amidation reaction with an acid chloride. For this, pentenoyl chloride was slowly added to a solution of dimethyl cystinate and TEA in DCM. The pure product was obtained with a yield of 85% (Figure 31).

Table 4: Isolated yield of the synthesized α,ω-dienes.

Entry	Synthesized Diene	Isolated Yield
1	**2a'**	50%
2	**2b**	60%
3	**2c**	89%
4	**2d**	85%

Side products like those found in the synthesis of **2a** were not observed in any of the other syntheses.

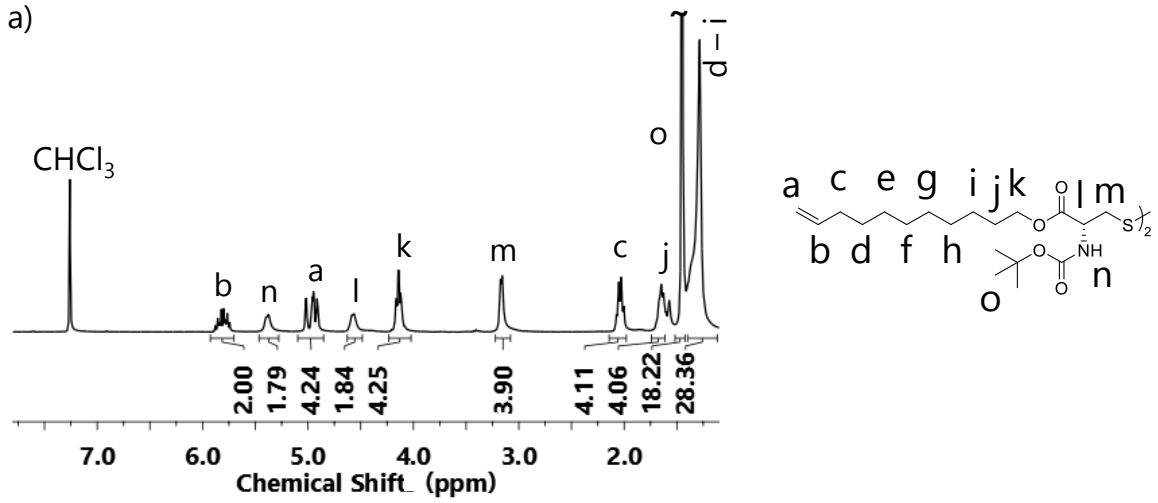

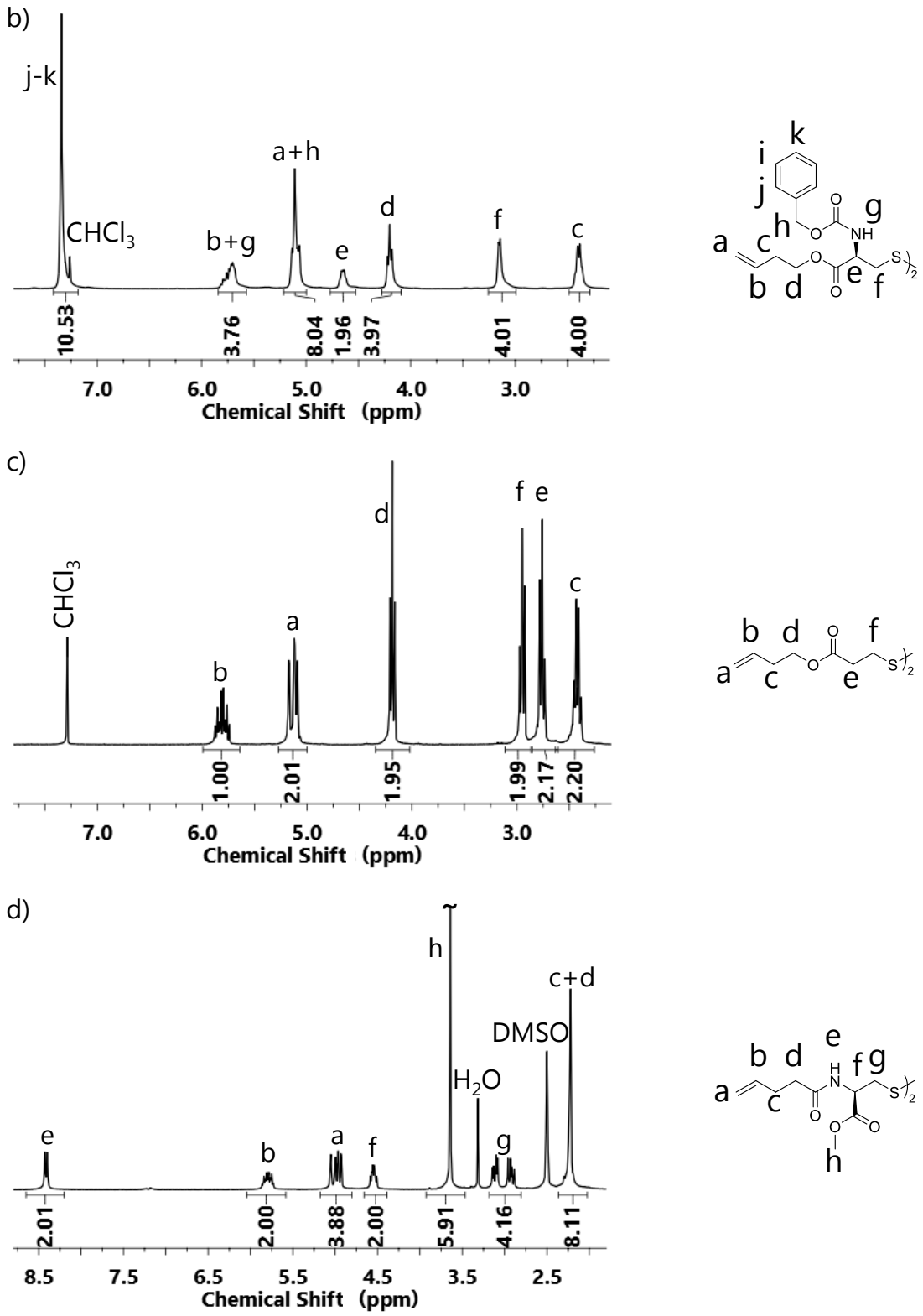

Figure 31: [1]H NMR (300 MHz) spectra of the α,ω-unsaturated cystine derivatives; a) **2a'** ($CDCl_3$), b) **2b** ($CDCl_3$), c) **2c** ($CDCl_3$), d) **2d** (DMSO-d_6).

6.5.1.2 Ring Closing Metathesis

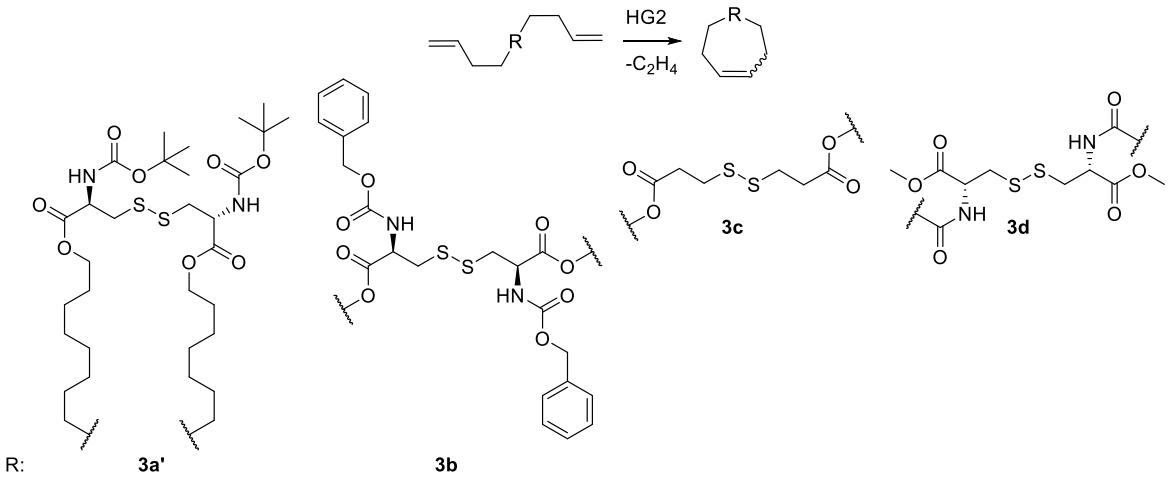

Scheme 13: Ring closing metathesis of the acyclic dienes **2a'**-**2d**.

The ring closing metathesis (RCM) of **2a'** was performed under the same conditions as for **2a**, however, the isolated yield was just 8%. To improve the yield, the amount of HG2 catalyst was increased from 0.01 equiv to 0.05 equiv relative to **2a'**. The resulting yield was substantially higher, *i.e.*, 31%. Since higher temperatures should promote the evaporation of ethylene, the use of higher boiling solvents at higher temperatures should further improve the yield of the ring closing reaction. Toluene is one of the standard solvents for olefin metathesis reactions. The use of toluene together with a higher reaction temperature of 110 °C led to an isolated yield of 81% after only 4 h.

Phenol is used as an additive in olefin metathesis reactions to improve reaction rate and the final yield of the reaction.[104,105] A set of test experiments were conducted to investigate the effect of phenol addition to the RCM of **2a'** using the HG2 catalyst. The addition of phenol had no effect on the conversion of double bonds after 22 h (Appendix I).

The RCM of **2b** was done under similar conditions as the RCM of **2a**. Thin-layer chromatography (TLC) analysis showed incomplete conversion even after 18 h of reflux in dry, degassed DCM. Another 0.01 equiv of HG2 was added and the reaction further refluxed for another 4 h. The isolated yield of **3b** was 77%.

Following a similar method as for the synthesis of **3a'**, the ring closing metathesis of **2c** was performed in refluxing toluene, with 0.02 equiv of HG2 and 0.02 equiv of *p*-Bq; the isolated yield of **3c** was 66%.

A first attempt to obtain the endocyclic amide **3d** by the same procedure as for **3a** (0.01 M in DCM, 0.01 equiv HG2, 0.02 equiv *p*-Bq) led to a yield of only 11%. By replacing DCM with toluene (110 °C, 4 h) and increasing the catalyst loading (0.02 equiv of HG and 0.04 equiv of *p*-Bq), the isolated yield reached 36%.

In general, the yields obtained for RCM in toluene at 110 °C were comparable or higher than yields obtained from reactions in DCM at 40 °C (Table 1). In addition, higher catalyst loadings led to higher yields. Double bond isomerization was not observed in any of the experiments. Additionally, the isolated yields of **3a** were significantly higher than for the other synthesized macrocycles. The reason for this is yet not understood.

Table 5: Reaction conditions and isolated yield of the cystine-based macrocycles.

Entry	Monomer	Solvent	Temperature [°C]	equiv HG2	equiv *p*-Bq	Isolated Yield
1	**3a**	DCM	40	0.01	0.02	86%
2	**3a**	Ethyl acetate	50	0.01	0.02	77%
3	**3a**	Toluene	110	0.01	0.02	87%
4	**3b**	DCM	40	0.02	0.02	73%
5	**3a'**	DCM	40	0.01	0.02	8%
6	**3a'**	$CHCl_3$	40	0.05	0.1	31%
7	**3a'**	Toluene	110	0.05	0.1	81%
8	**3c**	DCM	40	0.02	0.02	66%
9	**3d**	DCM	40	0.01	0.02	11%
10	**3d**	Toluene	110	0.02	0.04	31%

a)

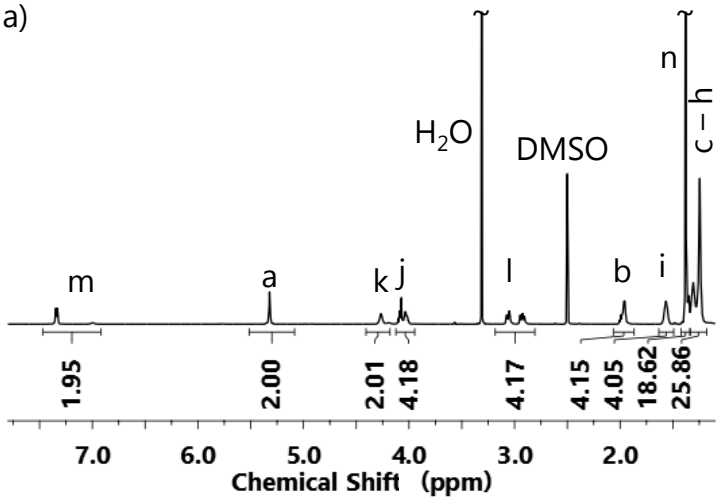
m
a
k
j
l
H2O
DMSO
b
i
n
c – h
1.95
2.00
2.01
4.18
4.17
4.15
4.05
18.62
25.86
7.0
6.0
5.0
4.0
3.0
2.0
Chemical Shift (ppm)

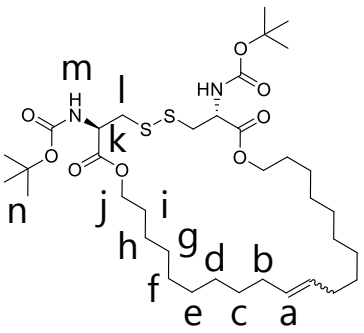
m
l
k
n
j
i
h
g
d
b
f
e
c
a

b)

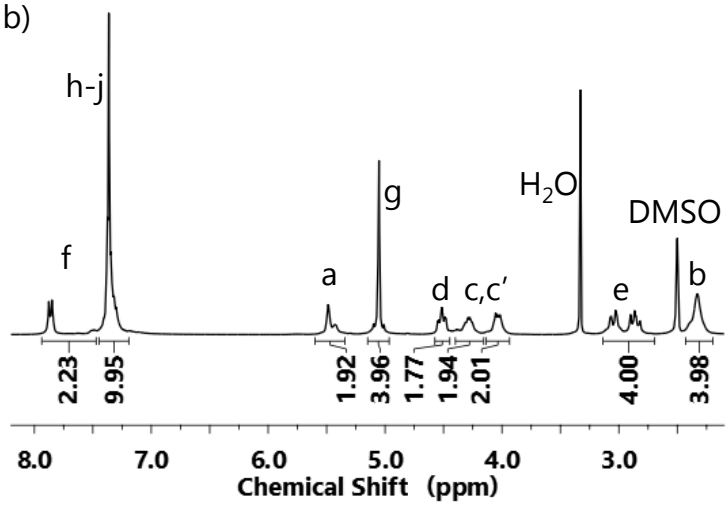
h-j
f
a
g
d
c,c′
H2O
e
DMSO
b
2.23
9.95
1.92
3.96
1.77
1.94
2.01
4.00
3.98
8.0
7.0
6.0
5.0
4.0
3.0
Chemical Shift (ppm)

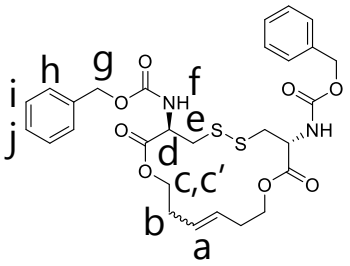
i
h
g
f
j
e
d
c,c′
b
a

c)

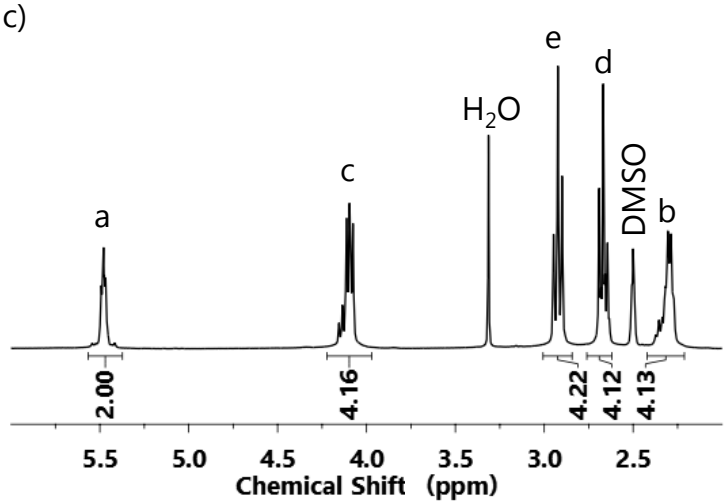
e
d
H2O
c
DMSO
a
b
2.00
4.16
4.22
4.12
4.13
5.5
5.0
4.5
4.0
3.5
3.0
2.5
Chemical Shift (ppm)

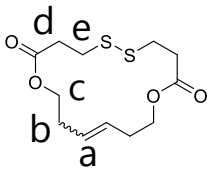
d
e
c
b
a

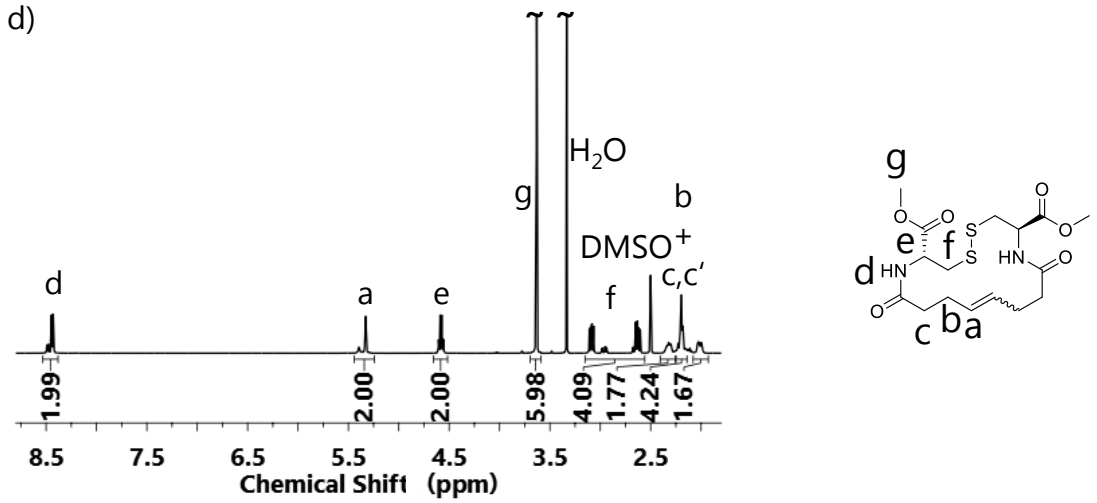

Figure 32: ^{1}H NMR spectra of the cystine-based macrocycles in DMSO-*d*$_6$; a) **3a'** (600 MHz), b) **3b** (300 MHz), c) **3c** (300 MHz), d) **3d** (500 MHz).

The ^{1}H NMR spectra of **3b** and **3d** show a geminal coupling at the methylene unit adjacent to the ester and amide group, respectively (Figure 33 and Appendix II). The reasons are the same as the ones discussed earlier for the macrocycle **3a**. However, no geminal coupling was observed in the NMR spectra of the **3a'** and **3c** derivatives. The macrocycle **3c** is an achiral compound, which explains the absence of a geminal coupling. The macrocycle **3a'**, on the other hand, is significantly larger than the other rings resulting in less conformational strain and thus no geminal coupling. All macrocycles exhibit an expected cis/trans ratio of 0.18-0.25.

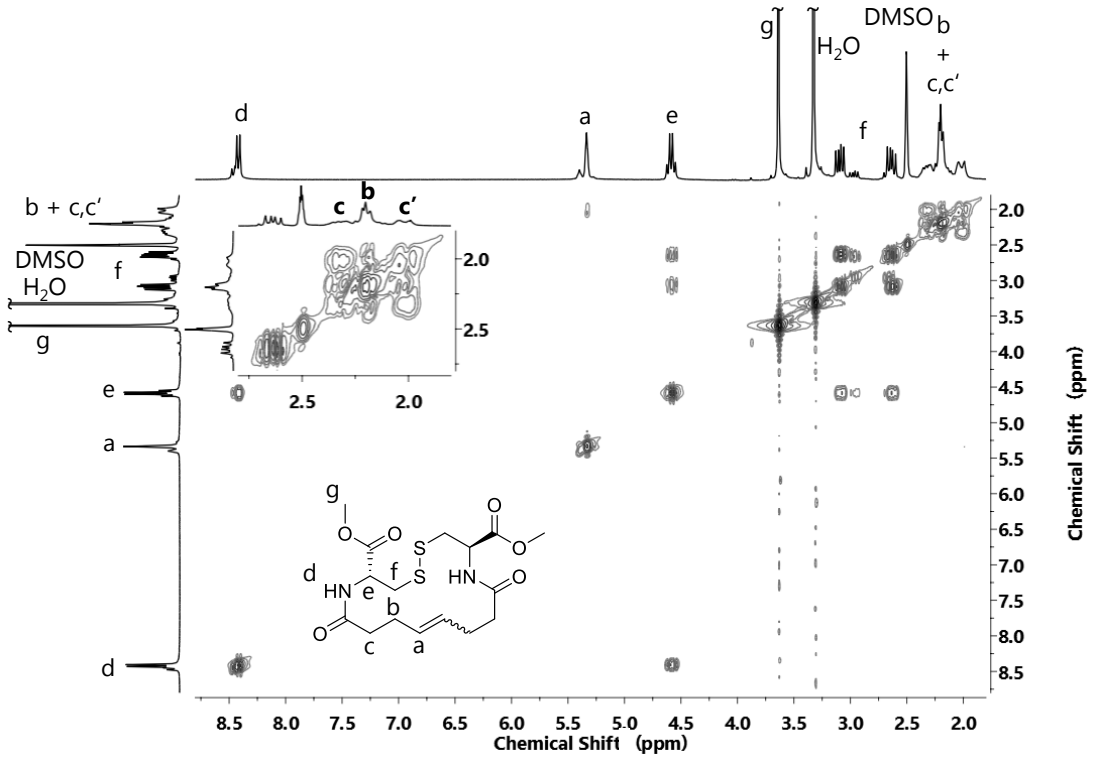

Figure 33: 2D [^{1}H,^{1}H] COSY NMR spectrum (300 MHz, DMSO-d_6) of **3d**. Magnified inset shows the region between 2.1 and 3.1 ppm, where the geminal coupling of -NCOCH$_2$- groups is observed.

6.5.2 Entropy-Driven Polymerizations

6.5.2.1 Polymerizations of Endocyclic Esters

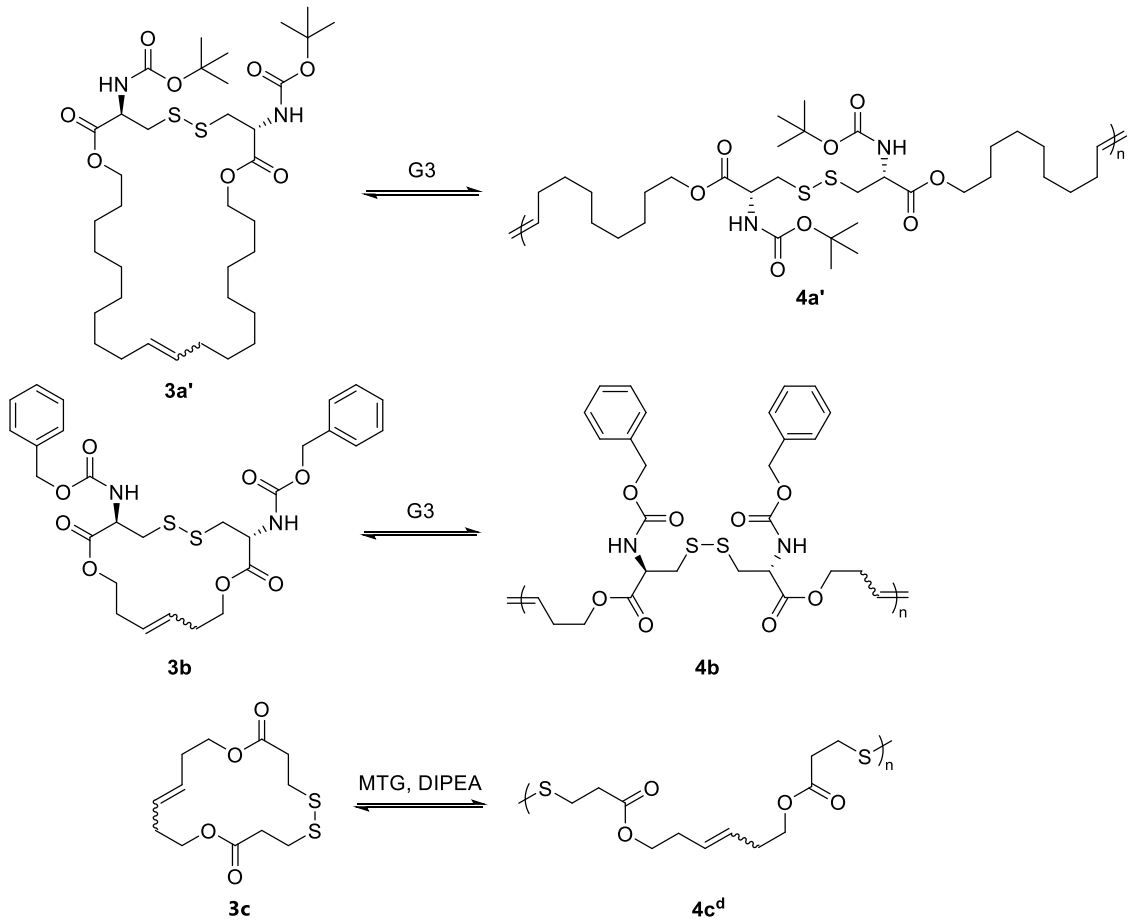

Scheme 14. Entropy-driven polymerizations of **3a'**, **3b** and **3c**.

ED-ROMP was also performed with the monomers **3a'** and **3b**. **3b** is only moderately soluble in $CHCl_3$, hence the polymerization was carried out at a 0.68 M concentration ($[\mathbf{3b}]_0/[G3]_0$ = 100:1) at 40 °C for 30 min. As expected, the polymerization led to only 60% conversion (analysis method 1) and a low molar mass (M_n^{app}) of 14 kDa. Polymerization of **3a'** ($[\mathbf{3a'}]_0/[G3]_0$ = 100:1) at 1.2 M in $CHCl_3$ at 40 °C yielded a polymer **4a'** with a M_n^{app} of 80 kDa after 30 min. **3c** was polymerized by ED-RODiMP in DMSO (85 °C, $[\mathbf{3c}]_0/[MTG]_0/[DIPEA]_0$= 100:1:1 at rt, 30 min). The purified polymer **4c**$^{\mathbf{d}}$ had a M_n^{app} of 55 kDa and a $Đ$ of 2.2.

6.5.2.2 Polymerization of the Endocyclic Amide

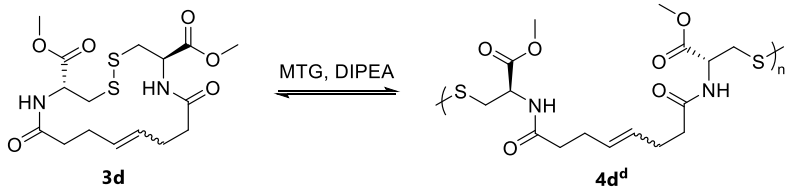

Scheme 15: Entropy-driven polymerization of **3d**.

The monomer **3d** was only soluble in polar solvents, such as DMAc, DMF or DMSO, and was poorly soluble in less polar solvents such as $CHCl_3$ or toluene, which are the recommended solvents for olefin metathesis. Therefore, **3d** cannot be polymerized by olefin metathesis. Hence, a ED-RODiMP was conducted, following a similar pathway as for the synthesis of **4a^d**, at 1.2 M in DMAc at 85 °C, $[\mathbf{3d}]_0/[MTG]_0/[DIPEA]_0$= 100:1:1. In the course of the reaction, the mixture turned more viscous, which is indicative of a successful polymerization. The polymerization was terminated by the addition of acetic acid and subsequently analyzed, by NMR and SEC. Since the resulting polymerization mixture was not soluble in $CDCl_3$ and tetrahydrofuran (THF), which were used for the analysis of **4a^d** and **4c^d**, DMSO-*d_6* and NMP were used instead. Although the viscosity of the crude polymerization mixture indicated a successful polymerization ^{1}H NMR and SEC analysis showed only low conversion and low molar mass products. It was hypothesized that the acidification of the polymerization with acetic acid was not efficient to completely terminate the reaction. Handling of the polymers with thiolate end-groups under dilute conditions in polar solvents would cause depolymerization by "back-biting". To test the hypothesis that thiol end groups cause depolymerization in dilute polar conditions even without an added base catalyst, the pure polymer **4a^d** was dissolved in DMSO-*d_6* and subsequently submitted to the NMR analysis. Indeed, **4a^d** depolymerized in polar dilute conditions (Figure 34).

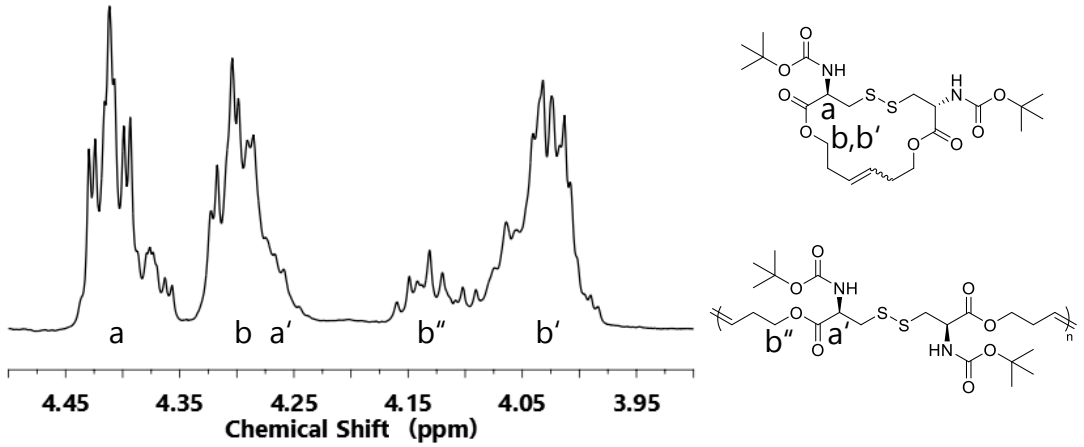

Figure 34: ^{1}H NMR (600 MHz) range from 4.5 to 3.9 ppm of **4a^d** diluted in DMSO-d_6.

Therefore, it was attempted to quench the polymer **4d^d** with a suitable end capping reagent to avoid depolymerization. Methyl maleimide as well as iodo aceto nitrile were thus used for the end capping of the active thiolate end groups. ^{1}H-NMR of the polymers in DMSO-d_6 indicated a monomer conversion of 84% for both end-capped polymers. An increased amount of monomer was detected in the maleimide-terminated polymer, after the purification (Figure 35). This indicates that a depolymerization took place during the polymer work up. The polymer that was end capped with iodo acetonitrile, on the other hand, showed no sign of monomer in the ^{1}H NMR.

SEC analysis of the polymer **4d^d** showed a molar mass of $M_w^{app} \approx 44$ kDa and $Đ \approx 3.5$. To investigate the stability of this acetonitrile end-capped polymer, it was kept under dilute conditions in NMP and SEC measurements were conducted to monitor possible degradation. The measurements revealed that, although the end-capping is sufficient enough to allow for polymer work up and analysis, the polymer still degrades slowly under dilution. However, the depolymerization is much slower, *i.e.* hours, compared to the minutes it takes to degrade the polymer before the end-capping. The polymerization of **3a** with the large $[M]_0/[I]_0$ feed ratio already showed that even trace amounts of thiolates are sufficient in order to reach the thermodynamic equilibrium (Page 51).

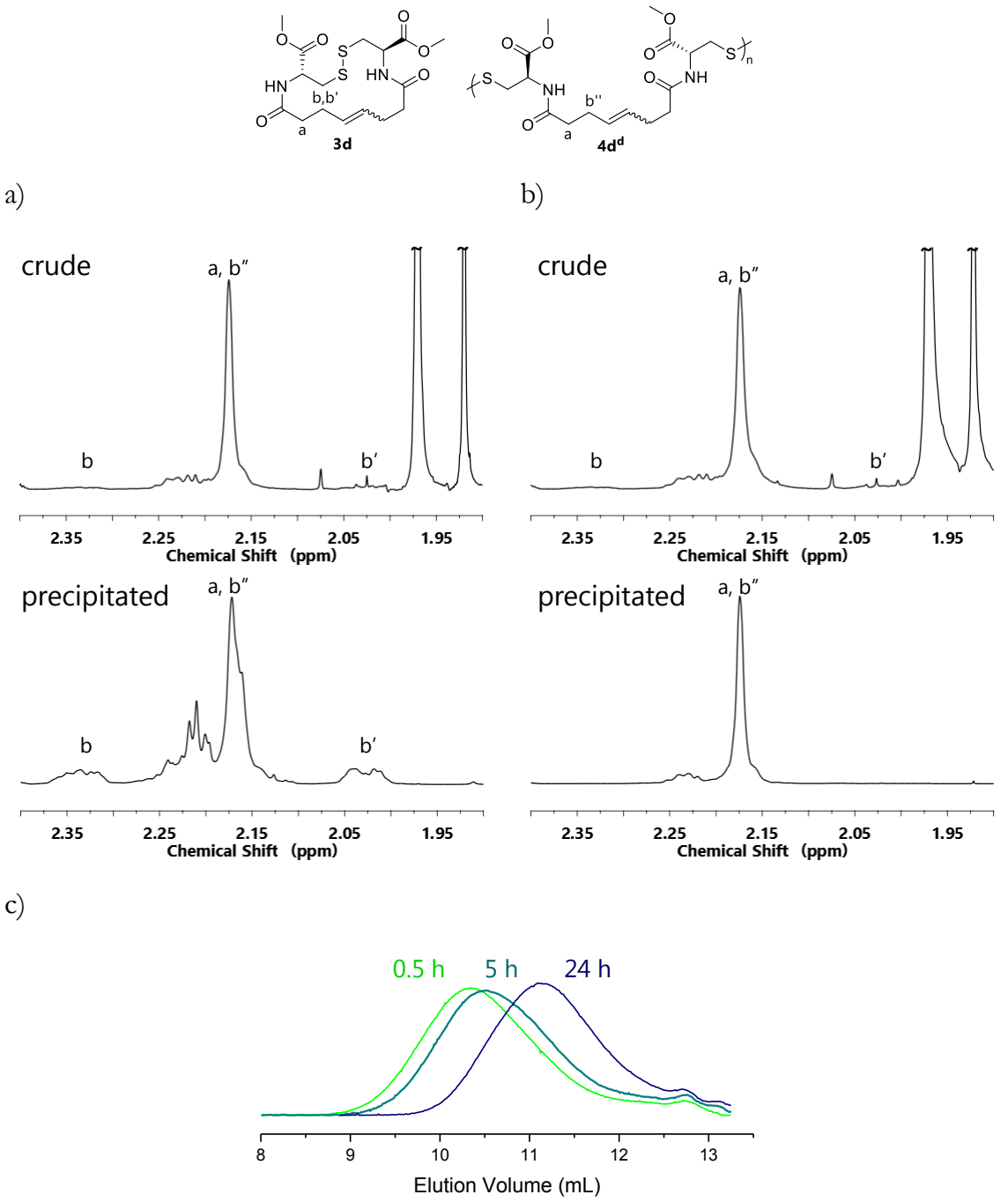

Figure 35: ^{1}H NMR spectra (600 MHz, DMSO-d_6) of the polymers terminated with a) methyl maleimide and b) iodo acetonitrile and c) SEC-RI trace (eluent NMP) of the precipitated polymer following the degradation.

6.6 Polymer Properties and Postpolymerization Reactions

6.6.1 Thermal Properties

Thermal decomposition of the polymers was analyzed by the onset of weight loss by TGA. For the polymers **4a**, **4a^{d}** and **4a'**, thermal decomposition started at ~160 °C and ~170 °C respectively. Since the polymers **4a** and **4a^{d}** only differ in their end groups, the TGA curves obtained for these polymers are, as expected, virtually identical (Appendix II). The decomposition temperatures obtained for these Boc containing polymers were lower than for the other polymers (Table 6). The Cbz-protected polymer **4b** shows an enhanced thermal stability, with an onset temperature of ~220 °C. Polymer **4c^{d}**, which lacks side-chains, exhibits the highest decomposition temperature of ~230 °C.

Table 6: Thermal properties of the polymers **4a**-**4d^{d}**.

Entry	Polymer	Decomposition Onset [°C]	T_g [°C]
1	**4a**	160	41
2	**4a^{d}**	160	31
3	**4a'**	170	2
4	**4b**	220	28
5	**4c^{d}**	230	-45
6	**4d^{d}**	210	39

All polymers were amorphous and exhibited a T_g ranging from -45 °C to 41 °C. While the polymers **4a**, **4a^{d}**, **4b**, and **4d^{d}** were found to have a comparable T_g in the range of 28-41 °C, the long alkyl chain in polymer **4a'** was thought to be responsible for the lower T_g. The lowest T_g was found in the polymer **4c**. This polymer does not contain a carbamate or amide group and is therefore not able to form inter-chain hydrogen bonds.

6.6.2 Polymer Degradation

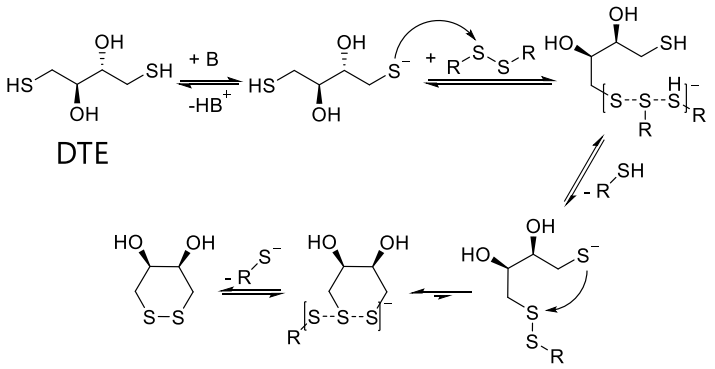

Scheme 16: Reduction mechanism of a disulfide with dithioerythritol (DTE).

The disulfide in the backbone of the polymer, allows for a reductively triggered degradation by forming two thiol groups. Standard reducing agents for disulfide reductions include aliphatic phosphines and thiols. Due to their effectiveness and ease of removal, by liquid extractions, dithiothreitol (DTT) and dithioerythritol (DTE) are standard reagents for this purpose. The mechanism of this reaction is a base-catalyzed S_N2 reaction. Scheme 16 shows the reduction of a disulfide by DTE. The first step of this reaction is the deprotonation of a thiol group. The formed thiolate of the DTE attacks the disulfide bridge, forming a mixed disulfide and a new thiolate as the product. After an attack of the second thiolate group of the DTE and the release of the second thiolate product, a stable six membered ring is formed.

The reductive S-S bond cleavage of the polymer **4a** by DTE was used for the polymer degradation. This reaction was achieved with an excess of DTE and catalytic amounts TEA as the base. The reduction was monitored by SEC and was found to be completed within less than 30 min (Figure 36).

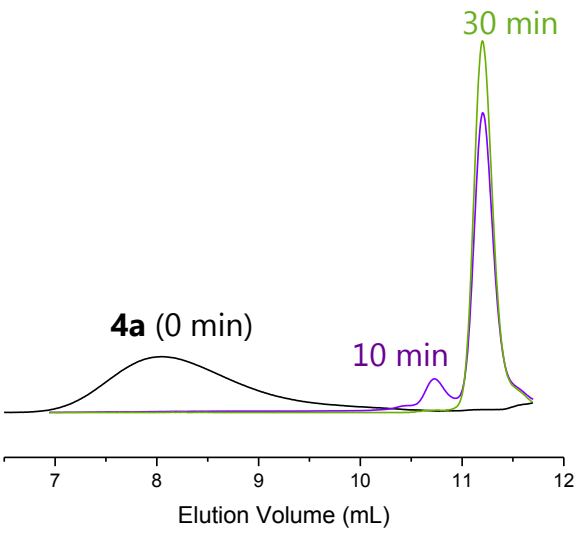

Figure 36: SEC-RI traces of the polymer **4a** and of the degradation products obtained after 10 min and 30 min (areas under RI signals are normalized).

The pure corresponding dithiol was obtained after liquid extraction. A reduction of the macrocycle **3a** done under the same reaction conditions demonstrated the consistency of the method. The ^{1}H NMR spectra of the degradation products, *i.e.*, dithiols, after liquid extraction for both reactions were found to be virtually identical (Figure 37). This further confirms the proposed structure of the polymer.

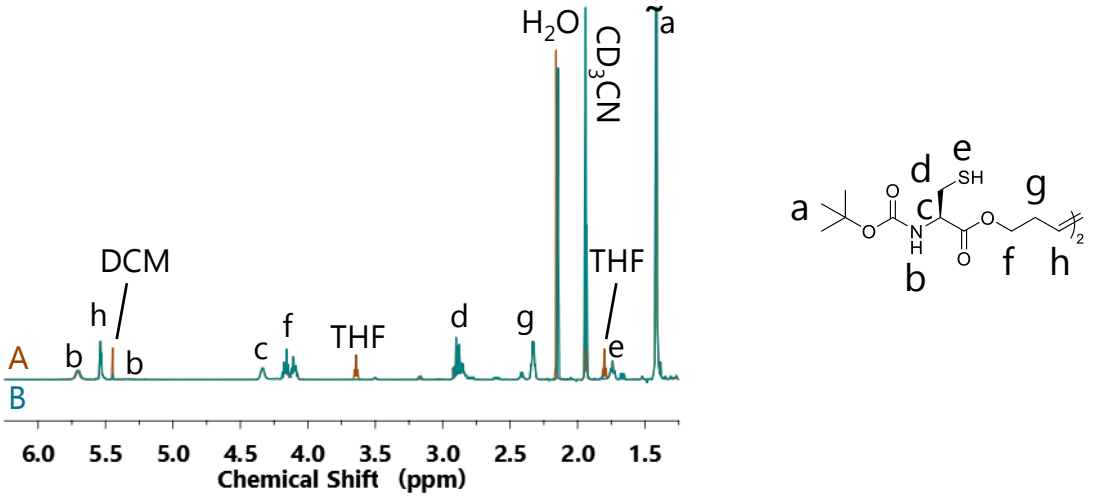

Figure 37: Stacked ^{1}H NMR spectra (600 MHz, CD_3CN) of the products obtained by the reduction of the macrocycle **3a** (A, brown) and the polymer **4a** (B, blue) with DTE.

6.6.3 Deprotection and Post Polymerization Modification

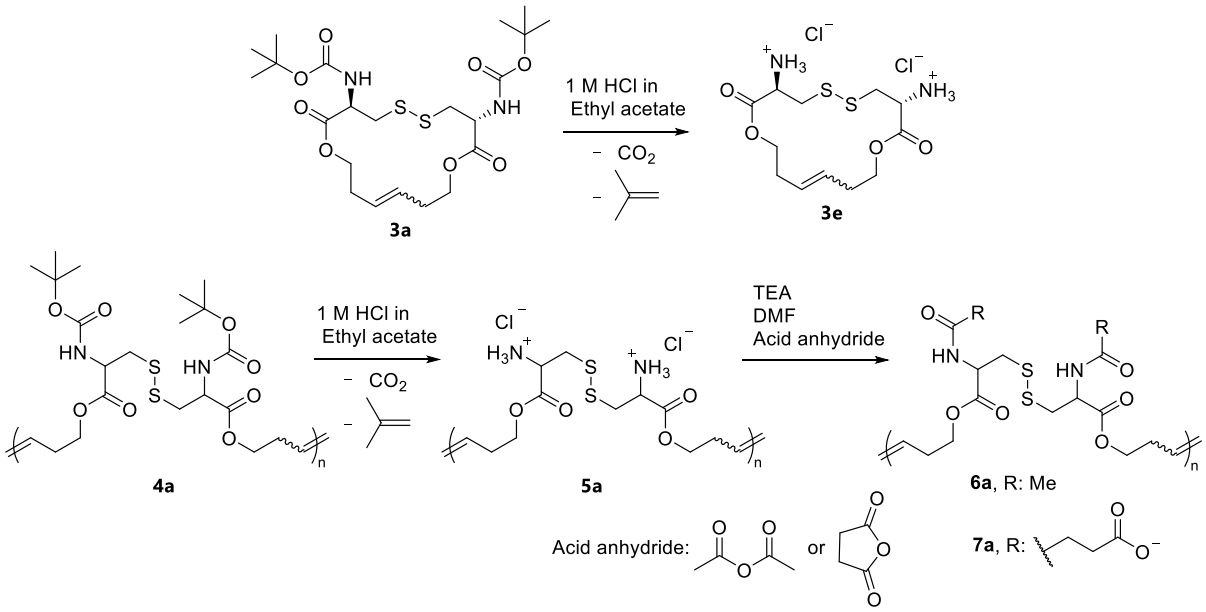

Scheme 17: Deprotection of the macrocycle **3a** and deprotection and functionalization of the polymer **4a**.

Polymers **4a** and **4a'** both contain the acid labile Boc-protecting group. To access the corresponding deprotected polymers **5a** and **5a'** a selective removal of the protecting group without affecting the polyester backbone was necessary. Rapoport et al. reported a selective procedure to remove the Boc-group in the presence of hydrolytically cleavable esters by using a 1 M solution of HCl in dry ethyl acetate.[106] Applying their procedure to the monomer **3a** led to a quantitative conversion of Boc-protected macrocycle to the corresponding ammonium chloride **3e** (Appendix I). Applied to the polymers **4a** and **4a'**, the deprotection reaction resulted in water-soluble polycations with a conversion of more than 99%.

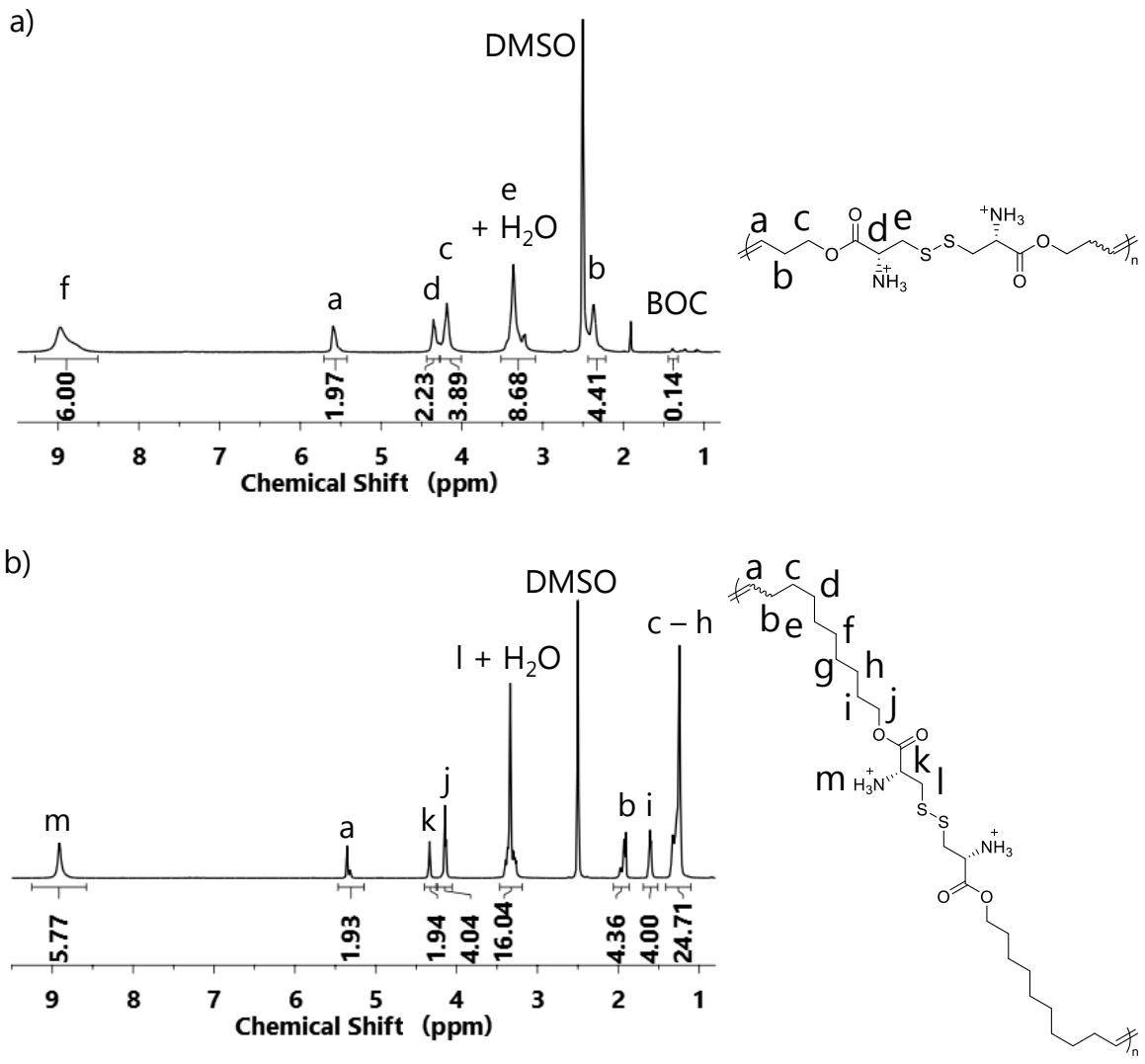

Figure 38: [1]H NMR spectra of the deprotected polymers (a) **5a** (300 MHz) and (b) **5a'** (600 MHz) in DMSO-d_6.

Static light scattering (SLS) of **4a** was performed before and after the deprotection. SLS analysis gave absolute M_w values of 23 ± 4 kDa for polymer **4a** and 15 ± 6 kDa for the deprotected polymer **5a** (Appendix II). Although the error in the SLS analysis is relatively high, the post-deprotected molar mass value is close to the theoretical value of 17 kDa. This indicates that no or very little ester cleavage took place during the reaction. The deprotection led to pendant ammonium chloride groups which can be further functionalized.

To study this, the polymer **4a** was deprotected as described before and subsequently treated with an excess of TEA, followed by a functionalization step by

the addition of either acetic anhydride or succinic anhydride. The expected structure for both functionalized polymers **6a** and **7a** was confirmed by ^{1}H NMR analysis (Figure 39). Additionally, the ^{1}H NMR spectra of the functionalized polymers showed no evidence for ester cleavage and suggest full conversion. SEC analysis of the polymers were not possible because of their low solubility in THF and NMP.

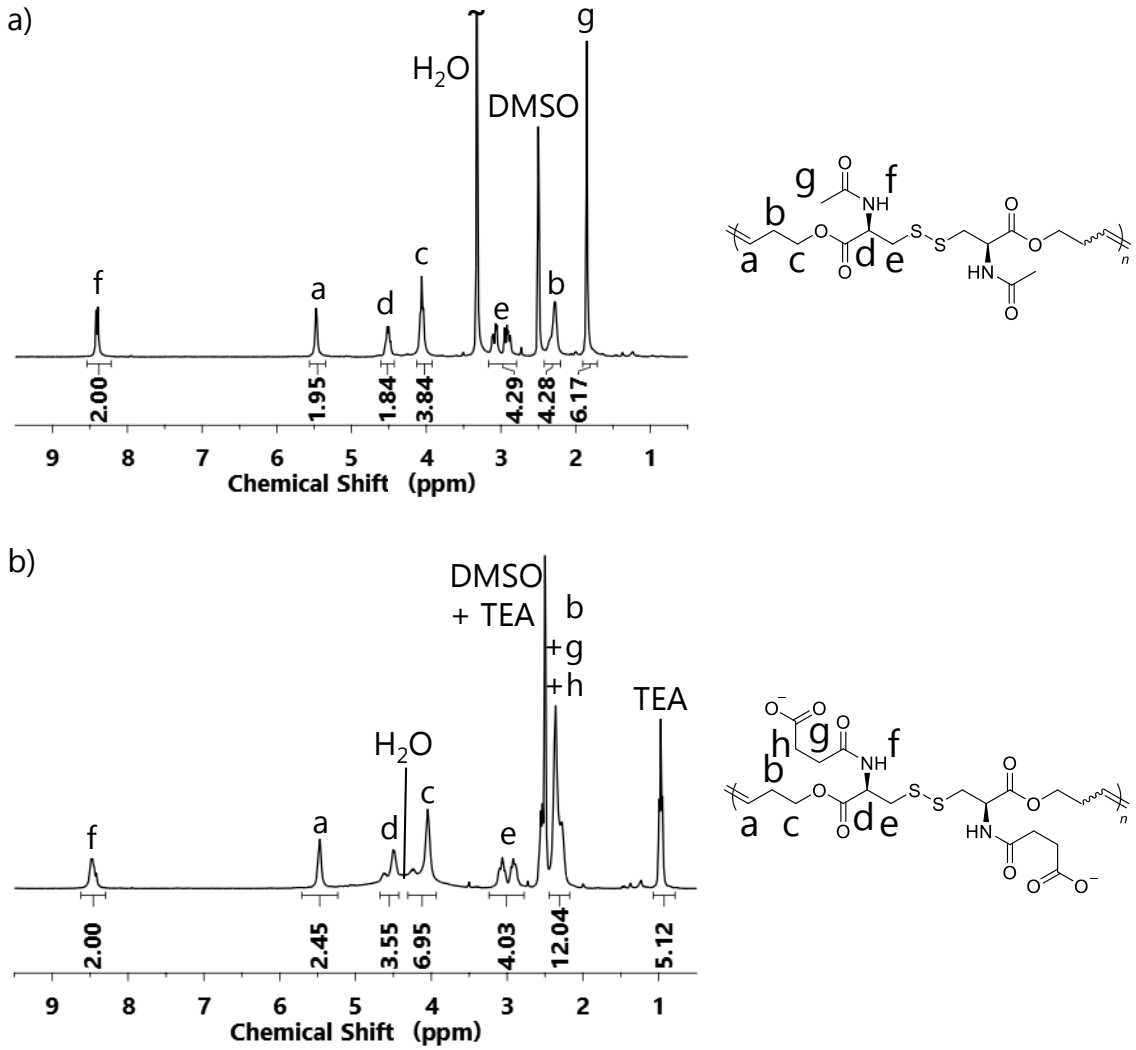

Figure 39: ^{1}H NMR spectra (300 MHz, DMSO d_6) of the functionalized polymers **6a** and **7a**.

6.7 Summary and Conclusion

During this work, novel cystine-based macrocycles were synthesized and polymerized. These monomers were polymerized by ED-ROMP and ED-RODiMP to yield functional polymers with molar masses up to 177 kDa. Furthermore, post-polymerization reactions, such as end-capping, deprotection, functionalization, and polymer degradation have been successfully studied (Scheme 18 and Scheme 19).

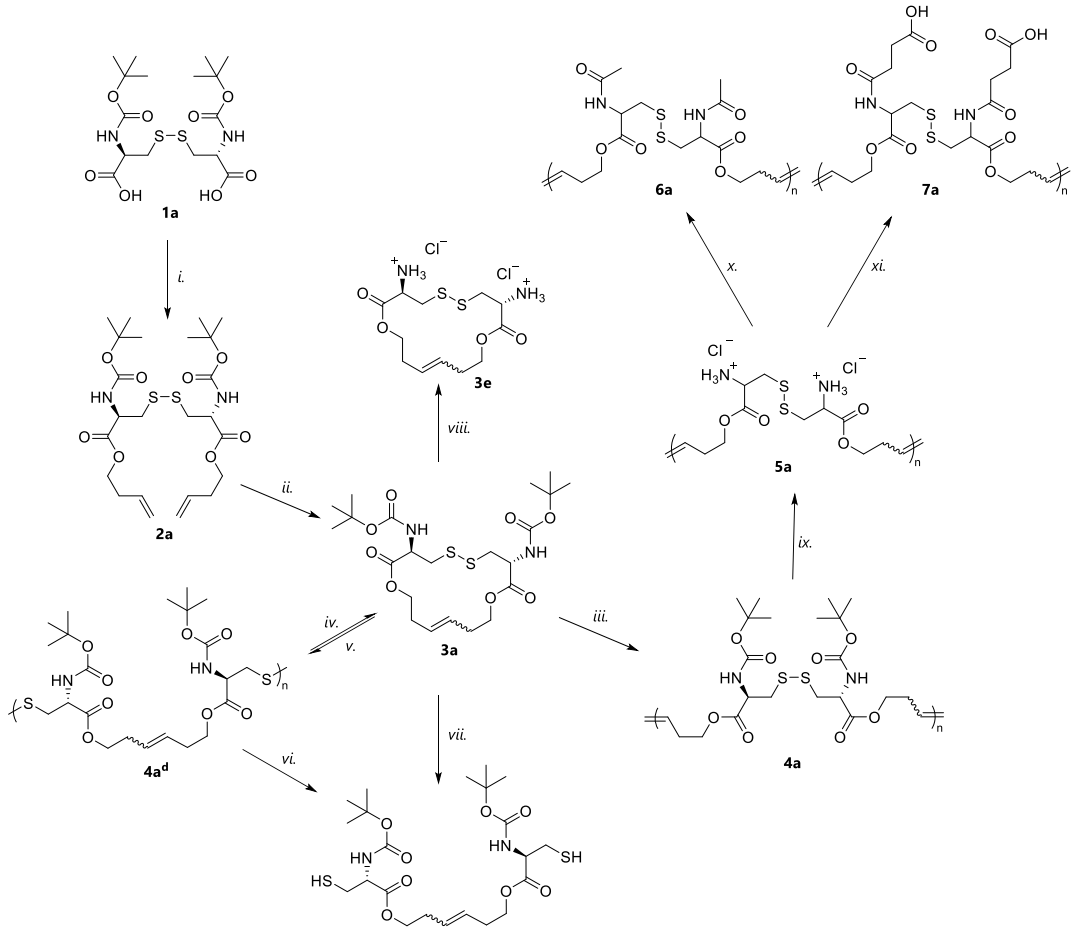

Scheme 18: Synthetic pathway: (i.) 4-bromobut-1-ene, K_2CO_3, DMF, rt, 4 d (ii.) HG2, *p*-benzoquinone, toluene, 110 °C, 4 h, (iii.) G3, $CHCl_3$, 60 °C, 15 min, (iv.) MTG, DIPEA, DMAc, 85 °C, 5 min, (v.) DMSO-d_6 (vi. and vii) DTE, TEA, THF, rt, 30 min, (viii. and ix.) 1M HCl, ethyl acetate, rt, 2d, (x.) acetic anhydride, TEA, DMF, rt 5 h (xi.) succinic anhydride, TEA, DMF, rt 5 h.

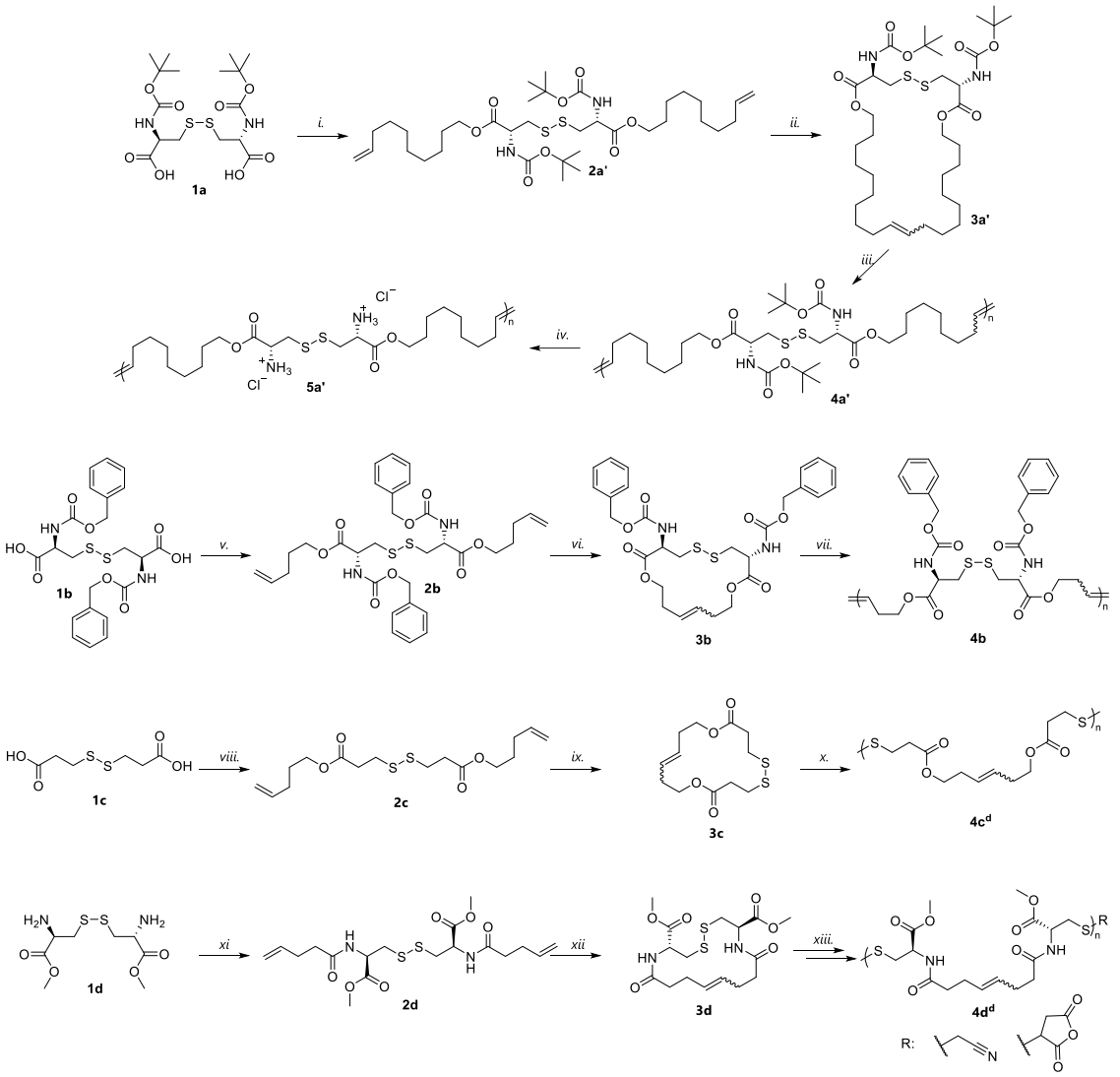

Scheme 19: Synthetic pathways towards various poly(disulfide)s; (i.) 11-bromoundec-1-ene, K_2CO_3, DMF, rt, 6 d, (ii.) HG2, *p*-benzoquinone, toluene, 110 °C, 4 h, (iii.) G3, $CHCl_3$, 40 °C, 30 min, (iv.) 1M HCl, ethyl acetate, rt, 2d, (v.) 4-bromobut-1-ene, K_2CO_3, DMF, rt, 6 d (vi.) HG2, *p*-benzoquinone, DCM, 40 °C, 22 h, (vii.) G3, $CHCl_3$, 40 °C, 30 min (viii.) HG2, *p*-benzoquinone, toluene, 110 °C, 4 h, (ix.) 4-bromobut-1-ene, K_2CO_3, DMF, 80 °C, 26 h, (x.) MTG, DIPEA, DMSO, rt, 1 h (xi.) 4-pentenoyl chloride, TEA, CH_2Cl_2, 0 °C, 30 min, rt, 4 h (xii) HG2, *p*-benzoquinone, toluene 110 °C, 4 h, (xiii.) MTG, DIPEA, DMAc, 85 °C, 1 h, and iodoacetonitrile or methyl maleimide, DMAc, 85°C, 10 min.

In more detail, the macrocycle **3a** was synthesized in a two-step pathway with a high overall yield of 77%. The structure of this macrocycle was confirmed by 1D and 2D NMR spectroscopy as well as by ESI-ToF MS and elemental analysis. The ED-ROMP of **3a** was successful and resulted in a high molar mass polymer of M_n^{app} = 59 kDa. This is the first example of homopolymerization of an endocyclic disulfide-based monomer by ROMP. The polymerization led to a maximum conversion of ~80% when the equilibrium is reached. The polymerization kinetics

of the ED-ROMP of **3a** were further studied. The reaction temperature did not affect the equilibrium or the molar masses, but faster equilibration was achieved at higher temperature. As expected for entropy-driven polymerizations, decreasing the concentration had a significant influence on the conversion, with lower concentrations leading to lower conversions. Lowering the catalyst loading led to a lower consumption of the monomer, which indicated that the catalyst was deactivated before reaching the equilibrium. The deactivation of the ruthenium catalyst was further supported by a dilution experiment, which showed that the catalyst was fully inactive after 60 min of the polymerization.

Catalyst deactivation and solvent restriction inspired the search for other means to polymerize such macrocycles. Even though the disulfide metathesis reaction is virtually unexplored as a polymerization reaction of unstrained macrocycles, it seems to be an ideal candidate for entropy-driven polymerizations. The polymerization of **3a** was conducted with MTG as the initiator and TEA or DIPEA as the basic catalyst. The polymerization was fast in a polar aprotic solvent (*i.e.*, DMAc) resulting in an equilibration in 15 min, with a conversion of up to 75% at 60 °C. Further increasing the temperature to 85 °C did led to a conversion of up to 77% after only 5 min, resulting in a polymer **4a**$^{\mathbf{d}}$ with an apparent molar mass M_n^{app} of 55 kDa. The polymerization was repeated in DMSO and GVL, which are less toxic and greener alternatives to DMAc. In DMSO, the maximum conversion was already reached within less than 1 min. The reaction in GVL proceeded similarly fast as the reaction in DMAc.

Unlike the olefin metathesis polymerization, the equilibrium of the ED-RODiMP was still achieved with an monomer-initiator feed ratio ([**3a**]/[MTG]) of 100:0.05. This led to a polymer with an apparent molar mass (M_n^{app}) of 177 kDa. A dilution experiment that was conducted similarly to the one described for ED-ROMP showed rapid depolymerization of the polymer. This demonstrates that the thiolate end groups of the polymers remain active throughout the polymerization and that only very small amounts of thiolates are needed to reach the equilibrium and achieve the polymerization.

A series of four additional macrocyclic disulfides were successfully synthesized, thereby demonstrating the robustness of the chosen synthetic strategy for different ring sizes and varying functional groups. The synthesis of these macrocycles was achieved with overall yields ranging from 26% (**3d**) and 59% (**3c**).

The polymerizations of **3a'**, **3b** and **3c** by ED-ROMP and ED-RODiMP were successful. Unexpected problems were encountered in the ED-RODiMP of **3d**. The polymer was found to rapidly depolymerize upon dilution in polar aprotic solvents that were used for the analysis. Therefore, end-capping with iodo acetonitrile and *N*-methyl maleimide was performed to stabilize the polymer. End-capping with *N*-methyl maleimide was sufficiently effective as to enable SEC analysis of the crude polymer. However, end-capping with iodo acetonitrile was more effective as it facilitated analysis the analysis of the crude as well as the purified polymer by greatly reducing the rate of depolymerization. Considering the reactivity of the thiolates towards disulfide groups, depolymerization in polar aprotic media can only be avoided by a quantitative and irreversible end-capping of the thiolates.

In conclusion, the ED-ROMP and the ED-RODiMP were shown to both have their respective advantages and drawbacks, while the choice of polymerization mechanism does not influence the equilibrium. Under certain conditions the ED-RODiMP is faster and can be performed in environmentally friendly solvents. Additionally, it does not require toxic transition metals, like ruthenium catalysts, and only uses thiols, which can be significantly cheaper. Furthermore, no deactivation of the thiolates was detected during the reactions, thereby yielding polymers with apparent molar masses of up to 177 kDa.

Depolymerization remains problematic when dilute polar aprotic conditions cannot be avoided. In this case, polymerization by ED-ROMP, which leads to polymers that are not prone to depolymerization is an effective alternative. The reaction can be run under kinetic control, where full equilibration can be achieved before catalyst deactivation.

Both polymerization complement each other and regarding their most suitable solvent choice. Together they offer a very broad scope of applicable different polymerization media. More precisely, similar to the polymerization of **3d**, which was, due to the solubility, not polymerizable with ED-ROMP, non-polar macrocycles can be envisioned that are not soluble in polar solvents required for ED-RODiMP and therefore be preferably polymerized by ED-ROMP.

In total five different monomers have been polymerized and the corresponding polymers were subsequently analyzed by thermal analytical methods. TGA revealed that the degradation temperature of the polymers was influenced by their respective side groups. All polymers were amorphous and showed glass transition temperatures ranging from -45 to 41 °C.

The side groups of the polymers can also be used for post-polymerization modifications. For instance, the Boc-group of the polymers **4a** and **4a'** can be removed by a treatment with dry HCl in ethyl acetate, to yield the weak polyelectrolytes **5a** and **5a'**. The resulting ammonium chloride groups can be further functionalized for instance with acid anhydrides and TEA.

As a proof of principle, polymer **4a** was treated with DTE to show the fast depolymerization of the polymer to the corresponding dithiol. The degradation of the polymers under reductive conditions can be an important property, for instance for medical applications.

6.8 Future Work

Poly(disulfide)s are of a particular interest for biomedical applications especially as gene or drug carrier systems. The advantages include the bio-degradability inside the cells and an enhanced cellular uptake mediated by the disulfide bond. Usually, polycations are used as gene carriers because of their ability to form polyplexes with DNA. It was shown that the deprotection of **4a** and **4a'** with hydrochloric acid in ethyl acetate led to the formation of polycations **5a** and **5a'**. These polymers and derivatives thereof are currently under investigation in our group regarding their aggregation behavior in water and in phosphate-buffered saline (PBS) solutions. While all investigated polymers were soluble in aqueous solution, the PBS buffer reduced the solubility of the polymers and led to a salting out effect at higher concentrations. The soluble samples were analyzed by dynamic light scattering (DLS) and transmission electron cryomicroscopy (cryo-TEM). First results showed aggregates typically in a range of 50-150 nm. Next steps would include degradability studies of the aggregates by glutathione and testing the drug loading of the aggregates. Furthermore, deprotection of the polymer **4d**^{d} (demethylation) would lead to a polyanion under physiological conditions. Unlike the polymers **5a** and **5a'**, the lack of the ester groups along the main chain of the polymer should lead to an enhanced hydrolytic stability, while still allowing for degradability under reductive conditions.

Additionally, current work is dedicated to reveal further insights of the ED-RODiMP, with a particular focus on the similarities with the ED-ROMP. The disulfide metathesis presents several advantages compared to the olefin metathesis regarding the polymerization of macrocyclic disulfides. However, disulfide polymerization in $CHCl_3$ was found to be ineffective and polymerization of very apolar monomers might not be feasible by this polymerization, due to their low solubility in polar solvents. Therefore, different bases and additives (*e.g.*, phosphazene bases and crown ethers) should be tested as catalysts and co-catalysts to facilitate ED-RODiMP in apolar conditions.

New functional macrocyclic disulfides and their subsequent polymerization via ED-RODiMP ought to be the topic of future research. Promising strategies for this include the focus on green chemistry, with synthesis of fully bio-based macrocycles and the synthesis of sequence encoded functional polypeptide-like polymers.

7 Experimental Section

7.1 Materials

7.1.1 Chemicals

Potassium carbonate (99+%), (triethyl)amine (TEA) (99%, pure), hydrogen chloride (1M solution in ethyl acetate), ethyl vinyl ether (99%, stabilized), iodoacetonitrile (95%), toluene (99.85%, extra dry), dimethylsulfoxide (DMSO) 99.7%, extra dry), *N,N*-dimethylacetamide (DMA) (99.5%, extra dry), were purchased from Acros Organics. *para*-Benzoquinone (≥98%, reagent grade), acetic anhydride (≥99%, puriss), succinic anhydride (96%), *N,N*-dimethylformamide (DMF) (≥99.8% puriss, absolute), 4-pentenoyl chloride (98%), dichloromethane (DCM) (99.8%, anhydrous), L-cystine dimethyl ester dihydrochloride (95%), DMSO-d_6 (99.9% atom D), 4-bromo-1-butene (97%), γ-valerolactone (GVL), (99%, reagent plus), *N*-methylmaleimide (97%), 11-bromo-1-undecene (95%), (1,3-Bis-(2,4,6-trimethylphenyl)-2-imidazolidinylidene)dichloro(*o*-isopropoxyphenylmethylene)-ruthenium (Hoveyda-Grubbs catalyst 2nd generation (HG2)) (97%), and [1,3-bis(2,4,6-trimethylphenyl)-2-imidazolidinylidene]dichloro(phenylmethylene)bis(3-bromopyridine)ruthenium(II) (Grubbs catalyst 3rd generation (G3)) (purity n/a, batch no. MKBS6084V) were purchased from Sigma-Aldrich. Heptanes (isomers, ≥99%, p.a.), tetrahydrofuran (THF) (99.5%), *N,N*-diisopropylethylamine (DIPEA) (99%, for synthesis) 1,4-dithioerythritol (DTE) (≥99%, p.a.) and acetic acid (100%, rotipuran) were received from Carl Roth. Ethyl acetate (technical 99%), *n*-pentane (99.0%, rectapur), toluene (99.0%, rectapur), acetonitrile-d_3 (99.8% atom D), 1,4-dioxane (99%, rectapur) and chloroform (HPLC) were received from VWR. *N,N'*-Di-(*tert*-butyloxycarbonyl)-L-cystine, (Boc-L-Cys-OH)$_2$, was purchased from Iris Biotech. Methylthioglycolate (MTG) (98%) was received from Alfa Aesar. Chloroform-d_1 (99.8% atom D) was received from Deutero GmbH. Silica gel (60M, 0.04–0.063 mm) was purchased from Macherey-Nagel.

Chloroform used for polymerizations was stored for at least one day over molecular sieves (3 Å), ethyl acetate, heptanes, and toluene were distilled in a rotatory evaporator prior to use. *n*-Butyl acetate was filtered over activated aluminum oxide.

7.2 Analytical Instrumentation and Methods

7.2.1 Nuclear magnetic resonance (NMR) spectroscopy

NMR spectra were recorded on Bruker Avance 300 MHz, 500 MHz, or Bruker Avance III 600 MHz spectrometers. Samples were prepared in $CDCl_3$, DMSO-*d*$_6$, or CD_3CN. Signals were referenced to the respective solvent peaks; $CDCl_3$ δ (^{1}H) 7.26 ppm, δ (^{13}C) 77.16 ppm; DMSO-*d*$_6$ δ (^{1}H) 2.50 ppm, δ (^{13}C) 39.52 ppm, CD_3CN δ (^{1}H) 1.94 ppm.

7.2.2 Elemental analysis

Elemental analyses were performed on a Vario EL III (Elementar) operated with helium as carrier gas.

7.2.3 Electronspray Ionization Time-of-Flight Mass Spectrometry (ESI-ToF MS)

ESI-ToF mass spectrometry was measured in positive ionization mode on a Micromass Q – Tof *micro*, Waters Inc. Samples were prepared in acetonitrile acidified with 0.2% formic acid. Ortho-phosphoric acid was used as the standard.

7.2.4 Melting point

Melting points were obtained by a MEL-TEMP II device (Laboratory Devices Inc., USA); measurements were conducted in open capillaries.

7.2.5 Size exclusion chromatography (SEC)

SEC with simultaneous UV and RI (differential refractive index) detection was performed with two different eluents and stationary phases: (*i*) THF, 0.5 mL·min^{-1}, rt, 300 x 8 mm^2 PSS SDV linear M column (3 µm particle size, molar mass range 10^2-10^6 Da) and (*ii*) NMP + 0.5 wt% LiBr, 0.5 mL·min^{-1}, 60 °C, 300 x 8 mm^2 PSS-GRAM analytical linear column (particle size 7 µm, separation range 10^2-10^6 Da). Solutions containing ~0.15 wt% polymer were filtered through 0.45 µm filters; the injected volume was 100 µL. Polystyrene standards (PSS, Mainz, Germany) were used for calibration.

Areas under the SEC-RI traces were normalized to 1. For a better comparability, the signal of the monomer **3a** in the shown SEC-RI traces was set to be at 13.37 mL.

7.2.6 Static light scattering (SLS)

SLS was performed at rt using an ALV-7004 multiple-tau digital correlator in combination with a CGS-3 compact goniometer and a He-Ne laser (Polytec, 34 mW, λ = 633 nm). The polymer stock solution was prepared by dissolution in ethyl acetate or water and subsequent filtration through 0.45 µm poly(tetrafluoroethylene) PTFE or poly(vinylidene difluoride) PVDF filters and measured at scattering angles from 70°-150° in 10° steps. Data evaluation was carried out using Zimm plot models. Refractive index increments (dn/dc) were measured with a PSS DnDc2010 device operating at λ = 620 nm.

7.2.7 Thermogravimetric analysis (TGA)

TGA was done on a Mettler Toledo TGA/SDTA851 from 25-900 °C at a heating rate of 10 K min^{-1} under a nitrogen flow of 20 mL min^{-1}.

7.2.8 Differential scanning calorimetry (DSC)

DSC was carried out on a Mettler Toledo DSC822e or Netzsch DSC 214 Polyma at -80-140 °C under a nitrogen flow. The glass transition temperature was determined at a heating rate of 10 K min^{-1}.

7.3 Synthetic Procedures

Unless otherwise noted, all reactions were performed in dry conditions under nitrogen atmosphere.

7.3.1 Monomer Synthesis

7.3.1.1 (*R,R*) Dibut-3-enyl (*N,N*'-di-Boc)-cystinate 2a

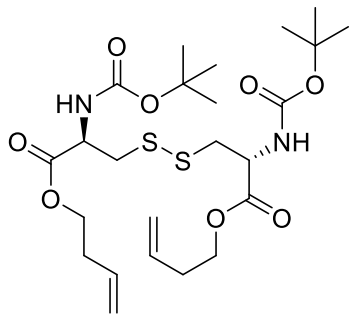

To a 0.25 M suspension of *N,N*'-di-Boc-L-cystine **1a** (1 equiv) and potassium carbonate (3 equiv) in DMF, 4-bromobut-1-ene (3 equiv) was slowly added. The resulting mixture was stirred for 1, 2, 3 or 4 days at room temperature. The suspension was poured into diethyl ether and the remaining solids were filtered to remove any residual solids and subsequently washed with additional diethyl ether. The clear yellowish solution was washed with saturated sodium bicarbonate solution, saturated sodium chloride solution and water. The organic phase was dried with magnesium sulfate. After the filtration the solution was concentrated on a rotatory evaporator and again solubilized in diethyl ether and filtrated over a silica pad. Removing the solvent *in vacuo* resulted the product as a white solid. Yields were 34%, 63%, 71%, and 90% for 1, 2, 3, and 4 days, respectively.

^{1}H NMR (300 MHz, DMSO-d_6) δ 7.45-6.94 (m, 2H), 5.79 (ddt, 2H), 5.19-4.99 (m, 4H), 4.24 (td, J = 9.0, 4.9 Hz, 2H), 4.19-4.01 (m, 4H), 3.12-2.83 (m, 4H), 2.34 (q, J = 6.5 Hz, 4H), 1.38 (s, 18H). ^{13}C NMR (75 MHz, DMSO-d_6) δ 170.80, 155.23, 134.22, 117.18, 78.44, 63.73, 52.78, 38.90, 32.46, 28.07. Anal. Calcd. for $C_{24}H_{40}N_2O_8S_2$: C, 52.5; H, 7.4; N, 5.1; S, 11.7. Found: C, 52.6; H, 7.7; N, 5.1; S, 11.9; Mp: 45-48 °C.

7.3.1.2 (*R,R*) Diundec-10-enyl (*N,N*'-di-Boc)-cystinate 2a'

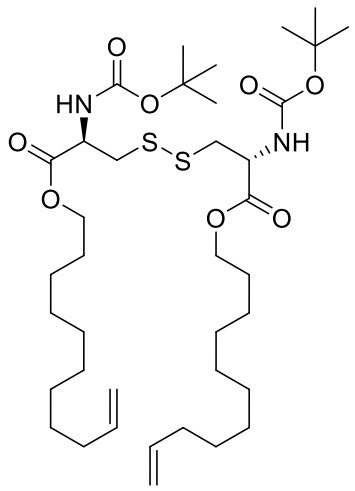

To a suspension of 2.5 g of *N,N*'-di-Boc-L-cystine **1a** (1 equiv, 5.68 mmol) and 2.35 g potassium carbonate (3 equiv, 17 mmol) in 23 mL DMF, 3.75 mL of 11-bromoundec-1-ene (3 equiv, 17 mmol) was slowly added. The resulting mixture was stirred for 6 days at room temperature. The suspension was poured on diethyl ether and the remaining solids were removed *via* filtration and washed with additional diethyl ether. The clear solution was washed with saturated sodium bicarbonate solution, saturated sodium chloride solution and water. The organic phase was dried with magnesium sulfate. After filtration, the solution was concentrated in a rotatory evaporator to yield a yellow oil, which was dissolved in 50 mL of *n*-pentane and put in a freezer at -20 °C overnight. The resulting gel was partially redissolved by warming it slightly and subsequently placed back in the freezer. After two hours, a precipitate was formed, which was filtered and redissolved in 50 mL of *n*-pentane. The gelation precipitation procedure was repeated to afford 2.6 g of a white solid (yield: 61%). ^{1}H NMR (300 MHz, DMSO-*d*$_6$) δ 7.54-6.79 (m, 2H), 5.78 (ddt, J = 16.9, 10.2, 6.6 Hz, 2H), 5.13-4.77 (m, 4H), 4.32-4.16 (m, 2H), 4.13-3.92 (m, 4H), 3.12-2.83 (m, 4H), 2.00 (dd, J = 13.8, 6.8 Hz, 4H), 1.65-1.49 (m, 4H), 1.38 (s, 18H), 1.25 (s, 24H). ^{13}C NMR (75 MHz, DMSO-*d*$_6$) δ 170.85, 155.20, 138.72, 114.51, 78.37, 64.68, 52.84, 33.15, 28.86, 28.76, 28.60, 28.48, 28.24, 28.05, 25.24. Anal. Calcd. for $C_{38}H_{68}N_2O_8S_2$: C, 61.3; H, 9.2; N, 3.8; S, 8.6. Found: C, 61.3; H, 10.5; N, 3.8; S, 8.8; Mp: 36-37 °C.

7.3.1.3 (*R,R*) Dibut-3-enyl (*N,N*'-di-Cbz)-cystinate 2b

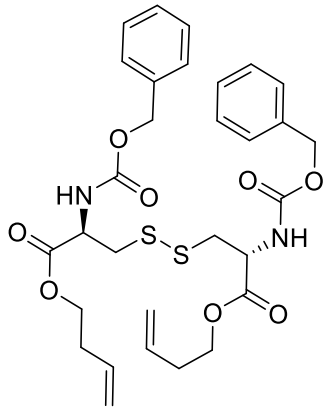

To a suspension of 1.0 g of *N,N*'-di-Cbz-L-cystine **1b** (1 equiv, 1.97 mmol) and 0.81 g potassium carbonate (3 equiv, 5.9 mmol) in 8 mL of DMF, 0.6 mL of 4-bromobut-1-ene (3 equiv, 5.9 mmol) was slowly added. The resulting mixture was stirred for 4 days at room temperature. The suspension was poured into diethyl ether and the remaining solids were removed *via* filtration and washed with additional diethyl ether. The clear yellowish solution was washed with saturated sodium bicarbonate solution, saturated sodium chloride solution and water. The organic phase was dried with magnesium sulfate. After filtration, the solution was concentrated on a rotatory evaporator. The resulting oil was dissolved in 1,4-dioxane, and freeze dried. Further purification was done by column chromatography over silica (gradient: heptanes/ethyl acetate 5:1 → ethyl acetate) to receive the product (650 mg, 53 % yield) as a white solid.

^{1}H NMR (300 MHz, $CDCl_3$) δ 7.34 (s, 10H), 5.87 – 5.59 (m, 4H), 5.19 – 5.01 (m, 8H), 4.73 – 4.55 (m, *J* = 7.2 Hz, 2H), 4.20 (t, *J* = 6.6 Hz, 4H), 3.15 (d, *J* = 4.6 Hz, 4H), 2.49 – 2.29 (m, *J* = 6.5 Hz, 4H); Mp: 72-73 °C.

^{13}C NMR (75 MHz, $CDCl_3$) δ 170.35, 155.78, 136.22, 133.57, 128.66, 128.37, 128.29, 117.83, 67.30, 65.05, 53.55, 41.38, 32.97.

7.3.1.4 Dibut-3-enyl dithiobispropionate 2c

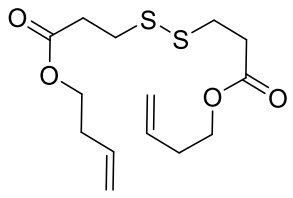

To a suspension of 1 g of 3,3'-dithiopropionic acid **1c** (1 equiv, 4.75 mmol) and 1.97 g potassium carbonate (3 equiv, 14.3 mmol) in 15 mL of DMF, 1.44 mL of 4-bromobut-1-ene (3 equiv, 14.3 mmol) was slowly added. The resulting mixture was stirred at 80 °C for 26 h. The suspension was poured into diethyl ether

and washed with saturated sodium bicarbonate solution, saturated sodium chloride solution and water. The organic phase was dried with magnesium sulfate. After filtration, the solution was concentrated on a rotatory evaporator to obtain the product (1.35 g, 89 % yield) as yellow oil.

^{1}H NMR (300 MHz, $CDCl_3$) δ 5.81 (ddt, *J* = 17.0, 10.2, 6.7 Hz, 2H), 5.26 – 5.01 (m, 4H), 4.19 (t, *J* = 6.7 Hz, 4H), 2.95 (t, *J* = 7.2 Hz, 4H), 2.76 (t, *J* = 7.1 Hz, 4H), 2.50 – 2.35 (m, 4H), 2.58 – 2.28 (m, 4H).

7.3.1.5 (*R,R*) Dimethyl (*N,N'*-dipent-4-enoyl)-cystinate 2d

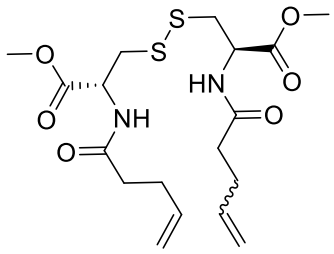

1.0 g L-Cystine dimethyl ester dihydrochloride **1d** (1 equiv, 2.9 mmol) and 1.7 mL TEA (4.2 equiv, 12.2 mmol) were suspended in 15 mL dry DCM in a 25-mL round bottom flask equipped with a septum. The resulting mixture was cooled to 0 °C and 0.72 mL 4-pentenoyl chloride (2.2 equiv, 6.5 mmol) was slowly added *via* a syringe. The reaction was stirred at 0 °C for 30 minutes and additionally for 4 hours at room temperature. The resulting suspension was diluted with 100 mL of ethyl acetate and washed with saturated sodium bicarbonate solution, saturated sodium chloride solution, and water. The organic phase was dried with magnesium sulfate. After filtration, the solution was concentrated *in vacuo* to yield a yellow solid. Recrystallization from toluene yielded the product (1.08 g, 85 % yield) as a white solid. ^{1}H NMR (300 MHz, DMSO-d_6) δ 8.41 (d, *J* = 7.8 Hz, 2H), 5.80 (ddt, *J* = 10.9, 9.1, 5.5 Hz, 2H), 5.13 – 4.88 (m, 4H), 4.55 (td, *J* = 8.7, 5.2 Hz, 2H), 3.64 (s, 6H), 3.17 – 2.82 (m, 4H), 2.31 – 2.15 (m, 8H). ^{13}C NMR (75 MHz, DMSO-d_6) δ 171.66, 170.91, 137.43, 114.95, 52.04, 51.11, 34.11, 28.99; Mp: 98-99 °C.

7.3.1.6 (*R,R*) Hex-3-en-1,6-diyl (*N,N*'-di-Boc)-cystinate 3a

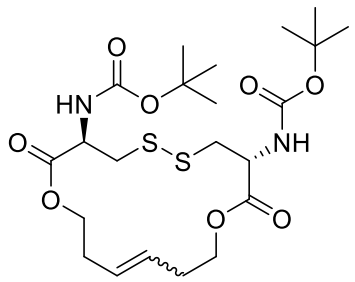

5.2 g of **2a** (1 equiv, 9.48 mmol), 63 mg of HG2 (0.01 equiv, 0.01mmol), and 22 mg of *p*-benzoquinone (0.02 equiv, 0.02 mmol) were dissolved in 1 L of DCM and refluxed for 6h. The reaction was monitored by TLC (heptanes/ethyl acetate 4:1) The reaction was quenched by addition of ethyl vinyl ether and refluxed for additional 15 minutes, followed by the addition of DMSO and refluxing for another 15 minutes. The reaction mixture was stirred overnight at room temperature and afterwards concentrated *in vacuo*. The brown oil was purified by column chromatography over silica (heptanes/ethyl acetate 5:1). The resulting off-white solid was suspended in warm heptanes. After cooling to room temperature the solvent was decanted, to obtain the product (4.4 g, yield: 85%) as a white solid.

1.48 g of **2a** (1 equiv, 2.7 mmol), 17 mg of HG2 (0.01 equiv, 0.027 mmol), and 6 mg of *p*-benzoquinone (0.02 equiv, 0.055 mmol) were dissolved in 270 mL of ethyl acetate and stirred over night at 50 °C. The reaction was quenched by the addition of ethyl vinyl ether and stirred at 50 °C for additional 15 minutes, followed by the addition of DMSO and stirring for another 15 minutes at 50 °C. The reaction mixture was stirred overnight at room temperature and afterwards concentrated *in vacuo*. The brown oil was purified by column chromatography over silica (heptanes/ethyl acetate 5:1), to obtain the product (1.0 g, yield: 73%) as a white solid.

4.5 g of **2a** (1 equiv, 8.2 mmol), 51 mg of HG2 (0.01 equiv, 0.081 mmol), and 18 mg of *p*-benzoquinone (0.02 equiv, 0.16 mmol) were dissolved in 820 mL of Toluene and refluxed for 4h. The reaction was cooled to 50 °C and subsequently quenched by the addition of ethyl vinyl ether and stirred at 50 °C for additional 15 minutes, followed by the addition of DMSO and stirring for another 15 minutes at 50 °C. The reaction mixture was stirred overnight at room temperature and afterwards concentrated *in vacuo*. The brown oil was purified by column chromatography over silica (Toluene/ethyl acetate 6:1). The resulting off-white solid was suspended in

warm heptanes. After cooling to room temperature the solvent was decanted, to obtain the product (3.7 g, yield: 87%) as a white solid.

^{1}H NMR (300 MHz, DMSO-*d*$_6$) δ 7.44-6.91 (m, 2H), 5.65-5.33 (m, 2H), 4.45-4.35 (m, 2H), 4.34-4.21 (m, 4.3 Hz, 2H), 4.09-3.93 (m, 2H), 3.07-2.72 (m, 4H), 2.43-2.20 (m, 4H), 1.38 (s, 18H). ^{13}C NMR (75 MHz, DMSO-*d*$_6$) δ 171.18, 155.42, 128.83, 78.45, 63.90, 51.00, 35.12, 31.00, 28.10, 26.62. ESI-ToF *m*/*z* calculated for $[C_{22}H_{37}N_2O_8S_2]^+$ $[M+H]^+$:521.1991, found: 521.1996. Anal. Calcd. for $C_{22}H_{36}N_2O_8S_2$: C, 50.8; H, 7.0; N, 5.4; S, 12.3. Found: C, 50.8; H, 7.3; N, 5.3; S, 12.5; Mp: 176-178 °C.

7.3.1.7 (*R,R*) Icos-10-en-1,20-diyl (*N,N*'-di-Boc)-cystinate 3a'

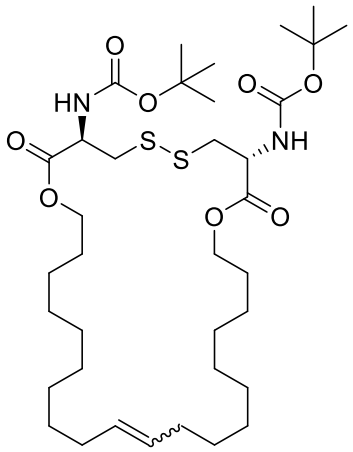

1.0 g of **2a'** (1 equiv, 1.34 mmol), 8.4 mg HG2 (0.01 equiv, 0.013 mmol), and 2.8 mg of *p*-benzoquinone (0.02 equiv, 0.027 mmol) were dissolved in 130 mL of DCM and refluxed for 24 h. The reaction was monitored by TLC (toluene/ethyl acetate 9:1). The reaction was quenched by the addition of ethyl vinyl ether and stirred at 50 °C for additional 15 minutes, followed by the addition of DMSO and another 15 minutes of stirring at 50 °C. The reaction mixture was stirred overnight at room temperature and subsequently concentrated *in vacuo*. The brown oil was dissolved in DCM, adsorbed on silica gel and purified by column chromatography over silica (toluene/ethyl acetate 9:1) to obtain the product (80 mg, 8% yield) as a white solid.

200 mg **2a'** (1 equiv, 0.27 mmol), 8.4 mg HG2 (0.05 equiv, 0.013 mmol), and 2.8 mg of *p*-benzoquinone (0.1 equiv, 0.027 mmol) were dissolved in 27 mL of $CHCl_3$ and stirred at 50 °C for 16 h. The reaction was monitored by TLC (toluene/ethyl acetate 9:1). The reaction was quenched by the addition of 200 μL of ethyl vinyl ether and stirred at 50 °C for additional 15 minutes, followed by the addition of 200 μL of DMSO and another 15 minutes of stirring at 50 °C. The reaction mixture was

stirred overnight at room temperature and afterwards concentrated *in vacuo*. The brown oil was dissolved in DCM, adsorbed on silica gel and purified by column chromatography over silica (toluene/ethyl acetate 9:1) to obtain the product (60 mg, 31% yield) as a white solid.

800 mg of **2a'** (1 equiv, 1.07 mmol), 33.6 mg HG2 (0.05 equiv, 0.054 mmol), and 11.2 mg of *p*-benzoquinone (0.1 equiv, 0.14 mmol) were dissolved in 135 mL of toluene and refluxed for 4 h. The reaction was monitored by TLC (toluene/ethyl acetate 9:1). The reaction was cooled to 50 °C and subsequently quenched by the addition of ethyl vinyl ether and stirred at 50 °C for additional 15 minutes, followed by the addition of DMSO and stirring for another 15 minutes at 50 °C. The reaction mixture was stirred overnight at room temperature and subsequently concentrated *in vacuo*. The brown oil was dissolved in DCM and adsorbed on silica gel and purified by column chromatography over silica (toluene/ethyl acetate 8:1) to obtain the product (625 mg, 81% yield) as purple solid.

^{1}H NMR (600 MHz, DMSO-d_6) δ 7.55-6.75 (m, 2H), 5.38-5.25 (m, 2H), 4.30-4.23 (m, 2H), 4.11-3.98 (m, 4H), 3.10-2.85 (m, 4H), 1.98-1.93 (m, 4H), 1.60-1.53 (m, 4H), 1.40-1.33 (m, 18H), 1.33-1.28 (m, 8H), 1.24 (s, 16H). ^{13}C NMR (151 MHz, DMSO-d_6) δ 170.93, 155.27, 130.30, 78.47, 64.77, 52.81, 38.93, 31.57, 28.80, 28.48, 28.39, 28.11, 28.03, 27.66, 26.27, 25.31. ESI-ToF m/z calculated for $[C_{36}H_{65}N_2O_8S_2]^+$ $[M+H]^+$: 717.4182, found: 717.4180. Anal. Calcd. for $C_{36}H_{64}N_2O_8S_2$: C, 60.3; H, 9.0; N, 3.9; S, 8.9. Found: C, 60.3; H, 9.6; N, 3.8; S, 9.3; Mp: 83-85 °C.

7.3.1.8 (*R,R*) Hex-3-en-1,6-diyl (*N,N*'-di-Cbz)-cystinate 3b

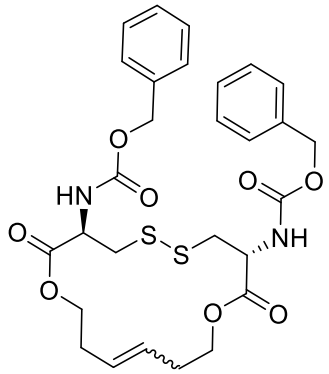

200 mg of **2b** (1 equiv, 0.325 mmol), 2 mg HG2 (0.01 equiv, 6.5 µmol) and 1 mg of *p*-benzoquinone (0.02 equiv, 13 µmol) were dissolved in 32 mL of DCM and refluxed for 16 h. The reaction was monitored by TLC (toluene/ethyl acetate 4:1). After 18 h additional 2 mg HG2 (0.01 equiv, 6.5 µmol) were added and the reaction was refluxed for further 4 h.The reaction was quenched by the addition of ethyl vinyl ether and stirred for additional 15 minutes, followed by the addition of DMSO and another 15 minutes of stirring. The reaction mixture was stirred overnight at room temperature and afterwards concentrated *in vacuo*. The brown oil was purified by column chromatography over silica (toluene/ethyl acetate 4:1) and subsequently recrystallized from methanol to obtain the product (148 mg, 77 % yield) as white needles.

^{1}H NMR (300 MHz, DMSO-d_6) δ 7.93 – 7.81 (m, 2H), 7.45 – 7.24 (m, 10H), 5.56 – 5.38 (m, 2H), 5.05 (s, 4H), 4.59 – 4.44 (m, 2H), 4.36 – 4.22 (m, 2H), 4.11 – 3.96 (m, 2H), 3.14 – 2.95 (m, 2H), 2.94 – 2.76 (m, 2H), 2.42 – 2.23 (m, 4H). ^{13}C NMR (75 MHz, DMSO) δ 171.03, 156.12, 136.73, 128.87, 128.37, 127.89, 127.77, 65.70, 64.11, 51.16, 34.76, 30.99. ESI-ToF m/z calculated for $[C_{28}H_{33}N_2O_8S_2]^+$ $[M+H]^+$: 589.1678, found: 589.1660; Mp: 175-177 °C.

7.3.1.9 Hex-3-en-1,6-diyl dithiobispropionate 3c

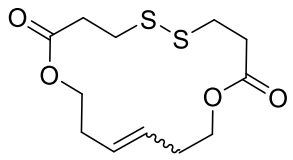

1.0 g **2c** (1 equiv, 3.14 mmol), 19.7 mg HG2 (0.01 equiv, 0.0314 mmol), and 6.8 mg *p*-benzoquinone (0.02 equiv, 0.063 mmol) were dissolved in 310 mL of toluene and The reaction was monitored by TLC. After 2.5 h additional 19.7 mg HG2 (0.01 equiv, 0.0314 mmol) were added and the reaction was further refluxed for 4 h. The reaction was quenched by the addition of ethyl vinyl ether and stirred additional 15 minutes, followed by the addition of a small amount of DMSO and another 15 minutes of stirring. The reaction mixture was stirred overnight at room temperature and subsequently concentrated *in vacuo*. The brown oil was purified by column chromatography over silica (heptanes/ethyl acetate 6:1) to obtain the product (600 mg, 66 % yield) as white crystals.

^{1}H NMR (300 MHz, DMSO) δ 5.55 – 5.38 (m, 2H), 4.23 – 3.96 (m, 4H), 2.92 (t, J = 7.1 Hz, 4H), 2.67 (t, J = 7.1 Hz, 4H), 2.41 – 2.21 (m, 4H). ^{13}C NMR (75 MHz, DMSO) δ 170.88, 128.85, 128.34, 63.59, 34.63, 33.96, 31.14, 26.62. ESI-ToF m/z calculated for $[C_{12}H_{19}O_4S_2]^+$ $[M+H]^+$: 291.0725, found: 291.0733; Mp: 67-69 °C.

7.3.1.10 (*R,R*) dimethyl (*N,N*'-oct-4-ene-1,8-dioyl) cystinate 3d

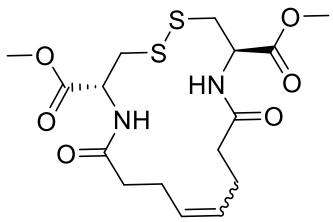

300 mg of **2d** (1 equiv, 0.7 mmol), 4.3 mg of HG2 (0.01 equiv, 0.007 mmol), and 1.5 mg of *p*-benzoquinone (0.02 equiv, 0.014 mmol) were dissolved in 70 mL of DCM and refluxed for 19 hours. The reaction was quenched by the addition of ethyl vinyl ether and refluxed for additional 15 minutes, followed by the addition of DMSO and refluxing for another 15 minutes. The reaction mixture was stirred overnight at room temperature and afterwards concentrated *in vacuo*. The obtained brown oil was purified by column chromatography over silica (gradient: heptanes/ethyl acetate 1:5 → ethyl acetate) to obtain the product (30 mg, 11% yield) as an off-white solid.

1.0 g **2d** (1 equiv, 2.3 mmol), 30 mg HG2 (0.02 equiv, 0.047 mmol), and 12.5 mg *p*-benzoquinone (0.04 equiv, 0.12 mmol) were dissolved in 250 mL of toluene and refluxed for 4 hours. The reaction was quenched by the addition of ethyl vinyl ether (1 mL, 10 mmol) and refluxed for additional 15 minutes, followed by the addition of 1 mL DMSO and refluxed for another 15 minutes. The reaction mixture was stirred overnight at room temperature and afterwards concentrated *in vacuo*. The obtained brown oil was purified by column chromatography over silica (ethyl acetate/methanol 100:3 v/v) to obtain the product (340 mg, 36% yield) as an off-white solid.

^{1}H NMR (500 MHz, DMSO-d_6) δ 8.51 – 8.41 (m, J = 23.1, 8.0 Hz, 2H), 5.44 – 5.27 (m, 2H), 4.58 (q, J = 7.9 Hz, 2H), 3.14 – 2.57 (m, 4H), 2.38 – 1.93 (m, 8H). ^{13}C NMR (126 MHz, DMSO-d_6) δ 171.39, 171.34, 128.90, 52.15, 50.84, 35.16, 33.76, 26.62, 23.27. ESI-ToF m/z calculated for $[C_{16}H_{25}N_2O_6S_2]^+$ $[M+H]^+$:405.1154, found: 405.1163; Mp: 185-188 °C.

7.3.2 Polymerization Procedures

7.3.2.1 General Procedure for ADMET Polymerizations of 2a

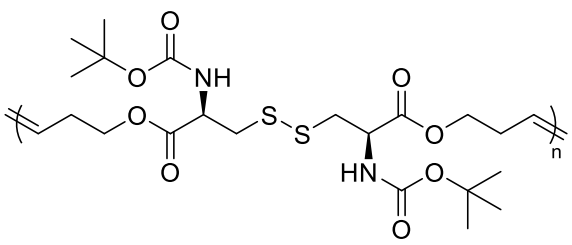

2a was placed in a flask equipped with a condenser and subsequently dissolved in the chosen solvent. To this HG2 and *p*-benzoquinone were added and the resulting solution was heated to the desired temperature. The headspace of the condenser was constantly flushed with nitrogen during the course of the reaction, to remove the ethylene. The reaction was quenched by the addition of an excess of ethyl vinyl ether.

7.3.2.2 Procedure for ED-ROMP

The macrocyclic monomer was placed in a 2.5 mL vial equipped with a stir bar and a septum cap and purged with nitrogen. One half of the total solvent amount was added *via* a syringe and the dispersion was tempered at the afforded reaction temperature. To this dispersion a stock solution containing the G3 (or HG2) catalyst in chloroform was added. The reaction was quenched by the addition of an excess of ethyl vinyl ether and stirred for additional 15 minutes. Purification of the polymers were done by dialysis (Spectra/Por® dialysis tubing, molecular weight cutoff: 3500 Da) against THF or precipitation in cyclohexane.

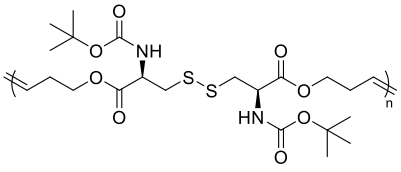

4a ^{1}H NMR (600 MHz, DMSO-d_6) δ 7.43-6.96 (m, 2H), 5.50 (s, 2H), 4.30-4.13 (m, 2H), 4.12-3.98 (m, 4H), 3.13-2.84 (m, 4H), 2.41-2.23 (m, 4H), 1.42-1.32 (m, 18H).

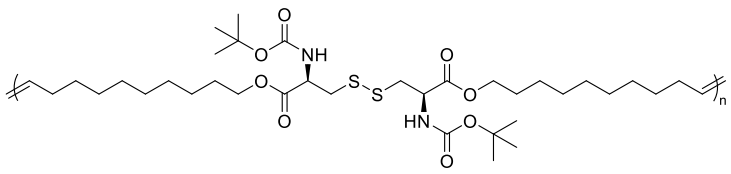

4a' ^{1}H NMR (600 MHz, $CDCl_3$) δ 5.45-5.30 (m, 4H), 4.63-4.51 (m, J = 5.7 Hz, 2H), 4.14 (qt, J = 10.7, 6.8 Hz, 4H), 3.25-2.99 (m, 4H), 2.05-1.91 (m, J = 29.3, 13.7, 8.2 Hz, 4H), 1.70-1.60 (m, 4H), 1.45 (s, 18H), 1.38-1.21 (m, 24H).

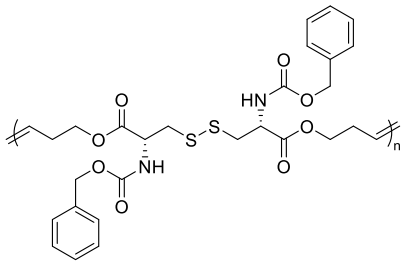

4b ^{1}H NMR (600 MHz, DMSO-*d*$_6$) δ 7.88 (d, *J* = 8.1 Hz, 2H), 7.38 – 7.26 (m, 10H), 5.50 – 5.34 (m, *J* = 28.3 Hz, 2H), 5.10 – 4.97 (m, 4H), 4.39 – 4.31 (m, *J* = 13.5, 8.8 Hz, 2H), 4.09 – 3.93 (m, *J* = 19.8 Hz, 4H), 3.14 – 2.89 (m, 4H), 2.36 – 2.21 (m, 4H).

7.3.2.3 Procedure for ED-RODiMP

The macrocyclic monomers were placed in a 2.5-mL vial equipped a septum cap. One half of the total solvent amount (DMAc, DMSO or GVL) was added via a syringe and the dispersion was tempered at the afforded reaction temperature under shaking. To this, a solution containing MTG and DIPEA (1:1 molar ratio) was added. The polymerizations were quenched by the addition of a dilute solution of acetic acid in dioxane and subsequently freeze dried. Purifications of the polymers were done by multiple precipitations from THF into cyclohexane.

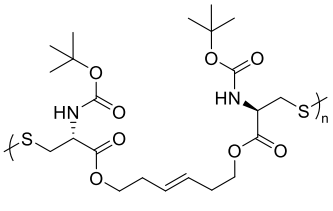

4a^d ^{1}H NMR (500 MHz, $CDCl_3$) δ 5.60 – 5.40 (m, *J* = 2.2 Hz, 4H), 4.67 – 4.36 (m, *J* = 91.7 Hz, 2H), 4.26 – 4.05 (m, *J* = 3.0 Hz, 4H), 3.26 – 3.03 (m, *J* = 4.5 Hz, 4H), 2.50 – 2.31 (m, 4H), 1.45 (s, 18H).

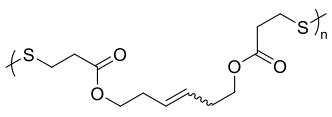

4c^d ^{1}H NMR (500 MHz, $CDCl_3$) δ 5.53 – 5.47 (m, 2H), 4.11 (t, *J* = 6.8 Hz, 4H), 2.92 (t, *J* = 7.2 Hz, 4H), 2.73 (t, *J* = 7.2 Hz, 4H), 2.43 – 2.30 (m, 4H).

7.3.2.4 Disulfide metathesis polymerization towards 4d[d]

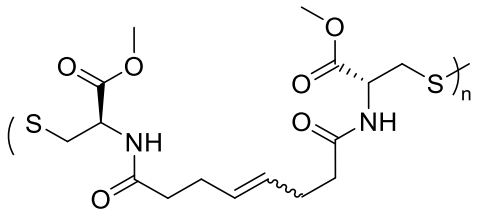

The macrocyclic monomer **3d** (100 mg, 25 mmol) was placed in a 2.5-mL vial equipped with a septum cap. 110 μL DMAc was added and the mixture was tempered at 85 °C under shaking. To this, 100 μL of a stock solution containing MTG (0.01 equiv, 2.5 μmol) and DIPEA (0.01 equiv, 2.5 μmol) in DMAc was added. The polymerization of **3d** was quenched with a 10-fold excess of iodoacetonitrile or methylmaleimide with respect to MTG. The reaction mixture was stirred at 85 °C for 10 minutes and then acetic acid was added. The end-capped polymer **4d[d]** was purified by multiple precipitations from DMF into methyl *tert*-butyl ether.

^{1}H NMR (600 MHz, DMSO-d_6) δ 8.45 – 8.34 (m, J = 7.9 Hz, 2H), 5.47 – 5.25 (m, 2H), 4.54 (td, J = 8.3, 5.3 Hz, 1H), 3.13 – 2.89 (m, 4H), 2.24 – 2.12 (m, 8H).

7.3.3 Post Modifications

7.3.3.1 Deprotection of the Polymers 4a and 4a'

The polymer **4a** (or **4a'**) (20 mg) was placed in a dried 2.5 mL vial equipped with a septum cap followed by the addition of 420 µL 1 M hydrochloric acid in ethyl acetate. The reaction was stirred at room temperature for 2 days. The solvent was removed *in vacuo* and the resulting solid was dispersed in diethyl ether. The solvent was again evaporated to give the deprotected polymer **5a** (or **5a'**).

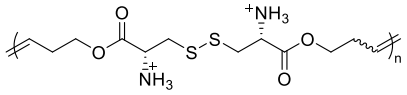

5a ^{1}H NMR (300 MHz, DMSO-d_6) δ 8.97 (bs, 6H), 5.59 (bs, 2H), 4.31 (bs, J = 18.5, 4.9 Hz, 2H), 4.18 (bs, 4H), 3.53-3.12 (bs, 4H), 2.37 (bs, 4H).

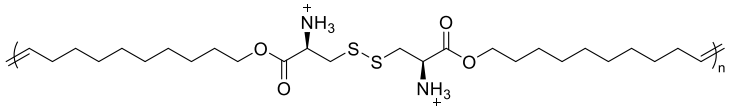

5a' ^{1}H NMR (600 MHz, DMSO-d_6) δ 8.91 (s, 6H), 5.46-5.23 (m, 2H), 4.33 (t, J = 5.5 Hz, 2H), 4.14 (t, J = 6.4 Hz, 4H), 3.46-3.19 (m, 4H), 2.01-1.86 (m, J = 33.6, 9.4 Hz, 4H), 1.68-1.52 (m, 4H), 1.38-1.16 (m, 24H).

7.3.3.2 Post-Polymerization Modification of the Deprotected Polymer 4a with Acid Anhydrides

The polymer **4a** (50 mg) was placed in a dried 4 mL vial equipped with a septum cap. To this, 1.1 mL of 1 M hydrochloric acid in ethyl acetate was added *via* a syringe. The reaction was stirred at room temperature for 2 days. The solvent was evaporated *in vacuo*. The resulting solid was dispersed in 2 ml of DMF. A solution of 670 µL TEA (50 equiv) in 3.2 mL of DMF was prepared in a second 4 mL vial. To this solution acetic anhydride or succinic anhydride was slowly added. An aliquot of 440 µL (correlating to 5 equiv of TEA and 3 equiv of acid anhydride) was taken and added to the deprotected polymer dispersion. After 5 hours the reaction mixture was diluted with THF and water and dialyzed against THF/water 1:1.

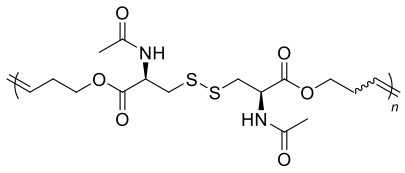

6a ^{1}H NMR (300 MHz, DMSO-d_6) δ 8.41 (d, J = 7.7 Hz, 2H), 5.47 (s, 2H), 4.51 (dd, J = 13.2, 7.9 Hz, 2H), 4.06 (t, J = 6.2 Hz, 4H), 3.14-2.82 (m, 4H), 2.39-2.16 (m, 4H), 1.85 (s, 6H).

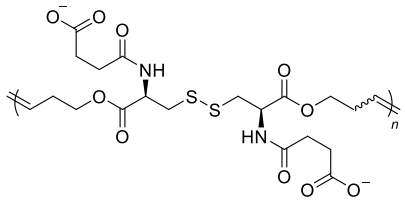

7a ^{1}H NMR (300 MHz, DMSO-d_6) δ 8.63-8.30 (m, 1H), 5.47 (s, 1H), 4.67-4.44 (m, J = 34.9, 6.8 Hz, 1H), 4.29-3.94 (m, 2H), 3.20-2.81 (m, 2H), 2.43-2.12 (m, J = 24.0 Hz, 6H).

7.3.3.3 Reduction of Main-Chain Disulfides

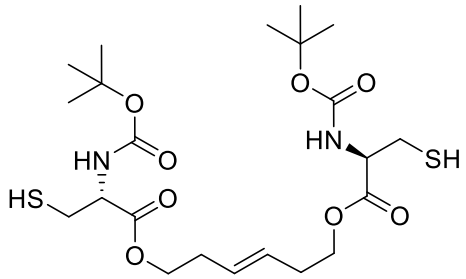

The polymer **4a** (or macrocycle **3a**) (15 mg) was placed in a 2.5 mL vial equipped with a septum cap. 44 mg of DTE and one drop of TEA were dissolved in 200 μL THF. The resulting solution was added to the polymer (or macrocycle). After 10 and 30 minutes an aliquot was taken and diluted to 1.5 mg mL^{-1} and analyzed by SEC. After 30 minutes the reaction was quenched by the addition of an aqueous saturated ammonium chloride solution. The resulting mixture was extracted with DCM and the organic phase was washed with brine and water. The solvent was evaporated *in vacuo*. ^{1}H NMR (600 MHz, CD_3CN) δ 5.78-5.60 (m, 2H), 5.61-5.47 (m, 2H), 5.36-5.28 (m, 1H), 4.42-4.21 (m, 2H), 4.20-4.06 (m, 4H), 2.95-2.79 (m, 4H), 2.45-2.28 (m, 4H), 1.74 (t, J = 8.7 Hz, 2H), 1.42 (s, 18H).

8 References

(1) Kovats, S.; Depledge, M.; Haines, A.; Fleming, L. E.; Wilkinson, P.; Shonkoff, S. B.; Scovronick, N. *Lancet* **2014**, *383* (9919), 757–758.

(2) Hill, M. *Lancet* **2014**, *383* (9936), 2211–2212.

(3) Robertson, C. Search Continues after Oil Rig Blast http://www.nytimes.com/2010/04/22/us/22rig.html (accessed Nov 9, 2017).

(4) Gaskill, M. *Nature* **2011**.

(5) PlasticsEurope. *Plastics – the Facts 2016*; 2016.

(6) Bajaj, I.; Singhal, R. *Bioresour. Technol.* **2011**, *102* (10), 5551–5561.

(7) Deming, T. J. *Advances in Polymer Science*. Springer-Verlag: Berlin/Heidelberg 2006, pp 1–18.

(8) Sanda, F.; Endo, T. *Macromol. Chem. Phys.* **1999**, *200* (12), 2651–2661.

(9) Sanda, F.; Nakamura, M.; Endo, T.; Takata, T.; Handa, H. *Macromolecules* **1994**, *27* (26), 7928–7929.

(10) Sanda, F.; Ogawa, F.; Endo, T. *Polymer* **1998**, *39* (22), 5543–5547.

(11) Mori, H.; Endo, T. *Macromol. Rapid Commun.* **2012**, *33* (13), 1090–1107.

(12) Skey, J.; O'Reilly, R. K. *J. Polym. Sci. Part A Polym. Chem.* **2008**, *46* (11), 3690–3702.

(13) Lu, A.; Smart, T. P.; Epps, T. H.; Longbottom, D. A.; O'Reilly, R. K. *Macromolecules* **2011**, *44* (18), 7233–7241.

(14) Conrad, R. M.; Grubbs, R. H. *Angew. Chemie - Int. Ed.* **2009**, *48* (44), 8328–8330.

(15) Kammeyer, J. K.; Blum, A. P.; Adamiak, L.; Hahn, M. E.; Gianneschi, N. C.; Tirrell, D. A.; Grubbs, R. H.; Cameron, N. R. *Polym. Chem.* **2013**, *4* (14), 3929.

(16) Sutthasupa, S.; Sanda, F.; Masuda, T. *Macromol. Chem. Phys.* **2008**, *209* (9), 930–937.

(17) Roweton, S.; Huang, S.; Swift, G. *J. Environ. Polym. Degrad.* **1997**, *5* (3), 175–181.

(18) Faghihi, K.; Hajibeygi, M.; Shabanian, M. *Macromol. Res.* **2009**, *17* (10), 739–745.

(19) Xing, T.; Lai, B.; Ye, X.; Yan, L. *Macromol. Biosci.* **2011**, *11* (7), 962–969.

(20) Sun, J.; Chen, X.; Lu, T.; Liu, S.; Tian, H.; Guo, Z.; Jing, X. *Langmuir* **2008**, *24* (18), 10099–10106.

(21) Anantharaj, S.; Jayakannan, M. *J. Polym. Sci. Part A Polym. Chem.* **2016**, *54* (18), 2864–2875.

(22) Herisson, J.-L.; Chauvin, Y. *Makromol. Chem.* **1971**, *141* (9), 161–176.

(23) Calderon, N.; Chen, H. Y.; Scott, K. W. *Tetrahedron Lett.* **1967**, *8* (34), 3327–3329.

(24) Nguyen, S. T. B. T.; Johnson, L. K.; Grubbs, R. H.; Ziller, J. W. *J. Am. Chem. Soc.* **1992**, *114* (10), 3974–3975.

(25) Chauvin, Y.; Grubbs, R. H.; Schrock, R. R. The Nobel Prize in Chemistry 2005 http://www.nobelprize.org/nobel_prizes/chemistry/laureates/2005/index.html (accessed Jun 27, 2017).

(26) Herbert, M. B.; Grubbs, R. H. *Angew. Chemie - Int. Ed.* **2015**, *54* (17), 5018–5024.

(27) Stewart, I. C.; Douglas, C. J.; Grubbs, R. H. *Org. Lett.* **2008**, *10* (3), 441–444.

(28) Buchmeiser, M. R. *Chem. Rev.* **2009**, *109* (2), 303–321.

(29) Velazquez, H. D.; Verpoort, F. *Chem. Soc. Rev.* **2012**, *41* (21), 7032.

(30) Sutthasupa, S.; Shiotsuki, M.; Sanda, F. *Polym. J.* **2010**, *42* (12), 905–915.

(31) Robert, T.; Friebel, S. *Green Chem.* **2016**, *18* (10), 2922–2934.

(32) Bai, Y.; De bruyn, M.; Clark, J. H.; Dodson, J. R.; Farmer, T. J.; Honoré, M.; Ingram, I. D. V.; Naguib, M.; Whitwood, A. C.; North, M. *Green Chem.* **2016**, *18* (14), 3945–3948.

(33) Türünç, O.; Meier, M. a. R. *Green Chem.* **2011**, *13* (2), 314.

(34) Lv, A.; Li, Z. L.; Du, F. S.; Li, Z. C. *Macromolecules* **2014**, *47* (22), 7707–7716.

(35) Hopkins, T. E.; Pawlow, J. H.; Koren, D. L.; Deters, K. S.; Solivan, S. M.; Davis, J. A.; Gómez, F. J.; Wagener, K. B. *Macromolecules* **2001**, *34* (23), 7920–7922.

(36) Terada, K.; Berda, E. B.; Wagener, K. B.; Sanda, F.; Masuda, T. *Macromolecules* **2008**, *41* (16), 6041–6046.

(37) Führer, F. N.; Schlaad, H. *Macromol. Chem. Phys.* **2014**, *215* (22), 2268–2273.

(38) Peres, L. B.; Preiss, L. C.; Wagner, M.; Wurm, F. R.; De Araújo, P. H. H.; Landfester, K.; Muñoz-Espí, R.; Sayer, C. *Macromolecules* **2016**, *49* (18), 6723–6730.

(39) Choi, T. L.; Chatterjee, A. K.; Grubbs, R. H. *Angew. Chemie - Int. Ed.* **2001**, *40*

(7), 1277–1279.

(40) Fürstner, A.; Langemann, K. *J. Am. Chem. Soc.* **1997**, *119* (39), 9130–9136.

(41) Fava, A.; Iliceto, A.; Camera, E. *J. Am. Chem. Soc.* **1957**, *79* (4), 833–838.

(42) Fernandes, P. A.; Ramos, M. J. *Chem. - A Eur. J.* **2004**, *10* (1), 257–266.

(43) Bach, R. D.; Dmitrenko, O.; Thorpe, C. *J. Org. Chem.* **2008**, *73* (1), 12–21.

(44) Nagy, P. *Antioxid. Redox Signal.* **2013**, *18* (13), 1623–1641.

(45) Winterbourn, C. C.; Hampton, M. B. *Free Radic. Biol. Med.* **2008**, *45* (5), 549–561.

(46) Singh, R.; Whitesides, G. M. In *The Chemistry of Sulphur-Containing Functional Groups*; John Wiley & Sons, Inc.: Chichester, UK, 1993; pp 633–658.

(47) Gamcsik, M.; Kasibhatla, M.; Teeter, S.; Colvin, O. *Biomarkers* **2012**, *17* (8), 671–691.

(48) Torres, A. G.; Gait, M. J. *Trends Biotechnol.* **2012**, *30* (4), 185–189.

(49) Gasparini, G.; Bang, E.-K. K.; Molinard, G.; Tulumello, D. V.; Ward, S.; Kelley, S. O.; Roux, A.; Sakai, N.; Matile, S. *J. Am. Chem. Soc.* **2014**, *136* (16), 6069–6074.

(50) Feillée, N.; Chemtob, A.; Ley, C.; Croutxé-Barghorn, C.; Allonas, X.; Ponche, A.; Le Nouen, D.; Majjad, H.; Jacomine, L. *Macromol. Rapid Commun.* **2016**, *37* (2), 155–160.

(51) Whistler, R. L.; Hoffman, D. J. *J. Polym. Sci. Part A Polym. Chem.* **1967**, *5* (8), 2111–2117.

(52) Marvel, C. S.; Olson, L. E. *J. Am. Chem. Soc.* **1957**, *79* (12), 3089–3091.

(53) Rosenthal, E. Q.; Puskas, J. E.; Wesdemiotis, C. *Biomacromolecules* **2012**, *13* (1), 154–164.

(54) Lin, C.; Zhong, Z.; Lok, M. C.; Jiang, X.; Hennink, W. E.; Feijen, J.; Engbersen, J. F. J. *J. Control. Release* **2007**, *123* (1), 67–75.

(55) Ou, M.; Wang, X.-L.; Xu, R.; Chang, C.-W.; Bull, D. A.; Kim, S. W. *Bioconjug. Chem.* **2008**, *19* (3), 626–633.

(56) Lin, C.; Engbersen, J. F. *Expert Opin. Drug Deliv.* **2009**, *6* (4), 421–439.

(57) Meng, F.; Hennink, W. E.; Zhong, Z. *Biomaterials* **2009**, *30* (12), 2180–2198.

(58) Phillips, D. J.; Gibson, M. I. *Biomacromolecules* **2012**, *13* (10), 3200–3208.

(59) Sakai, N.; Matile, S. *J. Am. Chem. Soc.* **2011**, *133* (46), 18542–18545.

(60) Lista, M.; Areephong, J.; Sakai, N.; Matile, S. *J. Am. Chem. Soc.* **2011**, *133* (39),

15228–15231.

(61) Sakai, N.; Lista, M.; Kel, O.; Sakurai, S.-I.; Emery, D.; Mareda, J.; Vauthey, E.; Matile, S. *J. Am. Chem. Soc* **2011**, *133* (39), 15224–15227.

(62) Ishida, H.; Kisanuki, A.; Endo, K. *Polym. J.* **2009**, *41* (2), 110–117.

(63) Endo, K.; Shiroi, T.; Murata, N.; Kojima, G.; Yamanaka, T. *Macromolecules* **2004**, *37* (9), 3143–3150.

(64) Sadownik, A.; Stefely, J.; Regen, S. L. *J. Am. Chem. Soc.* **1986**, *108* (24), 7789–7791.

(65) Stefely, J.; Markowitz, M. A.; Regen, S. L. *J. Am. Chem. Soc.* **1988**, *110* (22), 7463–7469.

(66) Illuminati, G.; Mandolini, L. *Acc. Chem. Res.* **1981**, *14* (4), 95–102.

(67) Liebman, J. F.; Greenberg, A. *Chem. Rev.* **1976**, *76* (3), 311–365.

(68) Jacobson, H.; Stockmayer, W. H. *J. Chem. Phys.* **1950**, *18* (12), 1600–1606.

(69) Hodge, P. *Chem. Rev.* **2014**, *114* (4), 2278–2312.

(70) Goodman, I.; Nesbitt, B. F. *J. Polym. Sci.* **1960**, *48* (150), 423–433.

(71) Youk, J. H.; Kambour, R. P.; MacKnight, W. J. *Macromolecules* **2000**, *33* (10), 3594–3599.

(72) Van Der Meulen, I.; Gubbels, E.; Huijser, S.; Sablong, R.; Koning, C. E.; Heise, A.; Duchateau, R. *Macromolecules* **2011**, *44* (11), 4301–4305.

(73) Focarete, M. L.; Scandola, M.; Kumar, A.; Gross, R. A. *J. Polym. Sci. Part B Polym. Phys.* **2001**, *39* (15), 1721–1729.

(74) Memeger, W.; Lazar, J.; Ovenall, D.; Leach, R. A. *Macromolecules* **1993**, *26* (14), 3476–3484.

(75) Weiss, R. M.; Short, A. L.; Meyer, T. Y. *ACS Macro Lett.* **2015**, *4* (9), 1039–1043.

(76) Tastard, C. Y.; Hodge, P.; Ben-Haida, A.; Dobinson, M. *React. Funct. Polym.* **2006**, *66* (1), 93–107.

(77) Kang, S.; Berkshire, B. M.; Xue, Z.; Gupta, M.; Layode, C.; May, P. A.; Mayer, M. F. *J. Am. Chem. Soc.* **2008**, *130* (46), 15246–15247.

(78) Xue, Z.; Mayer, M. F. *Soft Matter* **2009**, *5* (23), 4600.

(79) Marsella, M. J.; Maynard, H. D.; Grubbs, R. H. *Angew. Chemie Int. Ed. English* **1997**, *36* (10), 1101–1103.

(80) Maynard, H. D.; Grubbs, R. H. *Macromolecules* **1999**, *32* (21), 6917–6924.

(81) Gautrot, J. E.; Zhu, X. X. *Macromolecules* **2009**, *42* (19), 7324–7331.

(82) Gao, W.; Hagver, R.; Shah, V.; Xie, W.; Gross, R. A.; Ilker, M. F.; Bell, C.; Burke, K. A.; Coughlin, E. B. *Macromolecules* **2007**, *40* (2), 145–147.

(83) Gutekunst, W. R.; Hawker, C. J. *J. Am. Chem. Soc.* **2015**, *137* (25), 8038–8041.

(84) Song, L. N.; Xiao, M.; Shu, D.; Wang, S. J.; Meng, Y. Z. *J. Mater. Sci.* **2007**, *42* (4), 1156–1161.

(85) Regen, S. L.; Samuel, N. K. P.; Khurana, J. M. *Journal of the American Chemical Society*. October 1985, pp 5804–5805.

(86) Deiters, A.; Martin, S. F. *Chem. Rev.* **2004**, *104* (5), 2199–2238.

(87) Gradillas, A.; Pérez-Castells, J. *Angew. Chemie - Int. Ed.* **2006**, *45* (37), 6086–6101.

(88) Monfette, S.; Fogg, D. E. *Chem. Rev.* **2009**, *109* (8), 3783–3816.

(89) Hong, S. H.; Sanders, D. P.; Lee, C. W.; Grubbs, R. H. *J. Am. Chem. Soc.* **2005**, *127* (49), 17160–17161.

(90) Fokou, P. A.; Meier, M. A. R. *Macromol. Rapid Commun.* **2010**, *31* (4), 368–373.

(91) Ahn, Y. M.; Yang, K.; Georg, G. I. *Org. Lett.* **2001**, *3* (9), 1411–1413.

(92) Skowerski, K.; Białecki, J.; Tracz, A.; Olszewski, T. K. *Green Chem.* **2014**, *16* (3), 1125.

(93) Marcovici-Mizrahi, D.; Gottlieb, H. E.; Marks, V.; Nudelman, A. *J. Org. Chem.* **1996**, *61* (24), 8402–8406.

(94) Kost, D.; Kornberg, N. *Tetrahedron Lett.* **1978**, *19* (35), 3275–3276.

(95) Anderson, D. R.; Ung, T.; Mkrtumyan, G.; Bertrand, G.; Grubbs, R. H.; Schrodi, Y. *Organometallics* **2008**, *27* (4), 563–566.

(96) Choi, T. L.; Grubbs, R. H. *Angew. Chemie - Int. Ed.* **2003**, *42* (15), 1743–1746.

(97) Love, J. A.; Morgan, J. P.; Trnka, T. M.; Grubbs, R. H. *Angew. Chemie - Int. Ed.* **2002**, *41* (21), 4035–4037.

(98) Chang, C. C.; Emrick, T. *Macromolecules* **2014**, *47* (4), 1344–1350.

(99) Zhang, X.; Waymouth, R. M. *J. Am. Chem. Soc.* **2017**, *139* (10), 3822–3833.

(100) Wheeler, P.; Phillips, J. H.; Pederson, R. L. *Org. Process Res. Dev.* **2016**, *20* (7), 1182–1190.

(101) Gu, Y.; Jérôme, F. *Chem. Soc. Rev.* **2013**, *42* (24), 9550.

(102) Fritze, U. F.; von Delius, M. *Chem. Commun.* **2016**, *52* (38), 6363–6366.

(103) Menger, F. M.; Caran, K. L. *J. Am. Chem. Soc.* **2000**, *122* (47), 11679–11691.

(104) Forman, G. S.; McConnell, A. E.; Tooze, R. P.; Janse Van Rensburg, W.; Meyer, W. H.; Kirk, M. M.; Dwyer, C. L.; Serfontein, D. W. *Organometallics* **2005**, *24* (19), 4528–4542.

(105) Schmidt, B.; Hauke, S. *Org. Biomol. Chem.* **2013**, *11* (25), 4194.

(106) Gibson, F. S.; Bergmeier, S. C.; Rapoport, H. *J. Org. Chem.* **1994**, *59* (11), 3216–3218.

9 Appendix I: Additional Reactions and Results

9.1 Stability Test of *n*-Butyl Acetate under Disulfide Metathesis Conditions

A mixture of *n*-butyl acetate (2.8 mL), MTG (0.19 mL), and DIPEA (0.36 mL) in a 4-mL vial equipped with septum cap was stirred for 1 h at 85 °C. ^{1}H NMR analysis indicated that no reaction under formation of a thioester occurred.

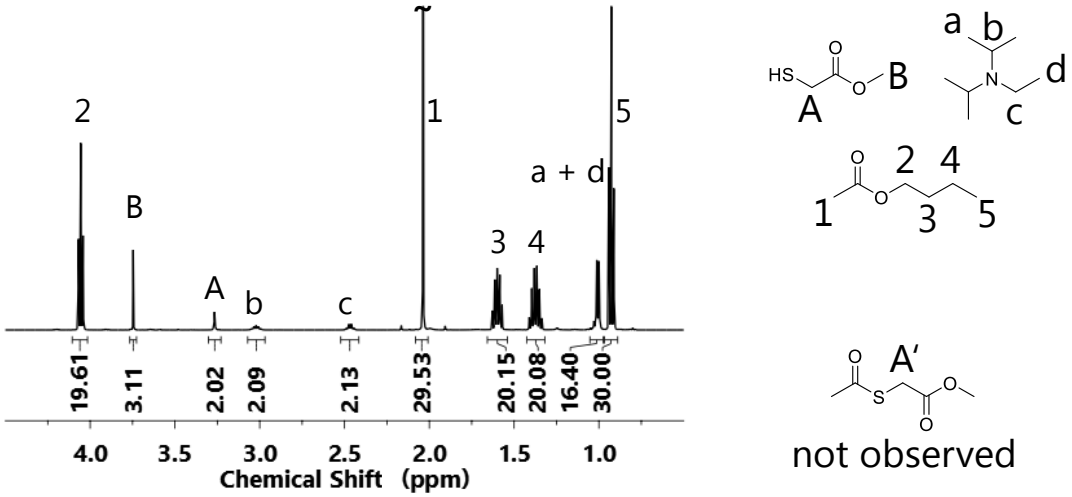

Appendix I, 1: ^{1}H NMR spectrum (500 MHz, $CDCl_3$) of *n*-butyl acetate under disulfide metathesis conditions.

9.2 Additives in the RCM of 2a'

Four small scale experiments have been done to investigate the impact of a phenol addition to the RCM of **2a'**.

Four times 15 mg of **2a'** (1 equiv, 20 μmol) and 1 mg HG2 (~0.1 equiv, 16 μmol) were placed in 4 mL vials equipped with a septum cap. The corresponding additives (1 mg *p*-benzoquinone (9 μmol) and 4 mg phenol (43 μmol)) were added and the

resulting mixtures were dissolved in 2.5 mL of toluene. The solutions were heated to 70 °C. The build-up pressures were released by puncturing the septa with a cannula. The solutions were stirred at 70 °C for 22 h and subsequently quenched by the addition of an excess of ethyl vinyl ether. The crude mixtures were analyzed by ^{1}H-NMR spectroscopy.

Table 7: Used additives in the RCM of **2a'**.

Entry	Reaction	*p*-Bq	Phenol	Conversion [%]
1	**A**	-	-	59
2	**B**	+	-	51
3	**C**	-	+	55
4	**D**	+	+	52

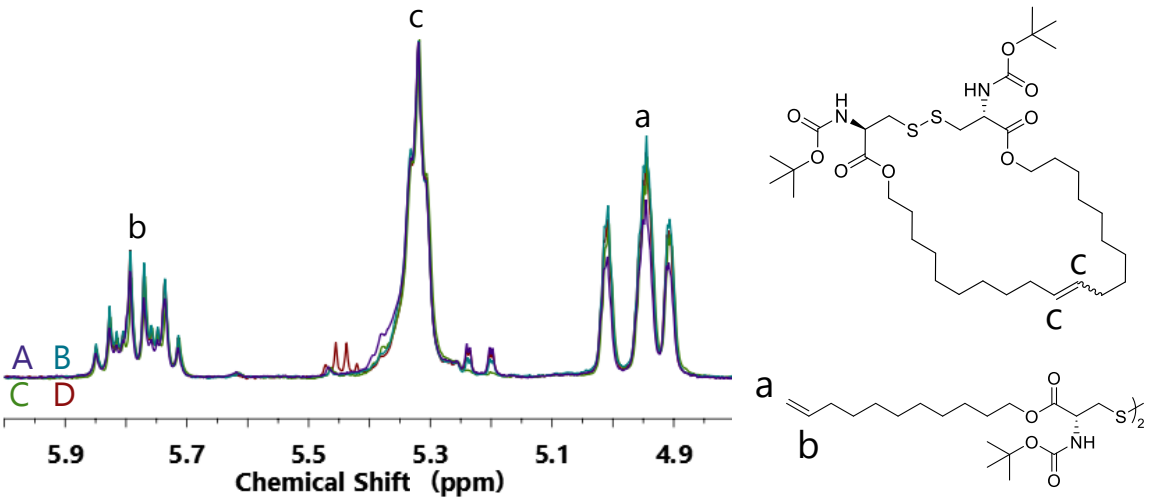

Appendix I, 2: Double bond region (4.8-6.0 ppm) of the ^{1}H-NMR spectra (300 MHz, DMSO-d_6) of the attempted RCM of **2a'**; A (purple), B (turquoise), C (green), and D (red).

9.3 Comparison of Method 1 and 2

In multiple entropy-driven polymerizations of **3a** the monomer conversion and the M_n^{app} were analyzed according to method 1 as well as to method 2. The results are compared in the following tables (Table 8 and Table 9).

Table 8: Comparison of the M_n^{app} obtained by method 1 and 2.

Entry	Method 1 [kDa]	Method 2 [kDa]	$\frac{M_w^{app}(1)}{M_w^{app}(2)}$
1	78	73	1.07
2	57	54	1.06
3	56	60	0.93
4	58	53	1.09
5	184	177	1.04
6		Average:	1.04

Table 9: Comparison of the monomer conv. obtained by method 1 and 2.

Entry	Method 1 [%]	Method 2 [%]	$\frac{conv.(1)}{conv.(2)}$
1	79	76	1.04
2	78	77	1.01
3	66	61	1.08
4	22	21	1.05
5		Average:	1.05

9.4 Polymerization *via* Homolytic Cleavage

50 mg of **3a** (0.1 mmol) were placed in a 2.5-mL vial equipped with a septum cap, followed by the addition of 80 µL $CHCl_3$. The resulting solution was sonicated in an ultrasonic bath at 40 °C for 16 h. Ultra-sonication was done in a bandelin sonorex RK 100 H with an ultrasonic frequency of 35 Hz and an ultrasonic output of 80 W**.** No polymer was detected with SEC analysis.

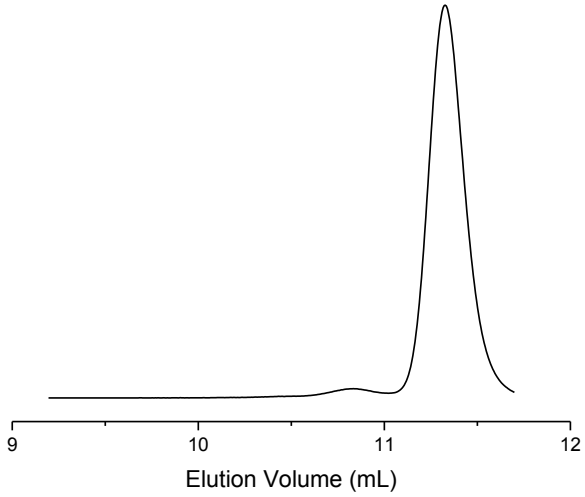

Appendix I, 3: SEC-RI trace of the attempted polymerization of **3a** using ultra-sonication.

9.5 Deprotection of the macrocycle 3a

20 mg of **3a** were placed in a dried 2.5 mL vial equipped with a septum cap. To this, 420 μL of 1 M hydrochloric acid in ethyl acetate was added *via* a syringe. The reaction was stirred at room temperature overnight. The solvent was evaporated *in vacuo* and the resulting solid was dispersed in diethyl ether. The solvent was again evaporated. ^{1}H NMR of the product revealed a conversion to **3e** of 98% (Appendix I, 4). ^{1}H NMR (600 MHz, DMSO-d_6) δ 8.92 (s, 6H), 5.62-5.45 (m, J = 37.6 Hz, 2H), 4.34-4.23 (m, 4H), 4.22-4.13 (m, 2H), 3.27 (ddd, J = 18.3, 14.3, 6.0 Hz, 4H), 2.46-2.29 (m, J = 56.6 Hz, 4H).

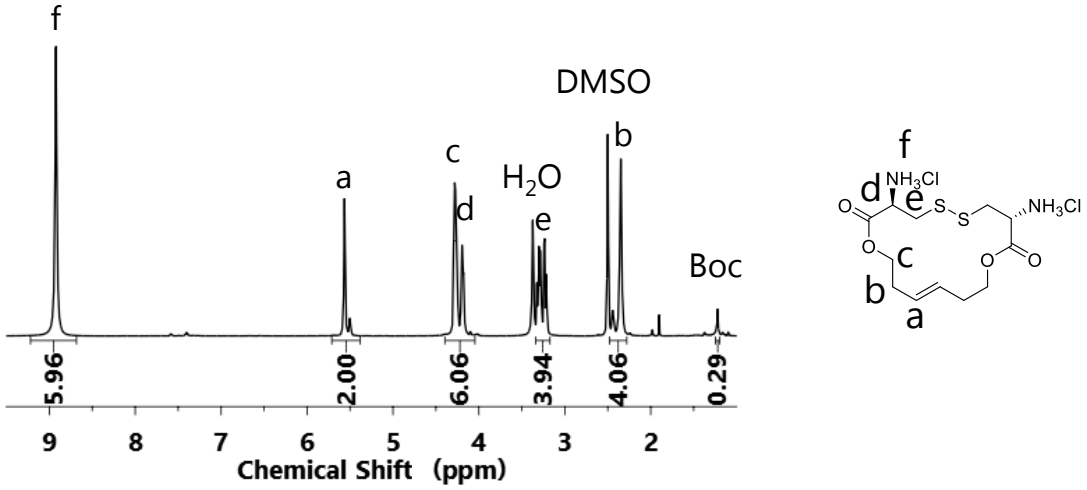

Appendix I, 4: ^{1}H NMR spectrum (600 MHz, DMSO-d_6) of the macrocycle **3e**.

9.6 Further ADMET polymerization attempts

Further ADMET attempts were conducted, under reduced pressure, with 55 mg **2a** (1 equiv, 0.1 mmol) and 3.6 mg HG2 (0.05 equiv, 5 μmol) in 4 mL vials equipped with a septum cap. The polymerizations were performed in (a) bulk, (b) in 4 drops of DMF, or (c) in 2 drops of o-xylene. The polymerization mixtures were heated to 100°C for two days and subsequently quenched by the addition of ethyl vinyl ether at 40 °C. The conversions were determined by ^{1}H NMR analysis of the crude polymerization attempts (Appendix I, 5). Conversions were 48%, 59%, and 79% for a), b), and c), respectively.

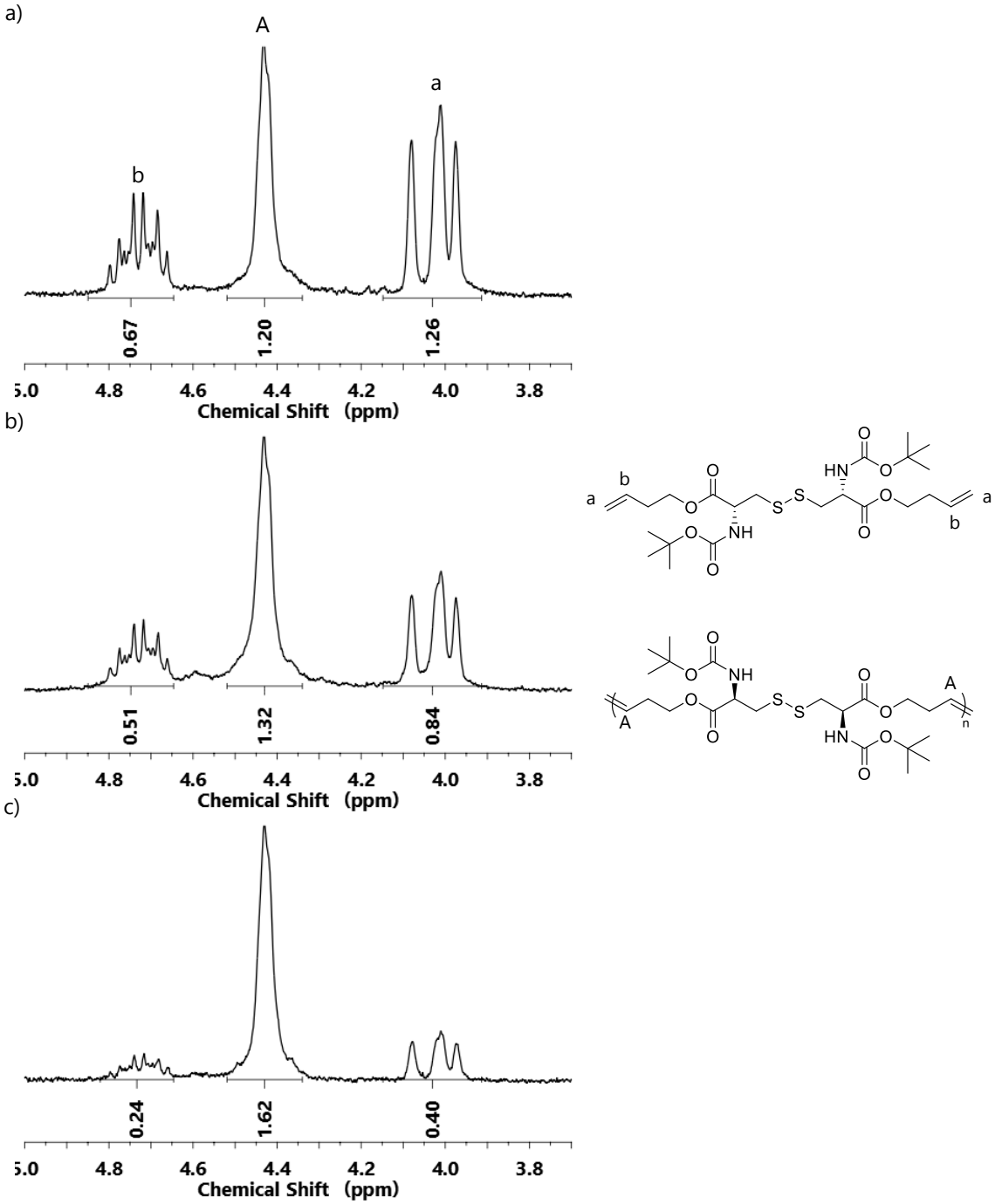

Appendix I, 5: ^{1}H NMR spectra of ADMET attempts of **2a**, showing the signals of the terminal and internal double bonds: (a) bulk polymerization, (b) in 4 drops of DMF, and (c) in 2 drops of *o*-xylene.

10 Appendix II:
Spectra and Analytical Data

10.1 NMR Spectra

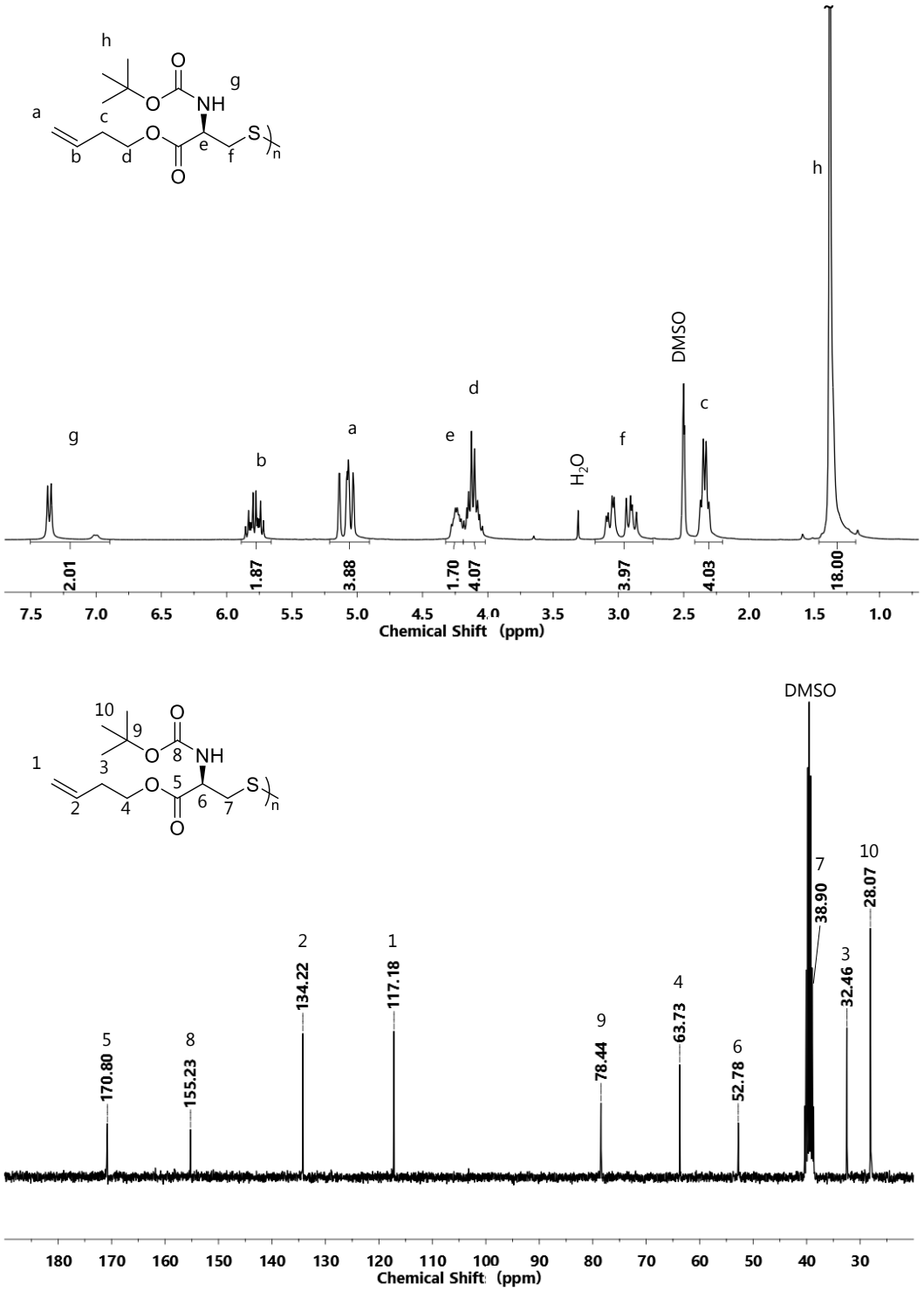

Appendix II, 1: NMR spectra of **2a** in DMSO-d_6: (top) ^{1}H NMR, 300 MHz and (bottom) ^{13}C NMR, 75 MHz.

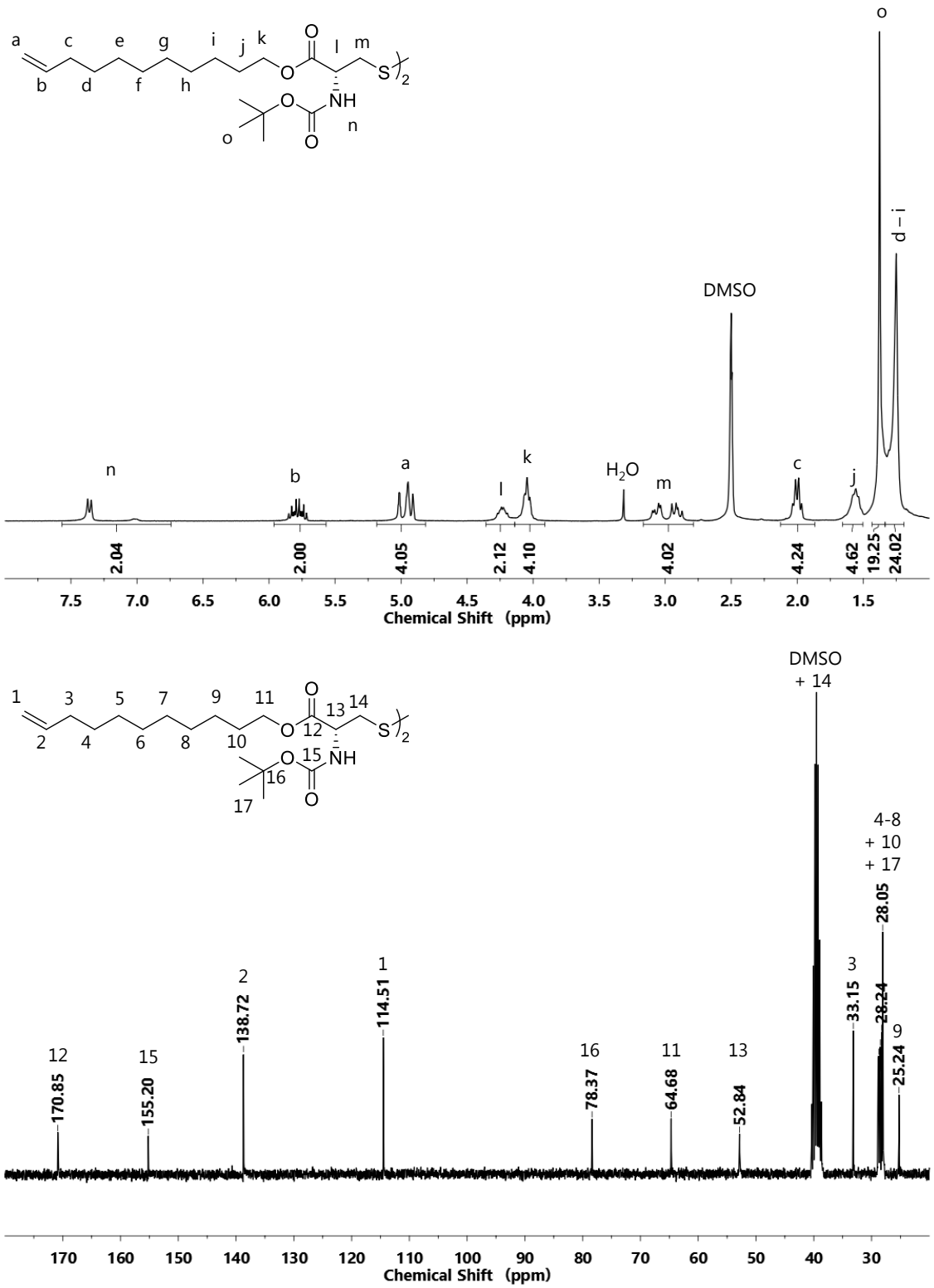

Appendix II, 2: NMR spectra of **2a'** in DMSO-d_6: (top) ^{1}H NMR, 300 MHz and (bottom) ^{13}C NMR, 75 MHz.

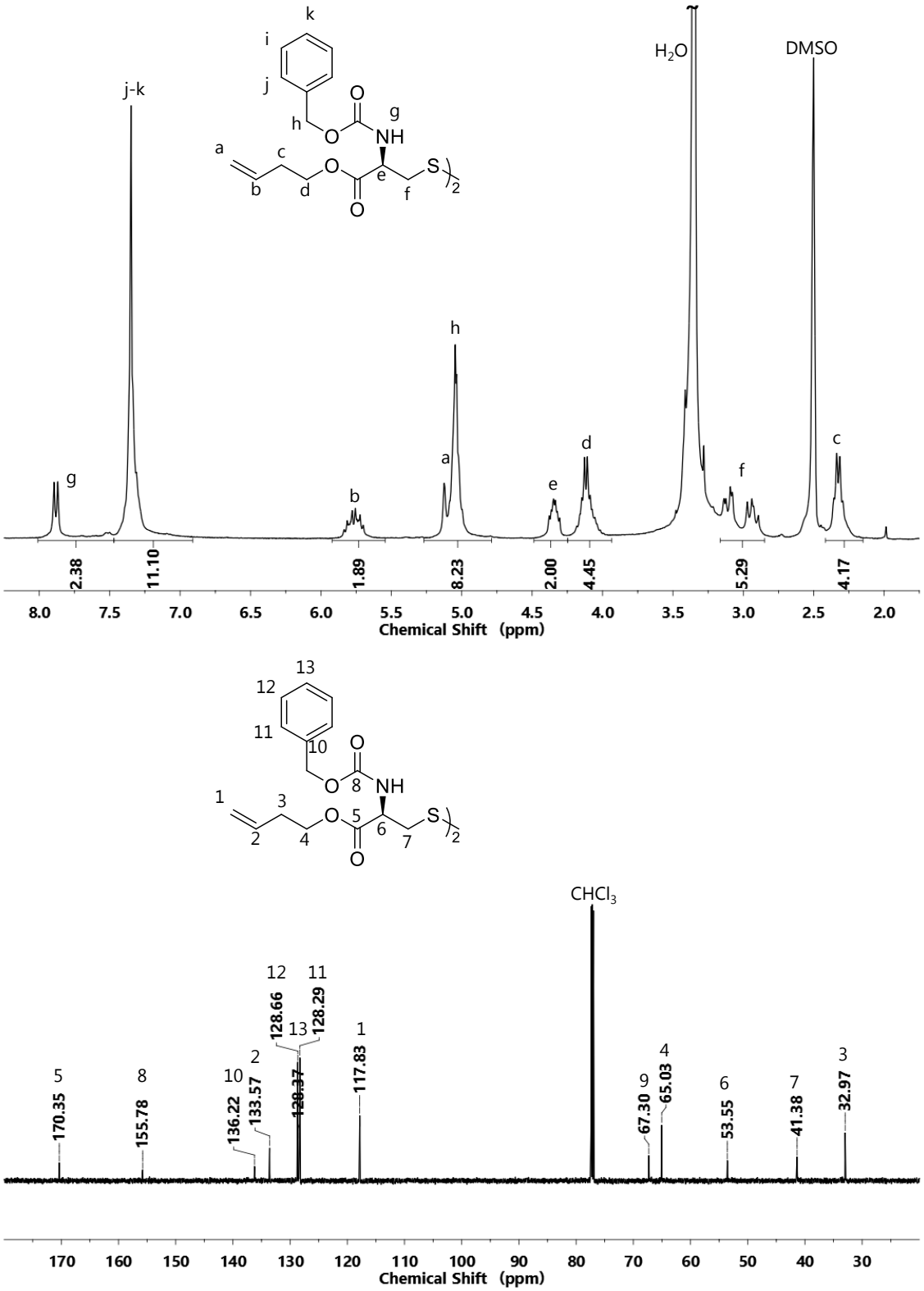

Appendix II, 3: NMR spectra of **2b**: (top) ^{1}H NMR, 300 MHz in DMSO-d_6 and (bottom) ^{13}C NMR, 151 MHz in $CDCl_3$.

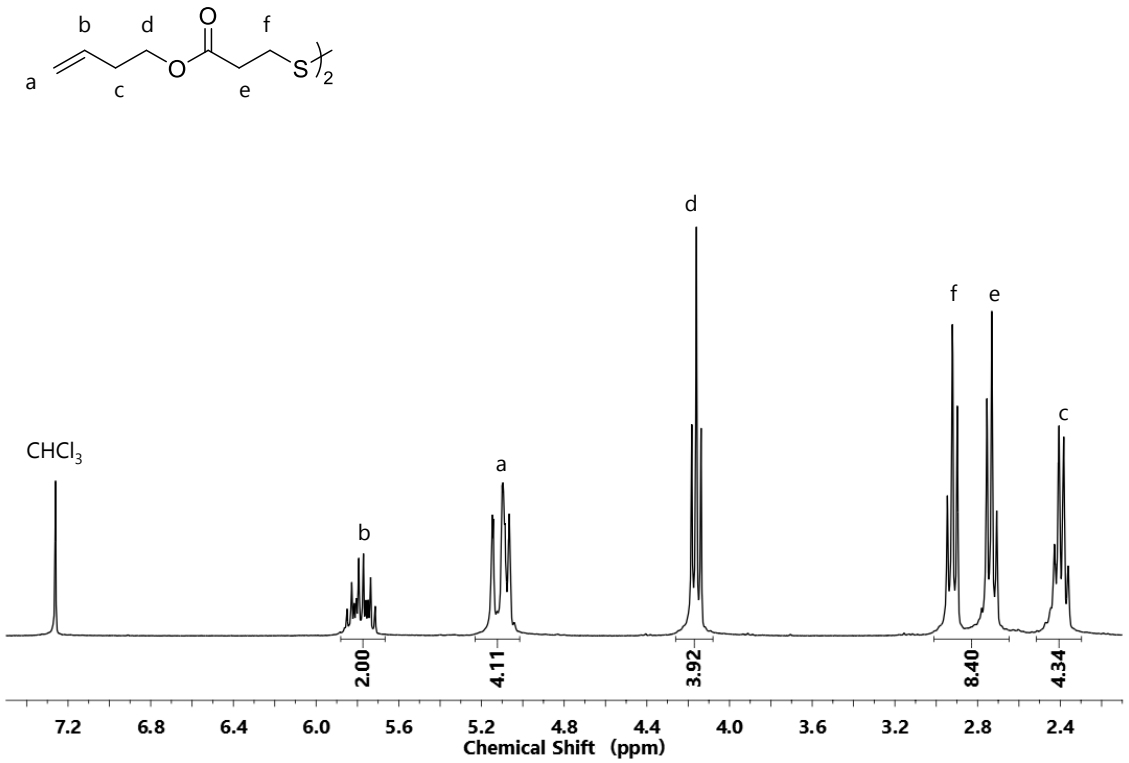

Appendix II, 4: ^{1}H NMR (300 MHz, $CDCl_3$) of **2c**.

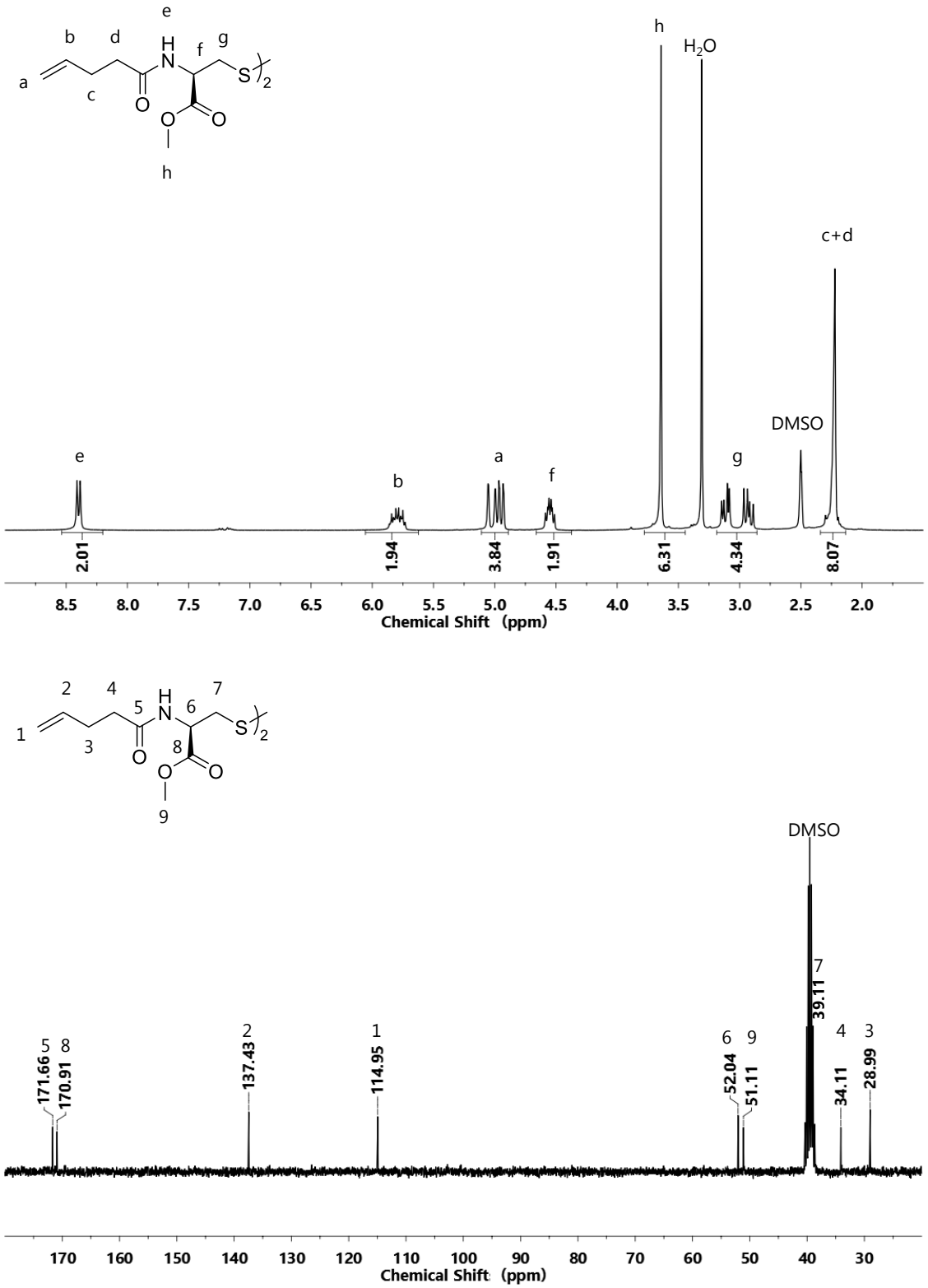

Appendix II, 5: NMR spectra of **2d** in DMSO-d_6: (top) ^{1}H NMR, 300 MHz and (bottom) ^{13}C NMR, 75 MHz.

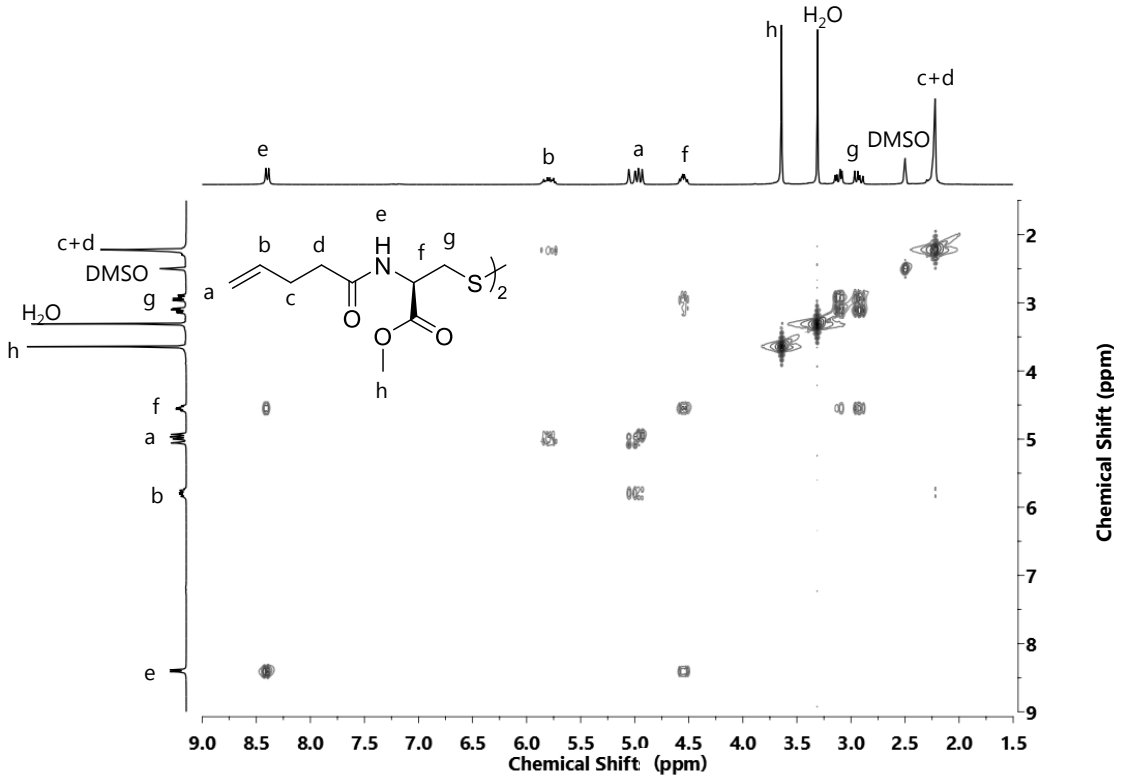

Appendix II, 6: $^{1}H,^{1}H$ COSY NMR spectrum (300 MHz, DMSO-d_6) of **2d**.

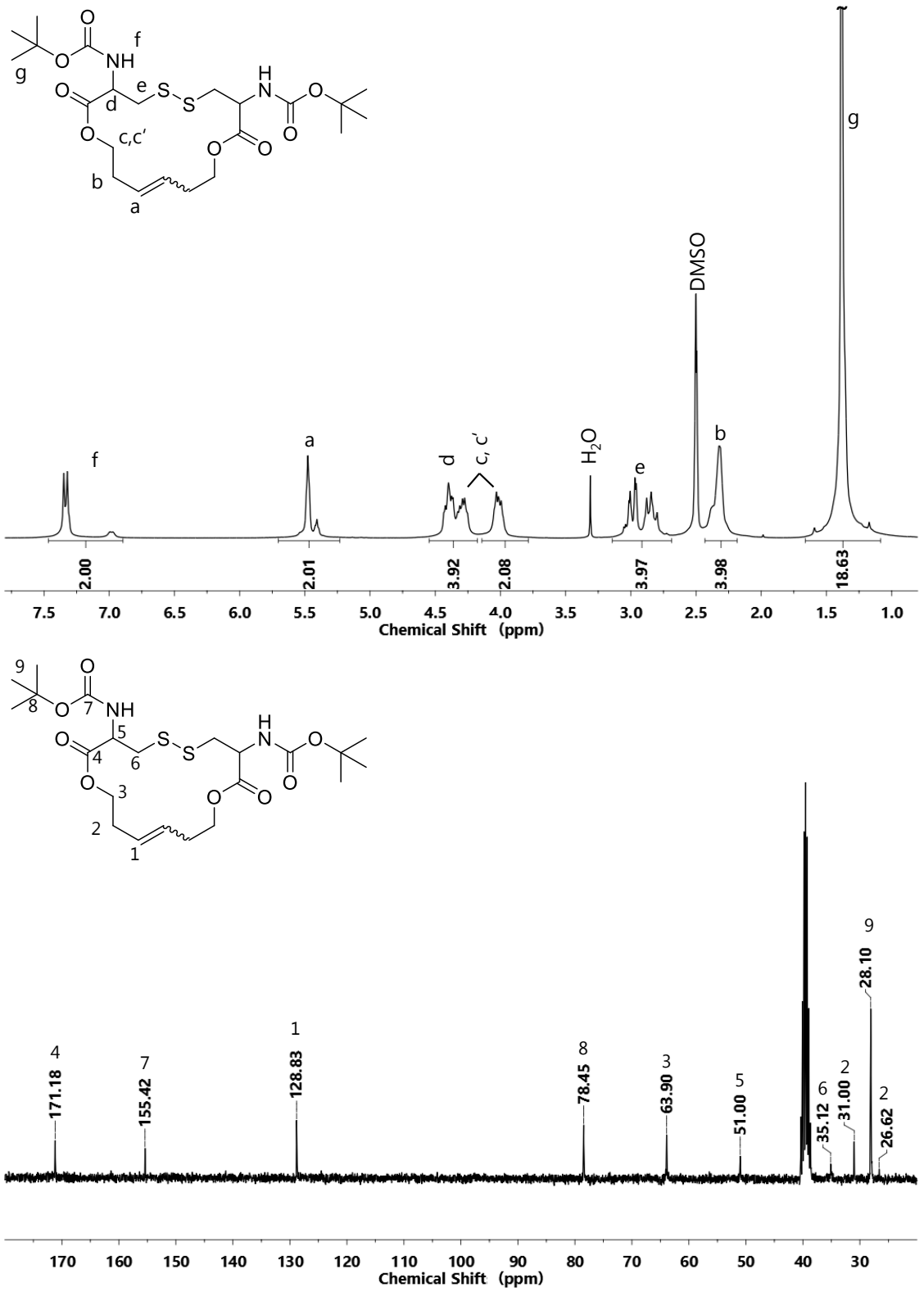

Appendix II, 7: NMR spectra of **3a** in DMSO-d_6: (top) ^{1}H NMR, 300 MHz and (bottom) ^{13}C NMR, 75 MHz.

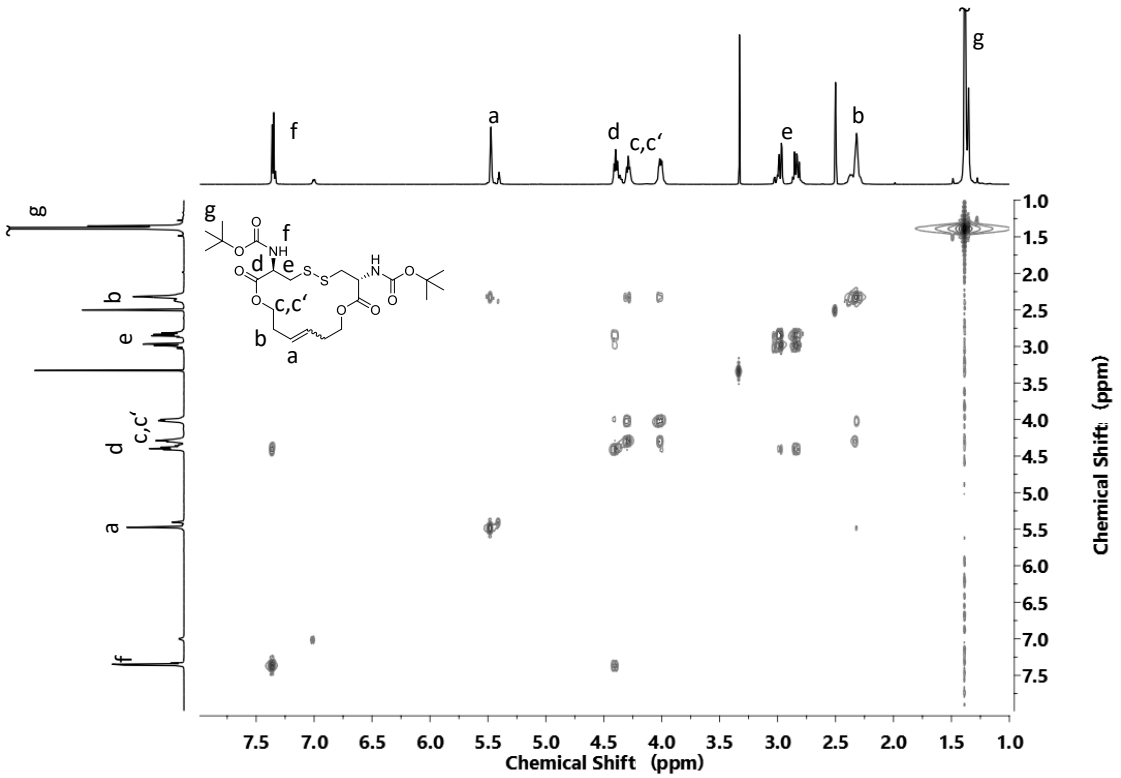

Appendix II, 8: ^{1}H,^{1}H COSY NMR spectrum (600 MHz, DMSO-*d*$_6$) of **3a**.

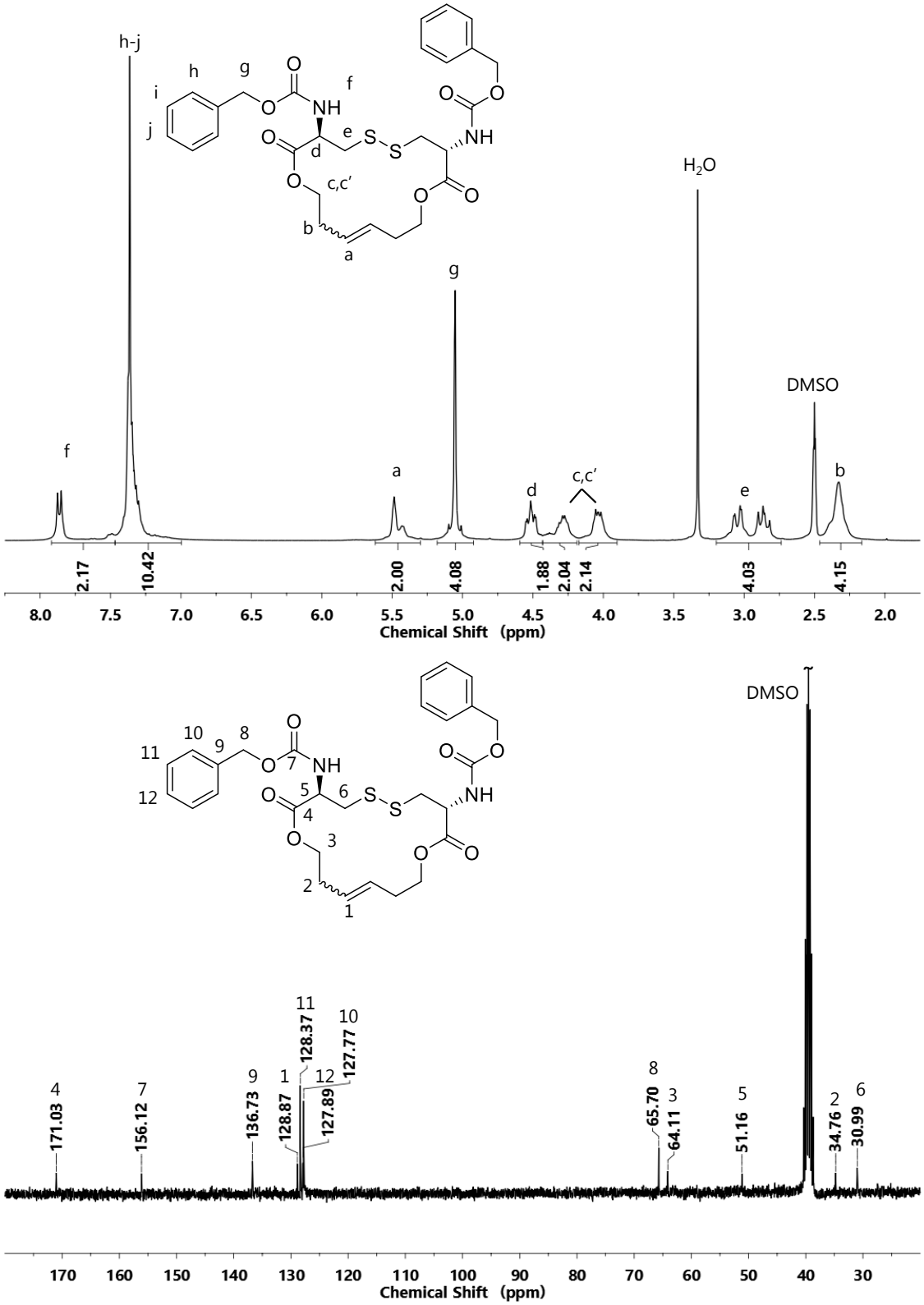

Appendix II, 9: NMR spectra of **3b** in DMSO-*d*$_6$: (top) ^{1}H NMR, 300 MHz and (bottom) ^{13}C NMR, 75 MHz.

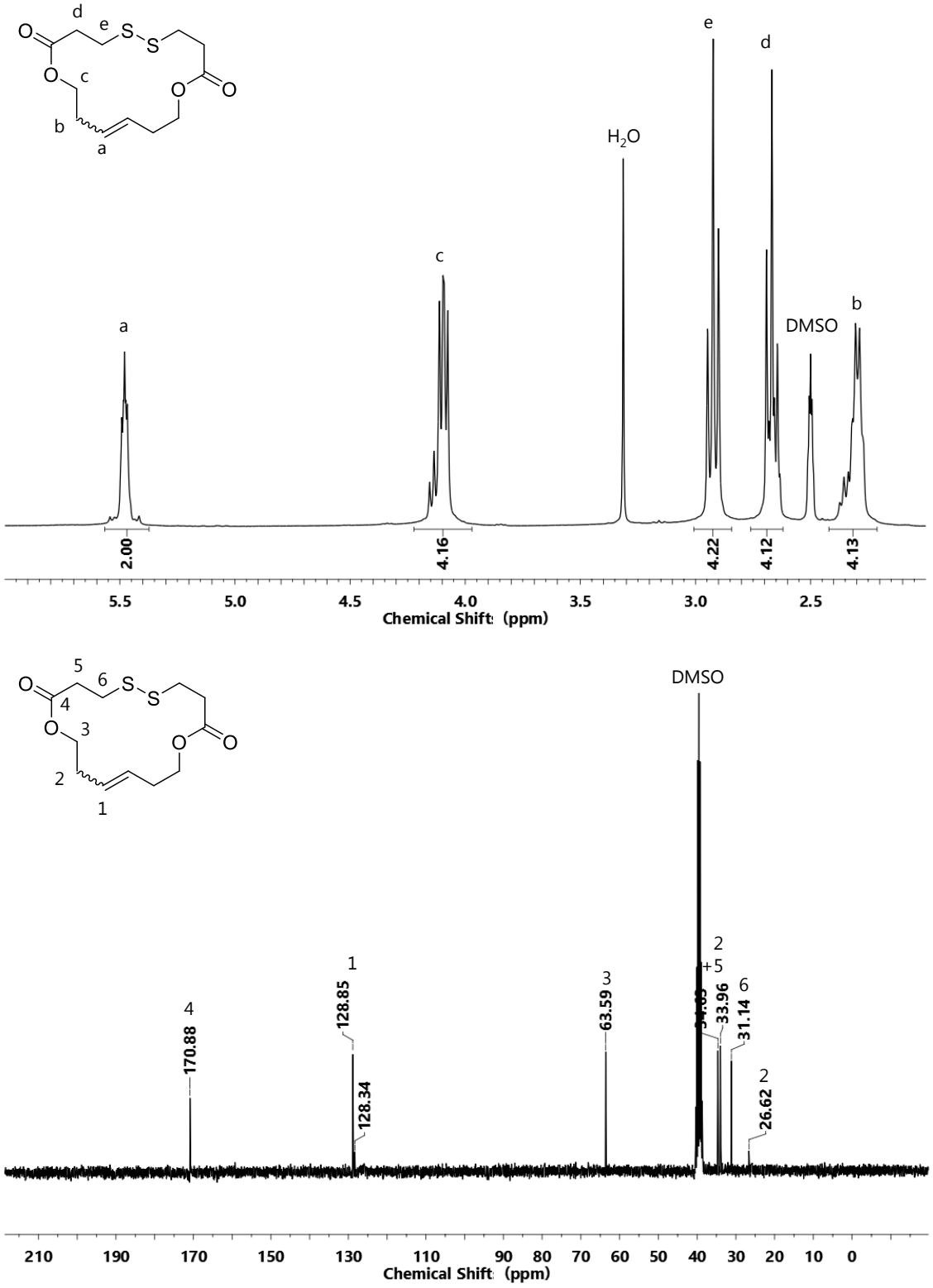

Appendix II, 10: NMR spectra of **2a** in DMSO-d_6: (top) ^{1}H NMR, 300 MHz and (bottom) ^{13}C NMR, 75 MHz.

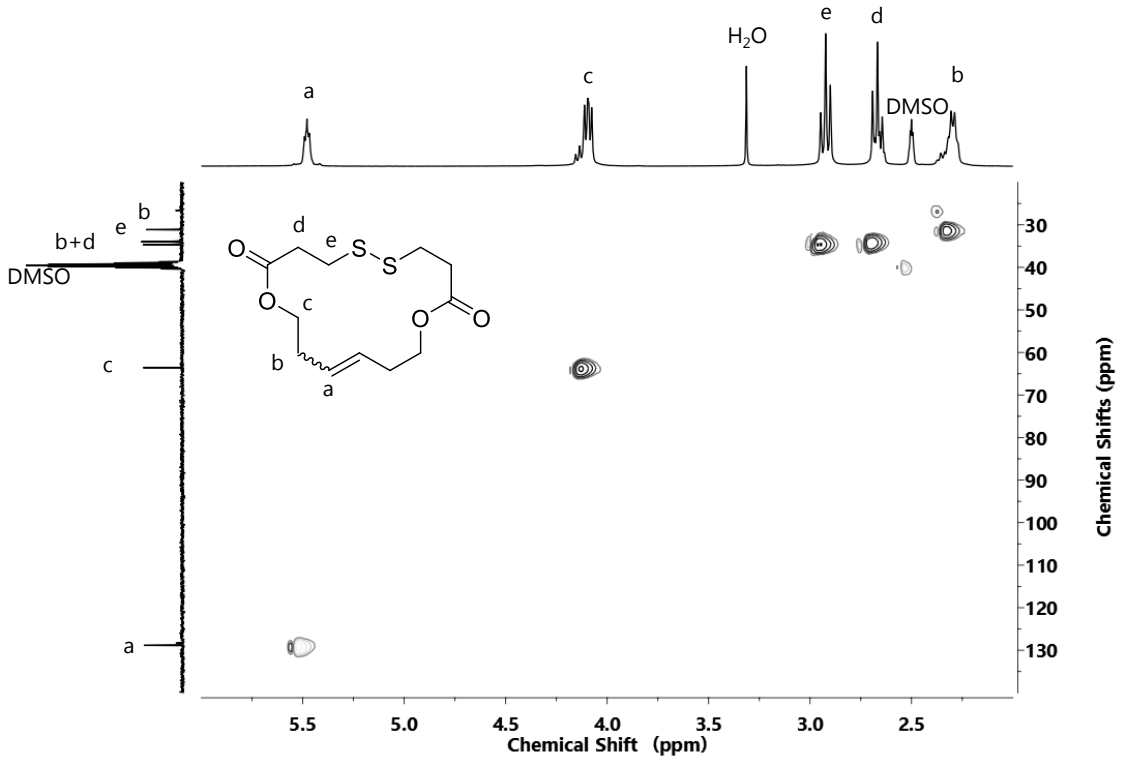

Appendix II, 11: $^{1}H,^{13}C$ HSQC NMR spectrum (300 MHz, DMSO-d_6) of **3c**.

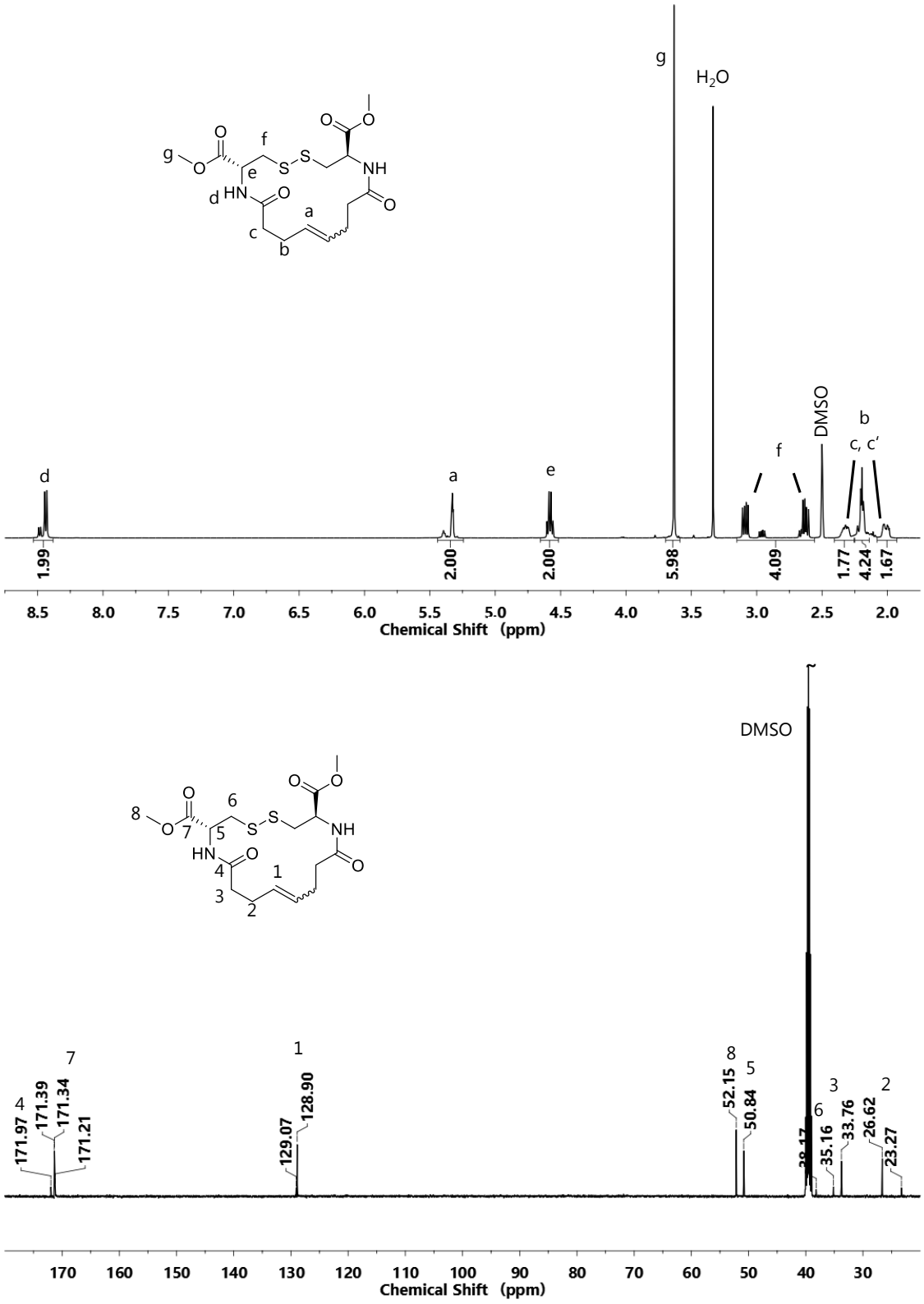

Appendix II, 12: NMR spectra of **3d** in DMSO-d_6: (top) ^{1}H NMR, 500 MHz and (bottom) ^{13}C NMR, 126 MHz.

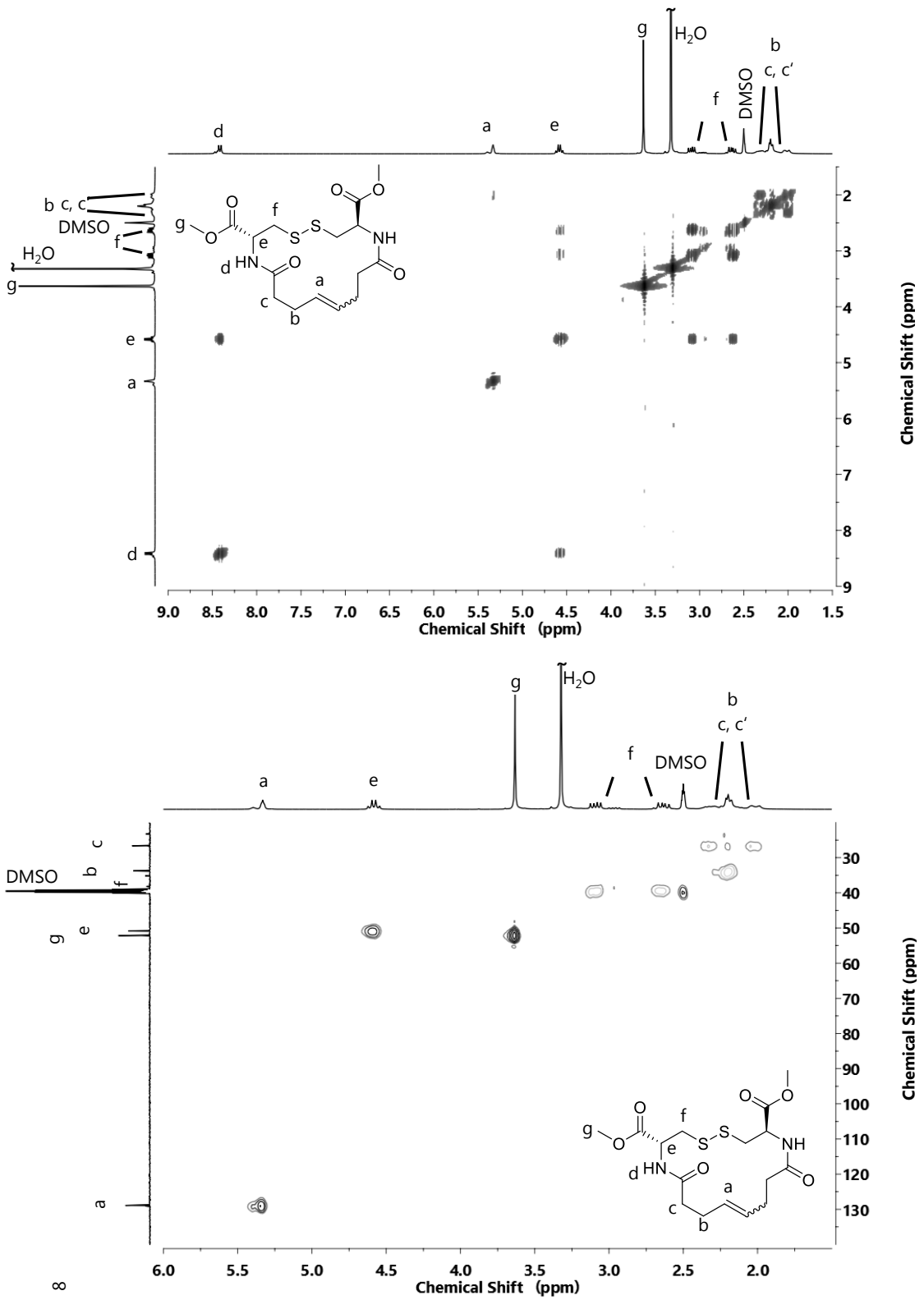

Appendix II, 13: 2D NMR spectra of **3d**: (top) $^{1}H,^{1}H$ COSY NMR spectrum (300 MHz, DMSO-*d*$_6$) and (bottom)) $^{1}H,^{13}C$ HSQC NMR spectrum (300 MHz, DMSO-*d*$_6$).

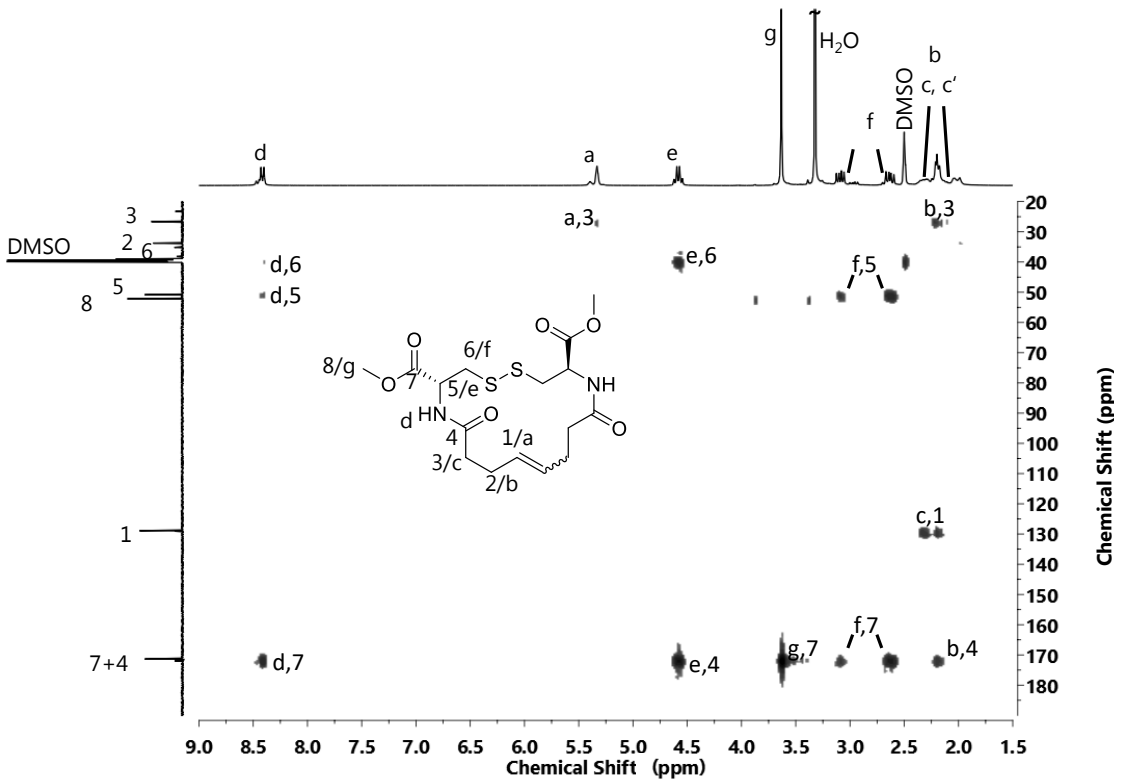

Appendix II, 14: $^{1}H,^{13}C$ HMBC NMR spectrum (300 MHz, DMSO-d_6) of **3d**.

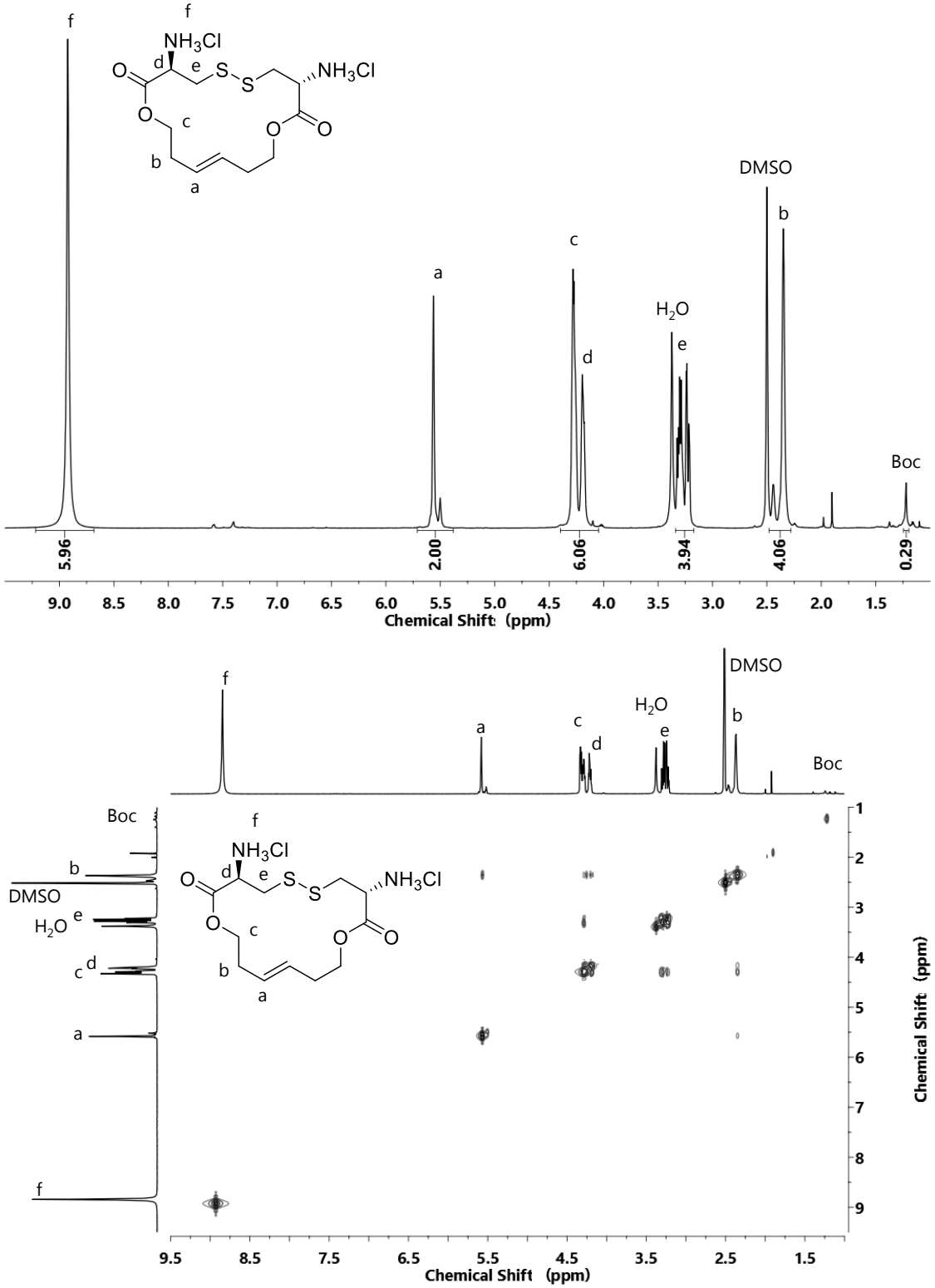

Appendix II, 15: NMR spectra of **3e**: (top) ^{1}H NMR (600 MHz, DMSO-*d*$_6$) and (bottom) ^{1}H,^{1}H COSY NMR (600 MHz, DMSO-*d*$_6$).

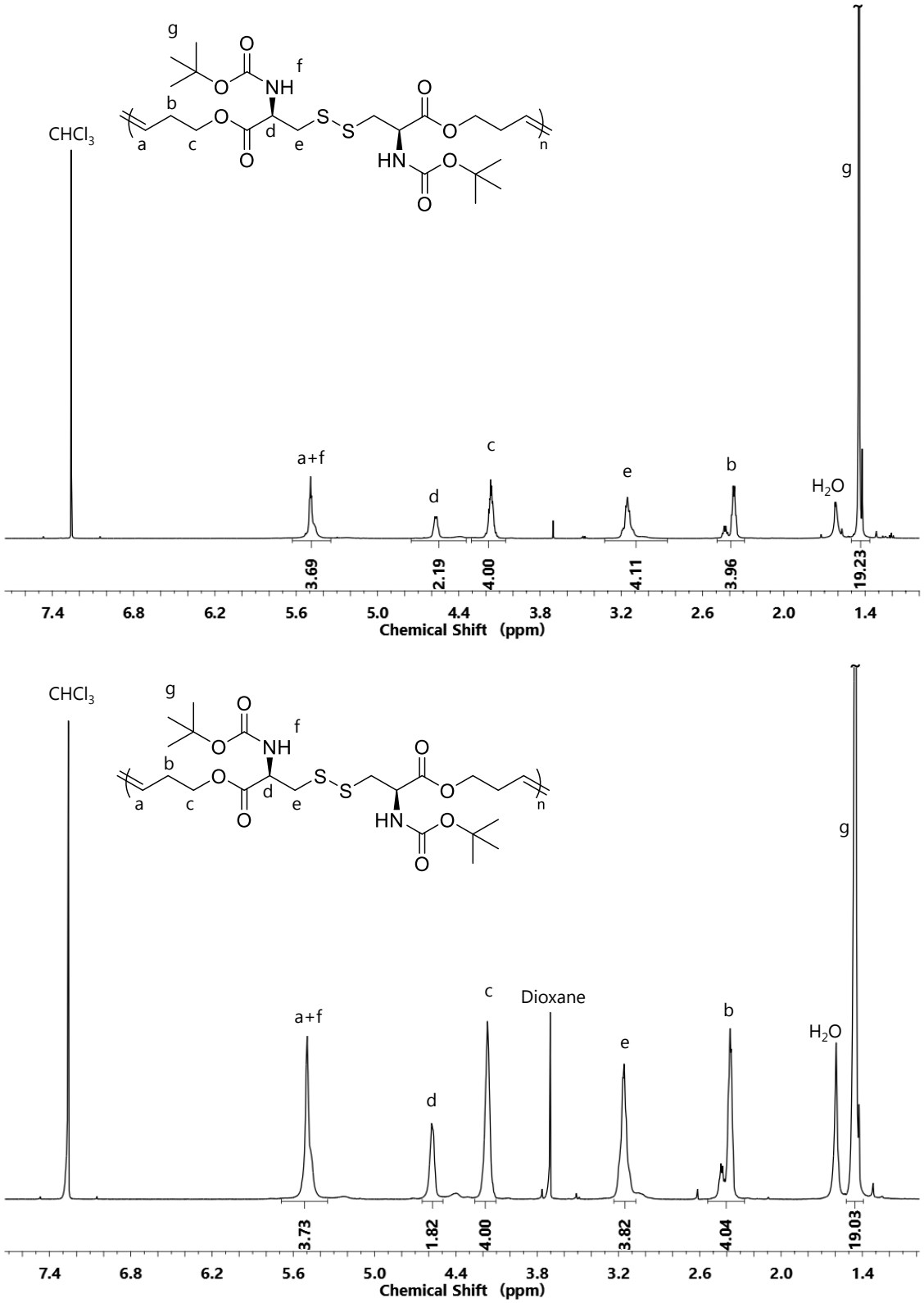

Appendix II, 16: ^{1}H NMR spectra (500 MHz, $CDCl_3$) of (top) **4a** and (bottom) **4a**[d].

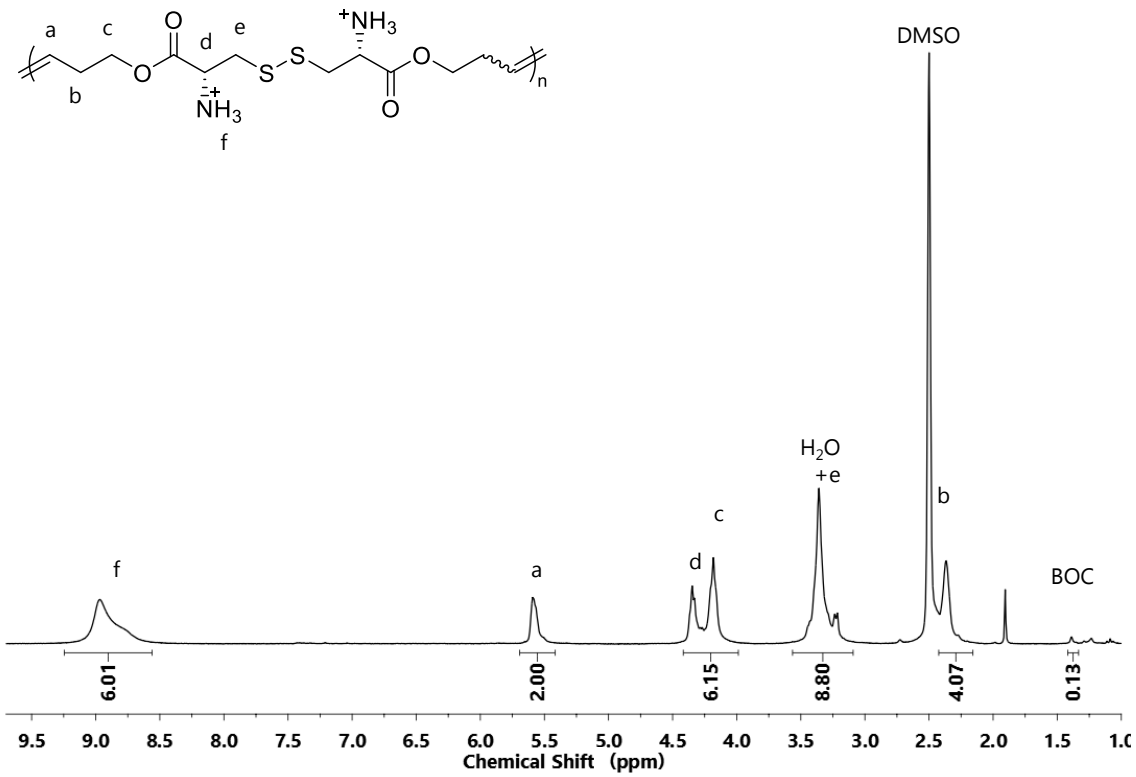

Appendix II, 17: ^{1}H NMR spectrum (300 MHz, DMSO-d_6) of **5a**.

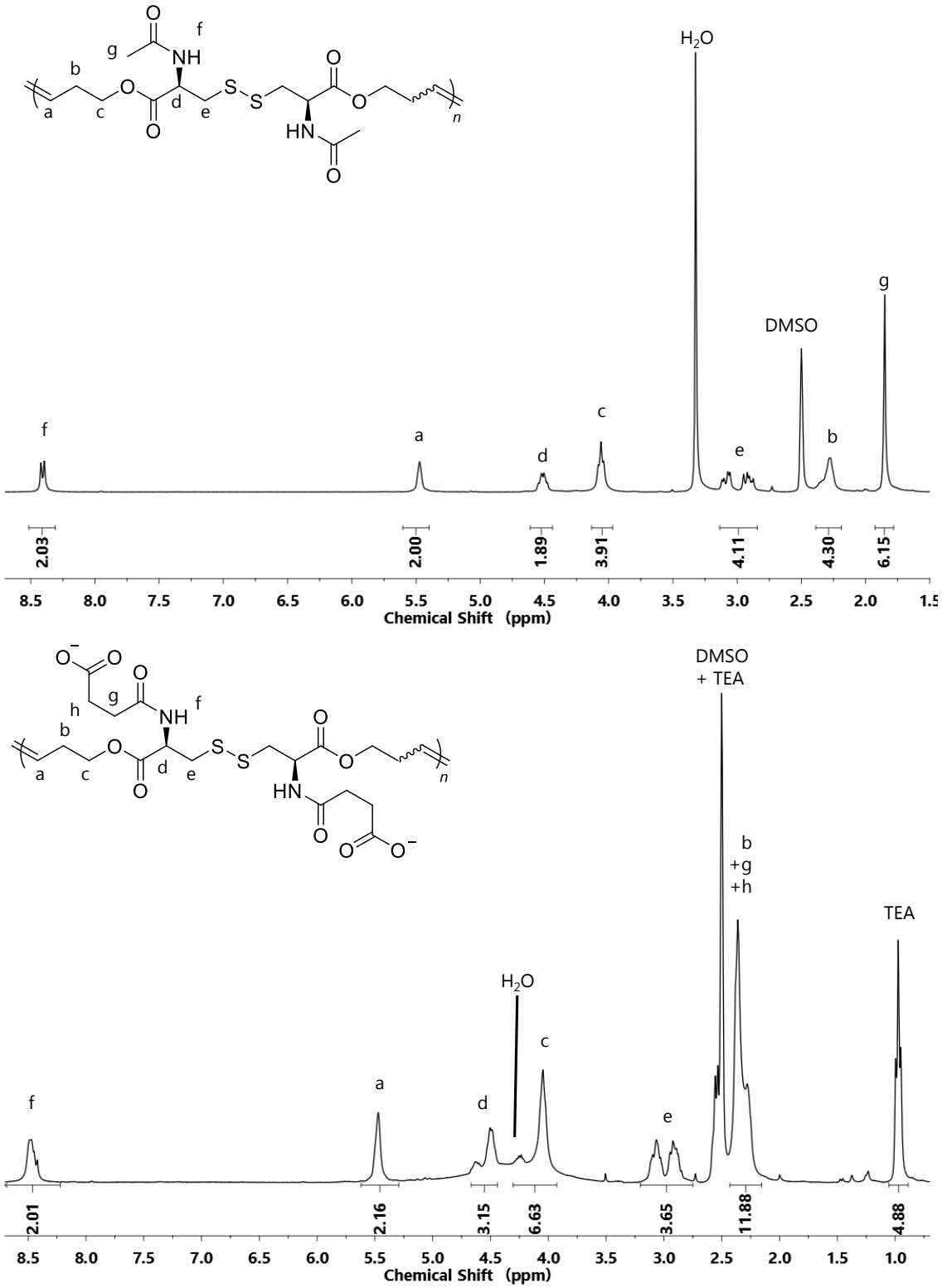

Appendix II, 18: ^{1}H NMR spectra (300 MHz, DMSO-d_6) of (top) **6a** and (bottom) **7a**.

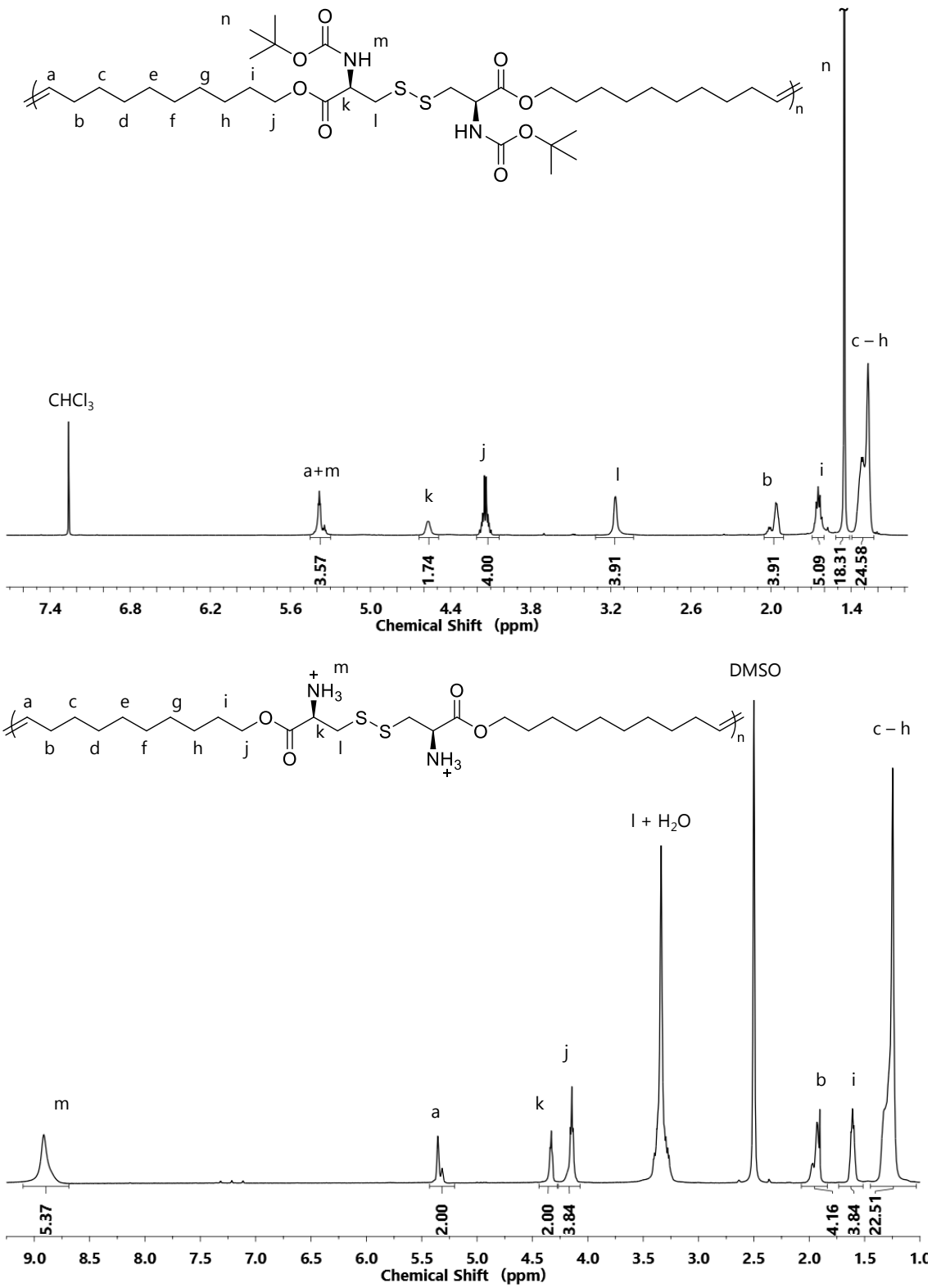

Appendix II, 19: ^{1}H NMR spectra of (top) **4a'** (600 MHz, $CDCl_3$) and (bottom) **5a'** (600 MHz, DMSO-d_6).

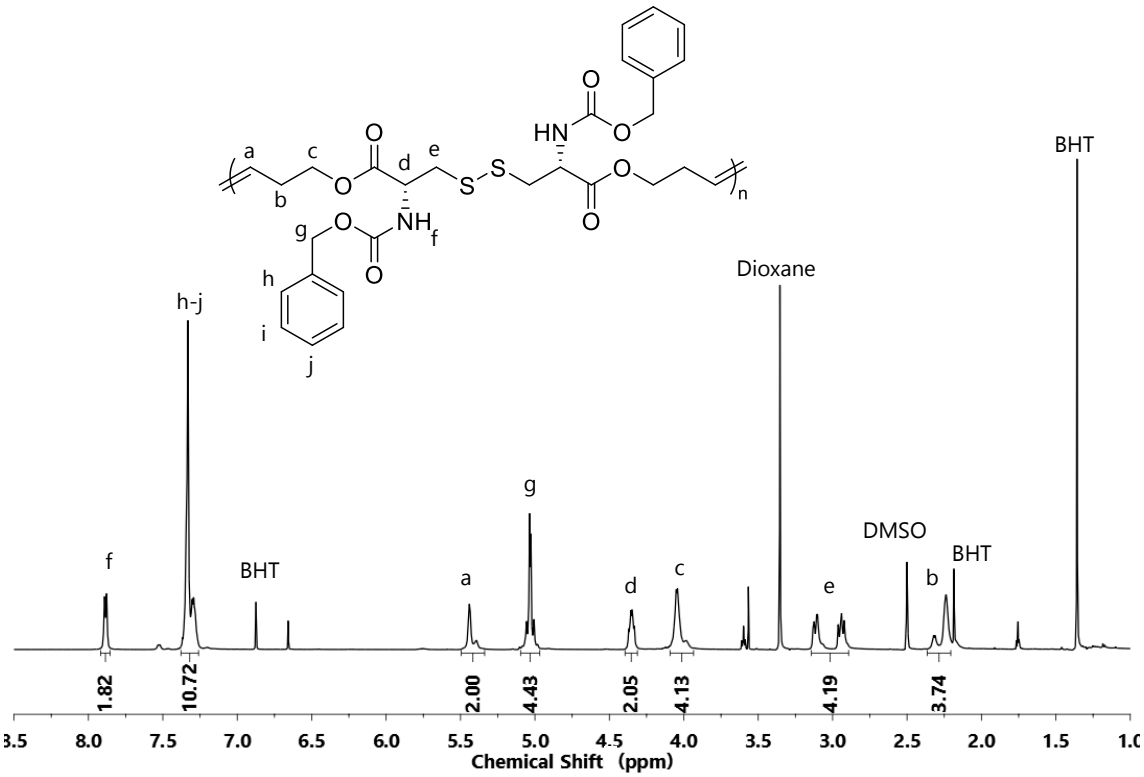

Appendix II, 20: ^{1}H NMR spectrum (500 MHz, DMSO-d_6) of **4b**.

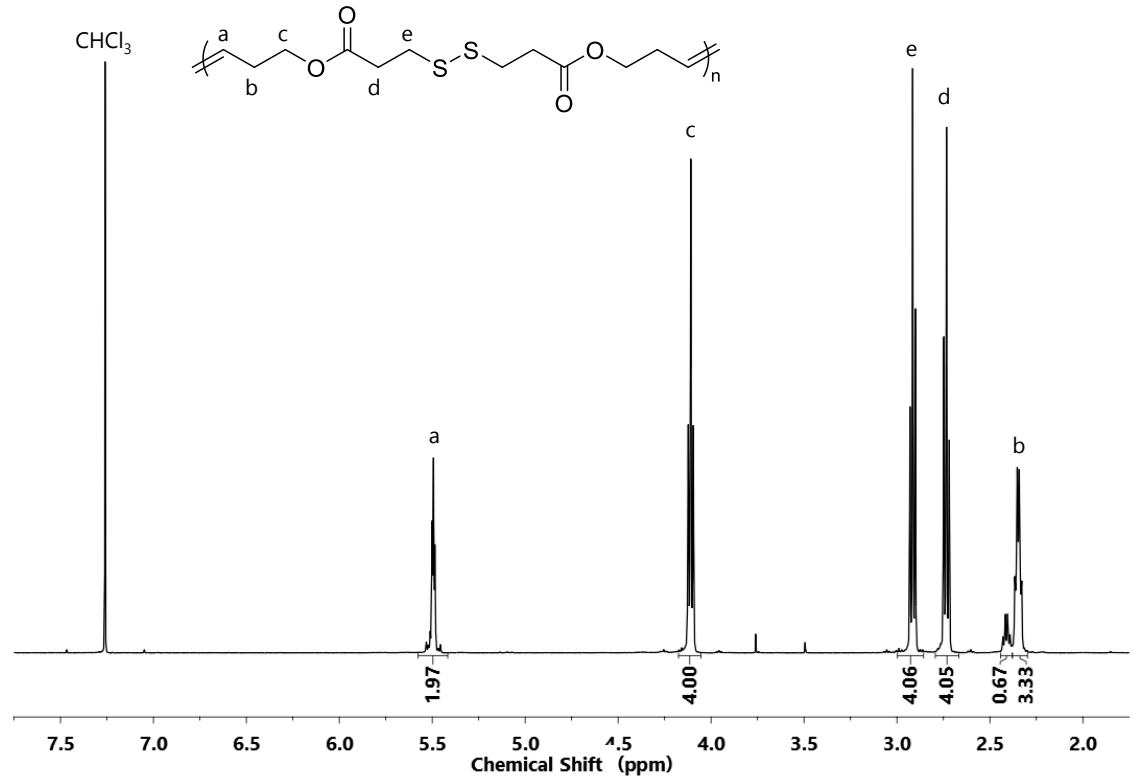

Appendix II, 21: ^{1}H NMR spectrum (500 MHz, $CDCl_3$) of **4c^{d}**.

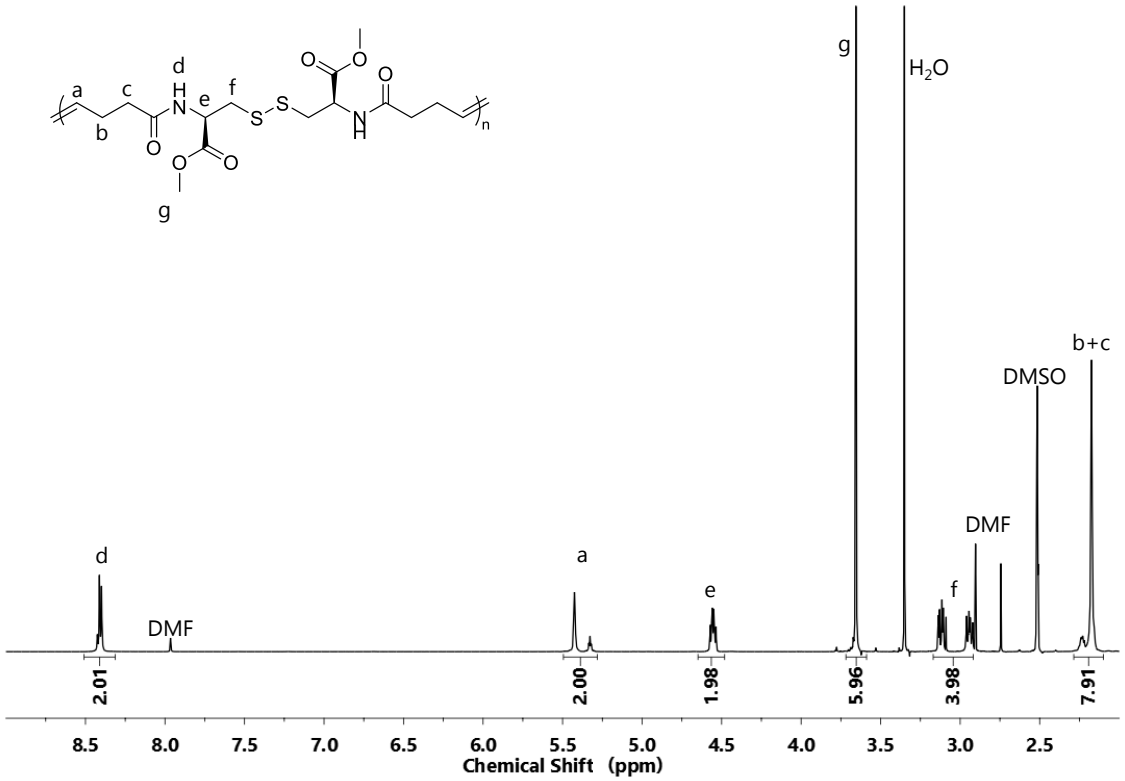

Appendix II, 22: ^{1}H NMR spectrum (600 MHz, DMSO-*d*$_6$) of **4d**^{d}.

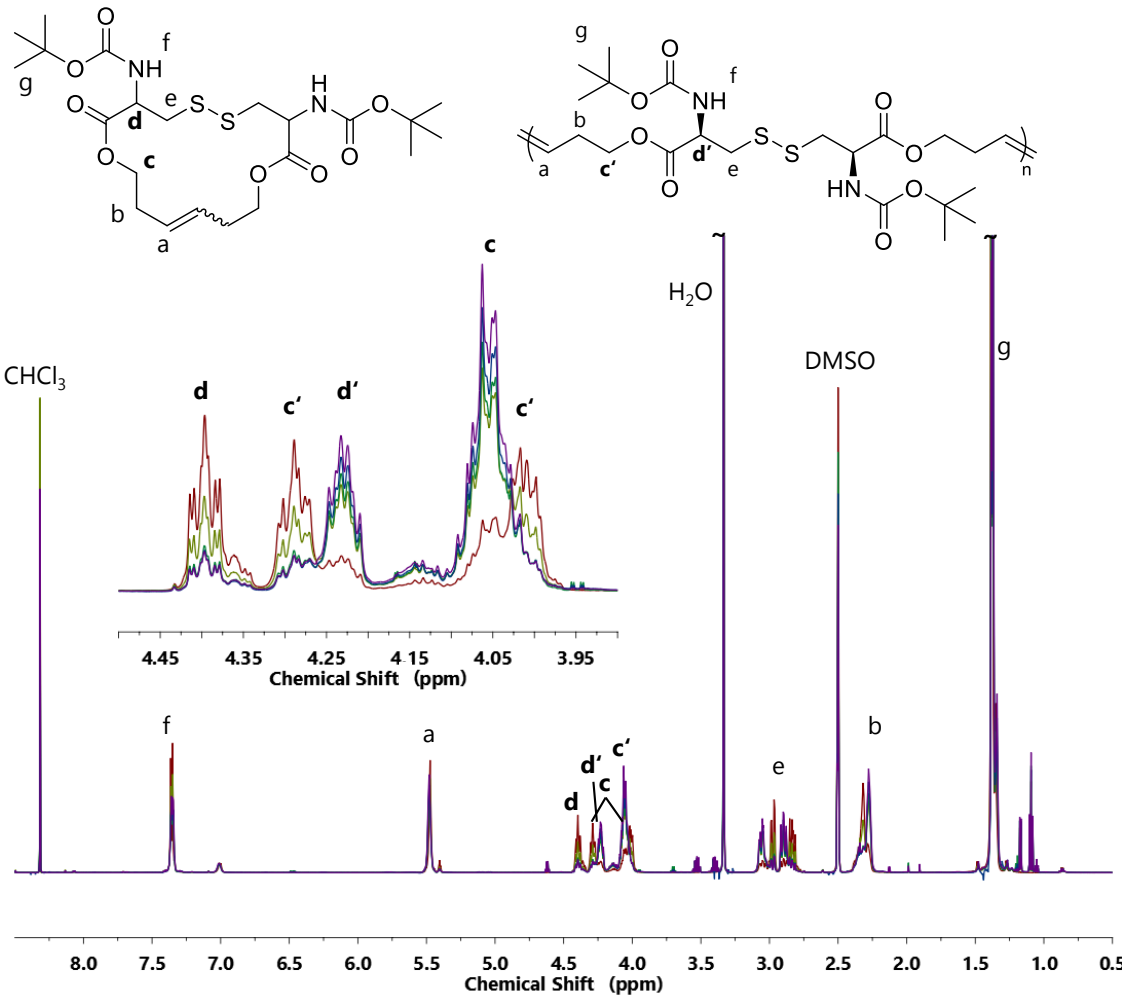

Appendix II, 23: ^{1}H NMR spectra (600 MHz, DMSO-*d*$_6$) following the polymerization of **4a** (1, 5, 15, 30, and 60 minutes), ([G3]$_0$/[**3a**]$_0$ = 0.01 in 1.2 M solution of chloroform at 40 °C). Magnified inlet (4.5-3.9 ppm) shows the disappearance of the geminal coupling of the monomer

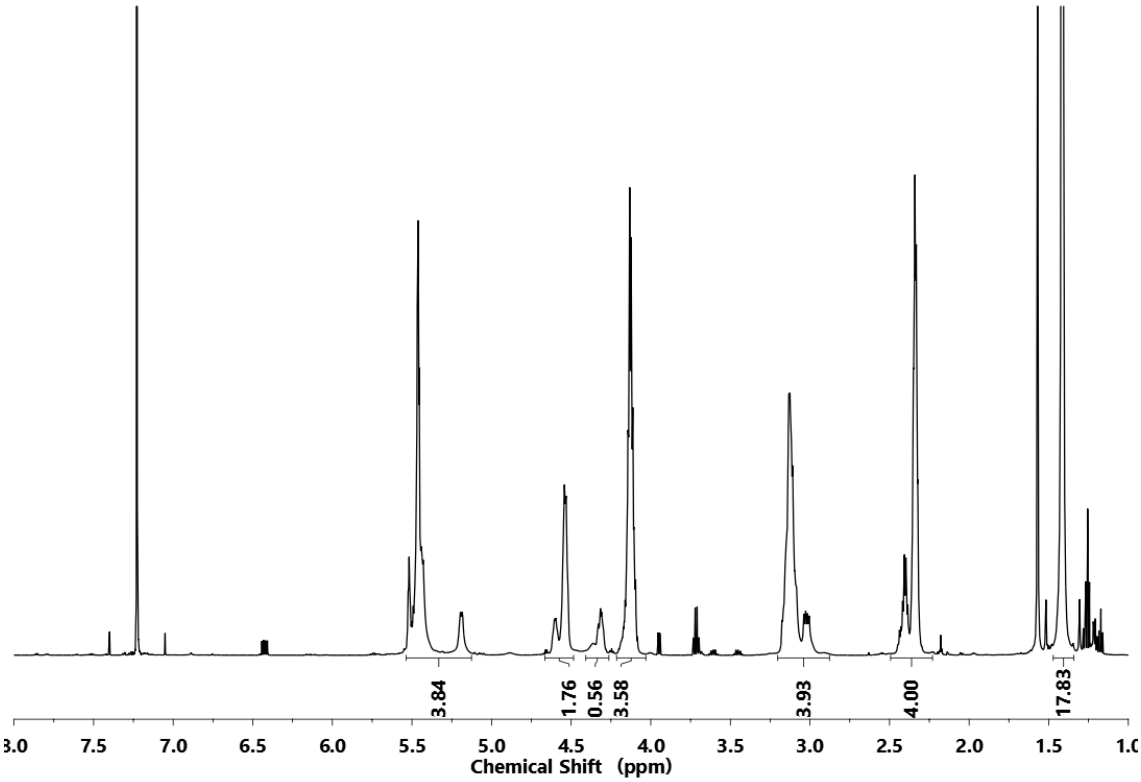

Appendix II, 24: ^{1}H NMR spectra (600 MHz, DMSO-d_6) of crude polymerization ([**3a**]$_0$/[G3]$_0$ = 100:1; 1.2 M in chloroform at 60 °C) towards **4a** obtained after full equilibration, with a conversion of 79% (conversion determined by integration of the signal at 4.3 ppm).

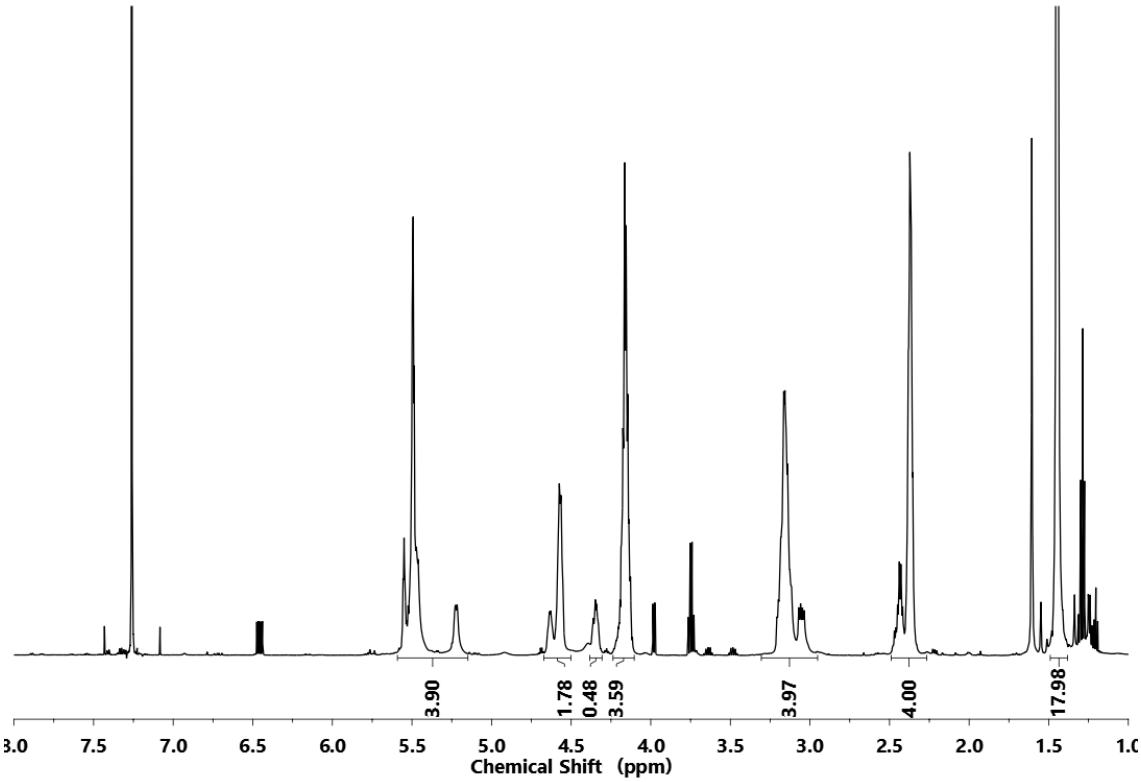

Appendix II, 25: ^{1}H NMR spectra (600 MHz, DMSO-d_6) of crude polymerization ([**3a**]$_0$/[G3]$_0$ = 100:1; 1.2 M in chloroform at 30 °C) towards **4a** obtained after full equilibration, with a conversion of 78% (conversion determined by integration of the signal at 4.3 ppm).

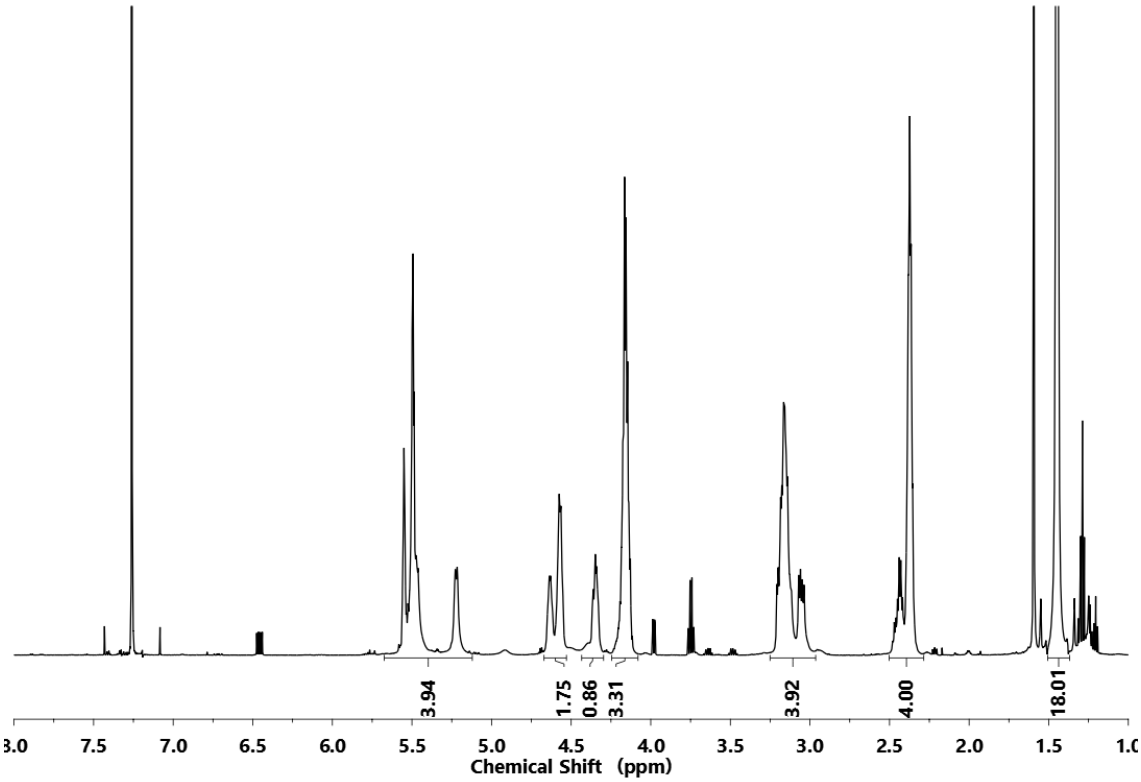

Appendix II, 26: ^{1}H NMR spectra (600 MHz, DMSO-d_6) of crude polymerization ([**3a**]$_0$/[G3]$_0$ = 100:0.5; 1.2 M in chloroform at 30 °C) towards **4a** obtained after full equilibration, with a conversion of 66% (conversion determined by integration of the signal at 4.3 ppm).

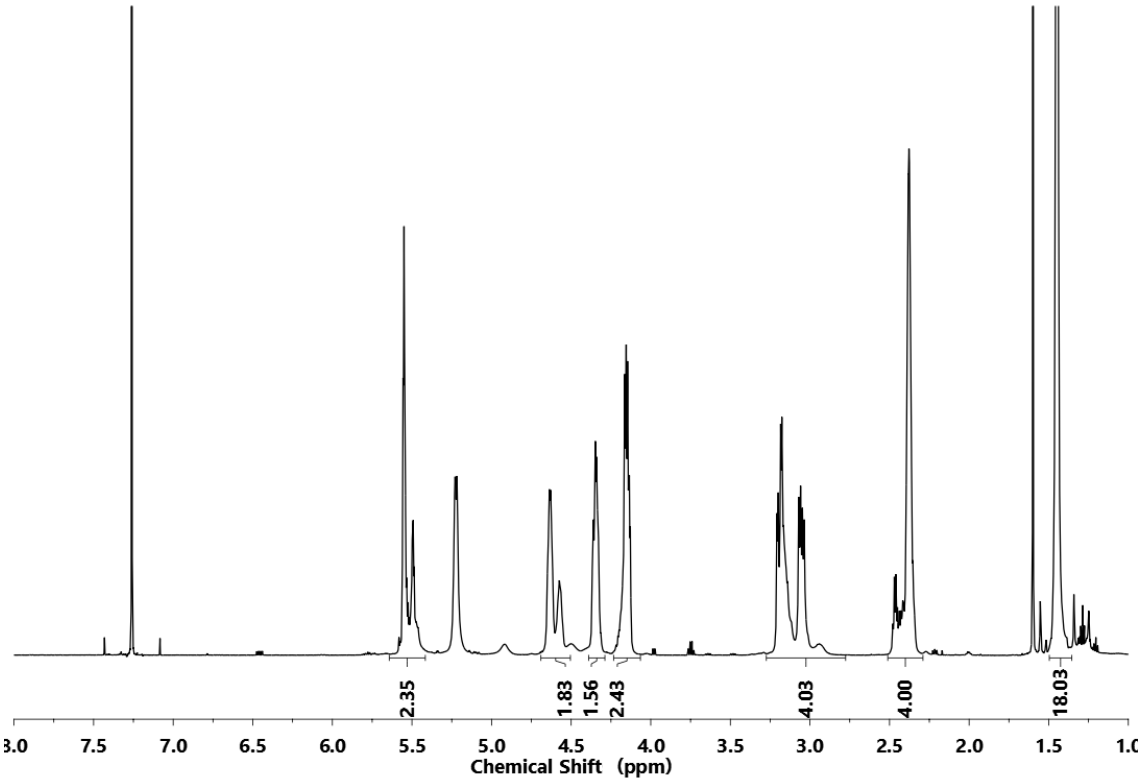

Appendix II, 27: ^{1}H NMR spectra (600 MHz, DMSO-d_6) of crude polymerization ([**3a**]$_0$/[G3]$_0$ = 100:0.1; 1.2 M in chloroform at 30 °C) towards **4a** obtained after full equilibration, with a conversion of 21% (conversion determined by integration of the signal at 4.3 ppm).

10.2 ESI-ToF MS spectra

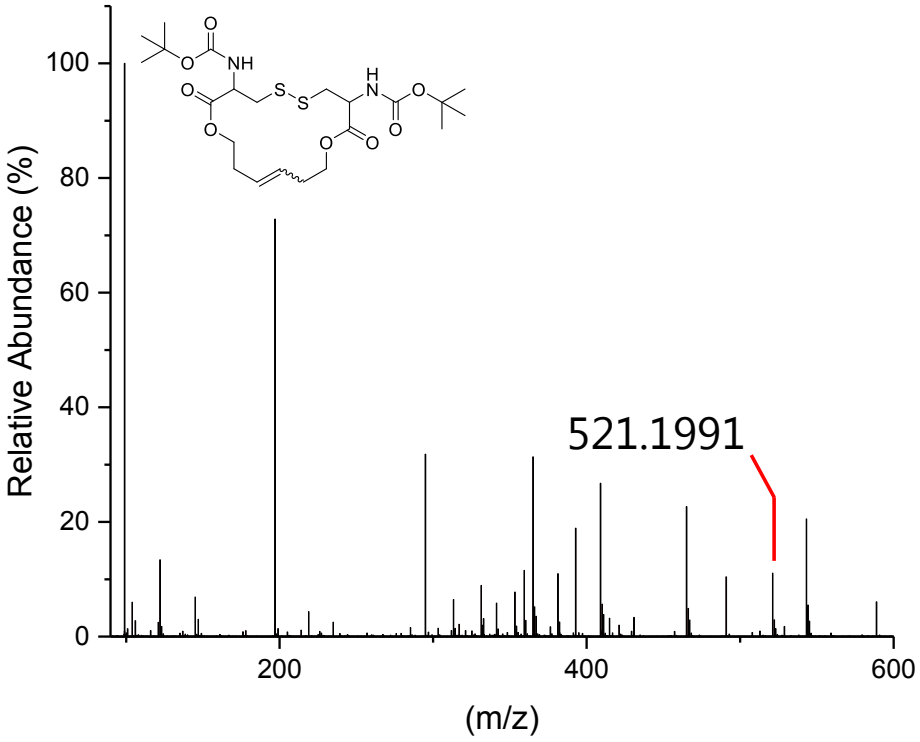

Appendix II, 28: ESI-ToF mass spectrum of **3a**.

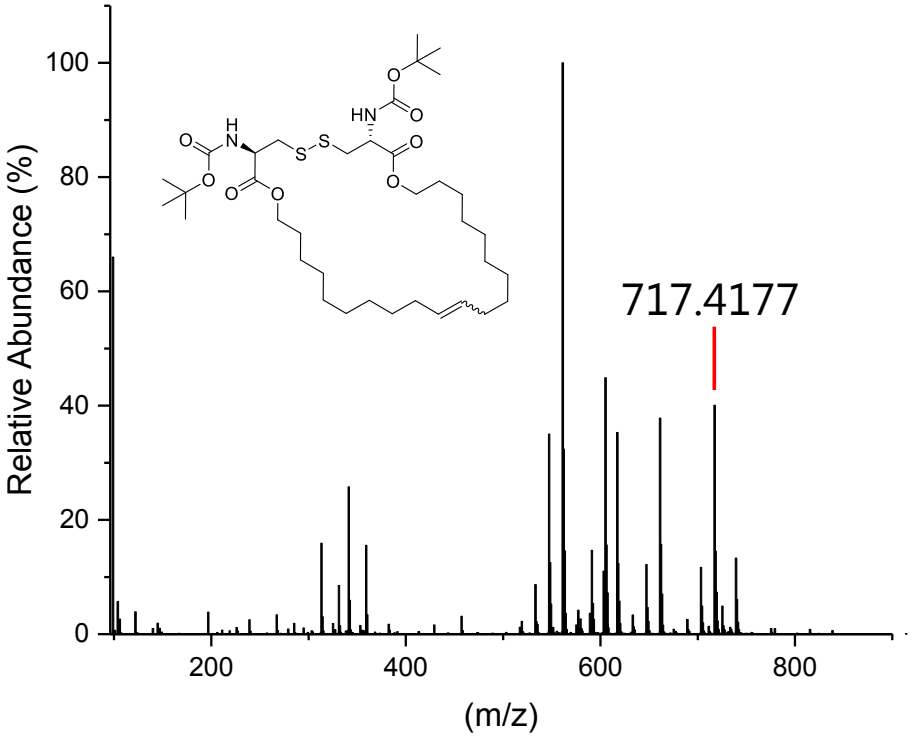

Appendix II, 29: ESI-ToF mass spectrum of **3a'.**

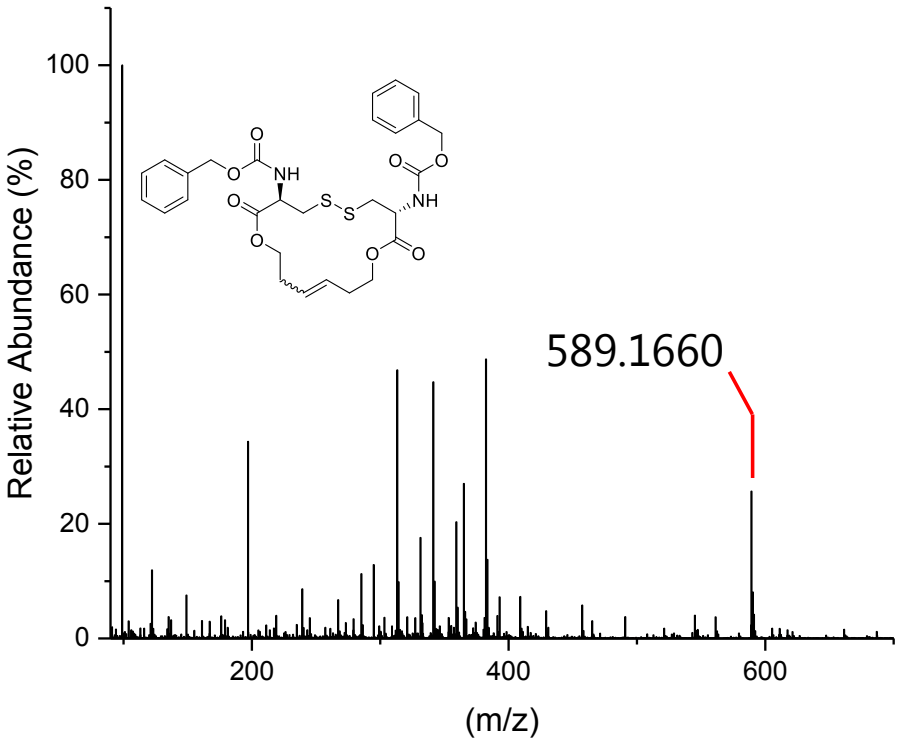

Appendix II, 30: ESI-ToF mass spectrum of **3b**.

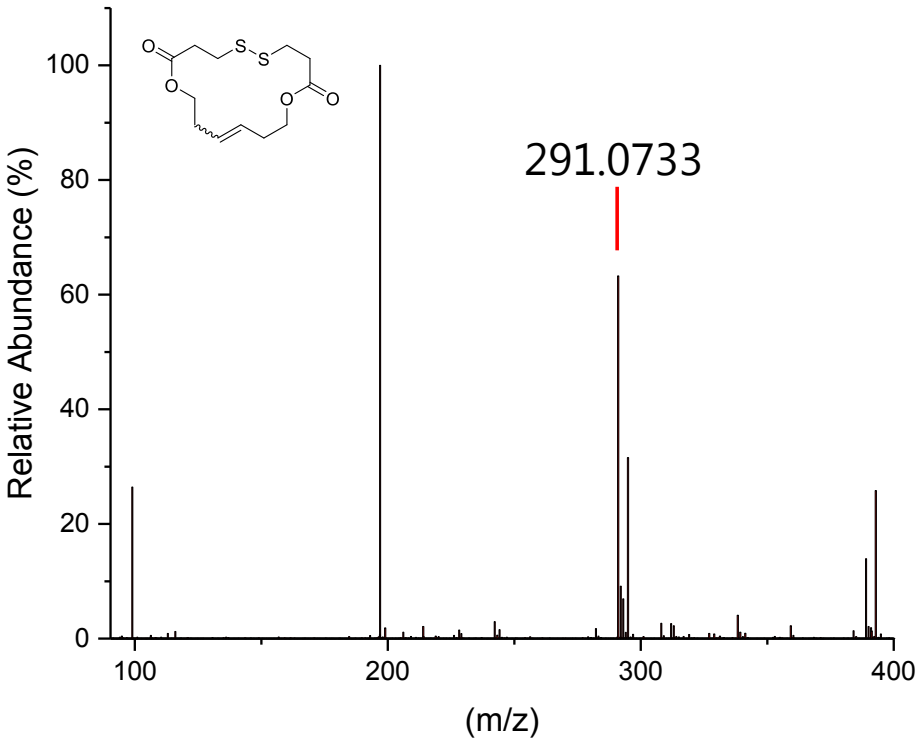

Appendix II, 31: ESI-ToF mass spectrum of **3c**.

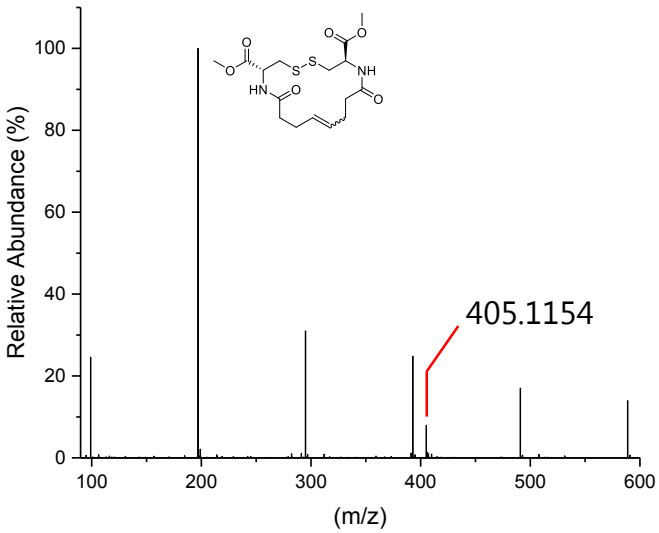

Appendix II, 32: ESI-ToF mass spectrum of **3d**.

10.3 Size Exclusion Chromatograms

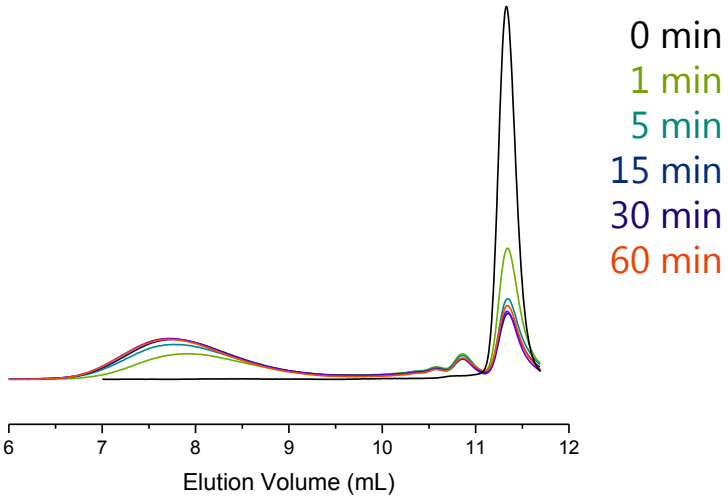

Appendix II, 33: SEC-RI traces (eluent: THF) of crude polymer **4a** obtained at different reaction times of the polymerizations ([**3a**]$_0$/[G3]$_0$ = 100:1; 1.2 M in chloroform at 60 °C (areas under RI signals are normalized).

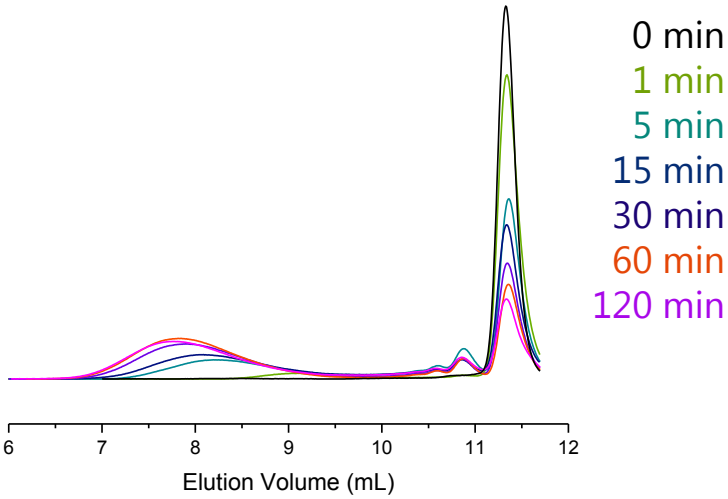

Appendix II, 34: SEC-RI traces (eluent: THF) of crude polymer **4a** obtained at different reaction times of the polymerizations ([**3a**]$_0$/[G3]$_0$ = 100:1; 1.2 M in chloroform at 30 °C (areas under RI signals are normalized).

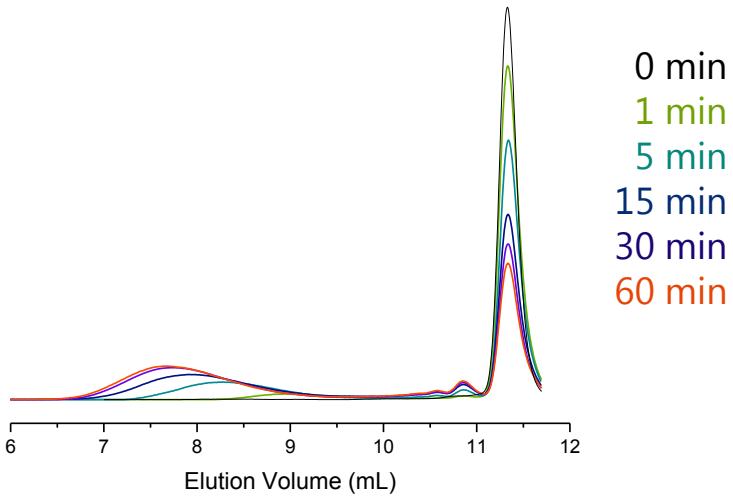

Appendix II, 35: SEC-RI traces (eluent: THF) of crude polymer **4a** obtained at different reaction times of the polymerizations ([**3a**]$_0$/[G3]$_0$ = 100:0.5; 1.2 M in chloroform at 30 °C (areas under RI signals are normalized).

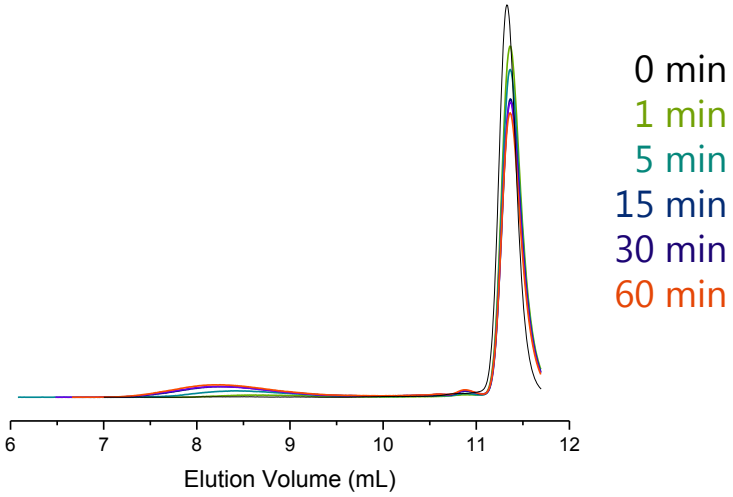

Appendix II, 36: SEC-RI traces (eluent: THF) of crude polymer **4a** obtained at different reaction times of the polymerizations ([**3a**]$_0$/[G3]$_0$ = 100:0.1; 1.2 M in chloroform at 30 °C (areas under RI signals are normalized).

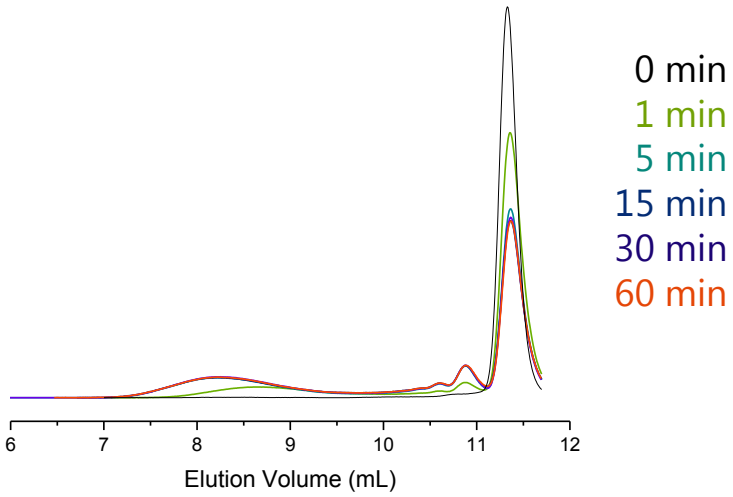

Appendix II, 37: SEC-RI traces (eluent: THF) of crude polymer **4a** obtained at different reaction times of the polymerizations ($[\mathbf{3a}]_0/[G3]_0 = 100:1$; 0.6 M in chloroform at 60 °C (areas under RI signals are normalized).

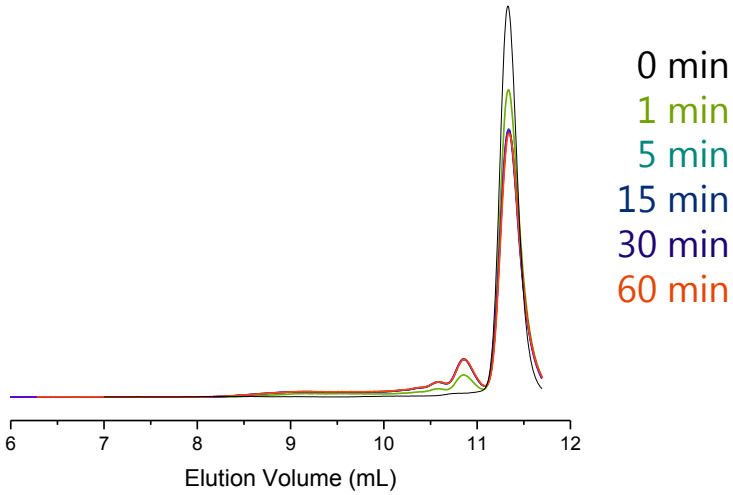

Appendix II, 38: SEC-RI traces (eluent: THF) of crude polymer **4a** obtained at different reaction times of the polymerizations ($[\mathbf{3a}]_0/[G3]_0 = 100:1$; 0.3 M in chloroform at 60 °C (areas under RI signals are normalized).

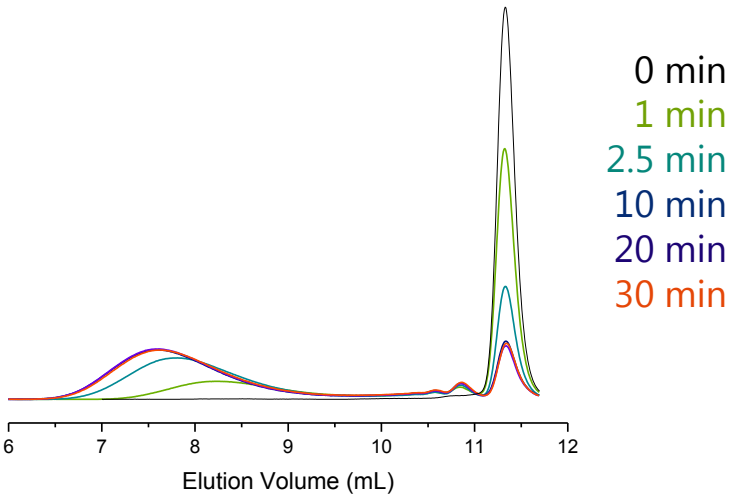

Appendix II, 39: SEC-RI traces (eluent: THF) of crude polymer **4a**^{d} obtained at different reaction times of the polymerizations ([**3a**]$_0$/[MTG]$_0$/[DIPEA]$_0$ = 100:1:1; 1.9 M solution in DMAc at 85 °C) (areas under RI signals are normalized).

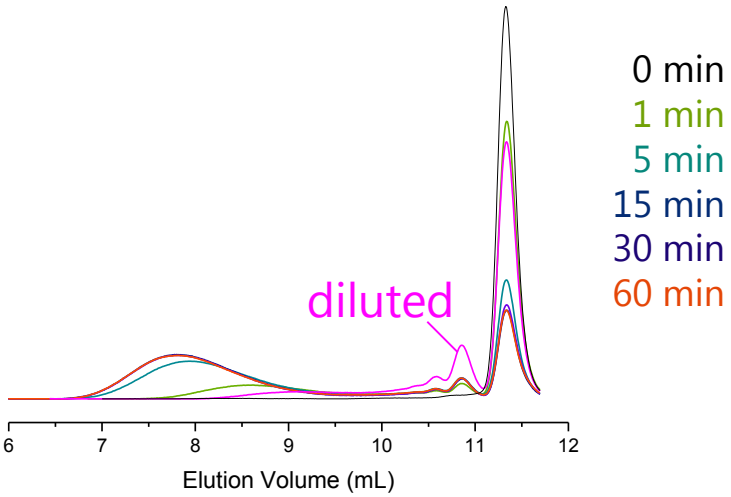

Appendix II, 40: SEC-RI traces (eluent: THF) of crude polymer **4a**^{d} obtained at different reaction times of the polymerizations ([**3a**]$_0$/[MTG]$_0$/[DIPEA]$_0$ = 100:1:1; 1.2 M solution in DMAc at 60 °C), and SEC RI trace after dilution with additional DMAc, showing depolymerization (areas under RI signals are normalized).

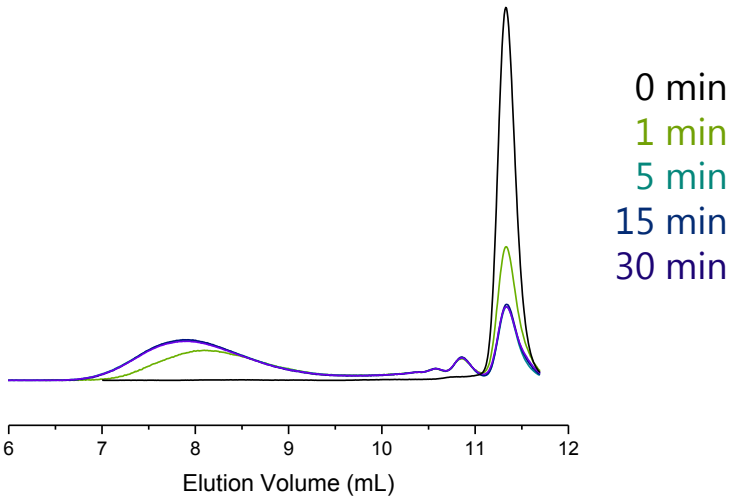

Appendix II, 41: SEC-RI traces (eluent: THF) of crude polymer **4a^{d}** obtained at different reaction times of the polymerizations ([**3a**]$_0$/[MTG]$_0$/[DIPEA]$_0$ = 100:1:1; 1.2 M solution in GVL at 85 °C) (areas under RI signals are normalized).

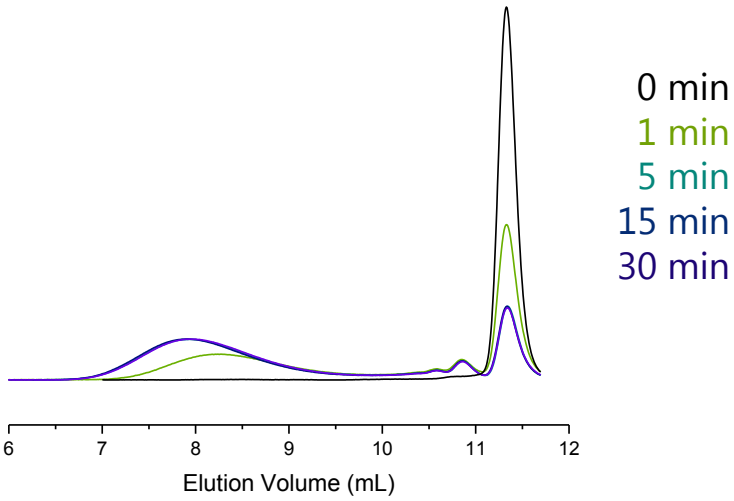

Appendix II, 42: SEC-RI traces (eluent: THF) of crude polymer **4a^{d}** obtained at different reaction times of the polymerizations ([**3a**]$_0$/[MTG]$_0$/[DIPEA]$_0$ = 100:1:1; 1.2 M solution in DMAc at 85 °C) (areas under RI signals are normalized).

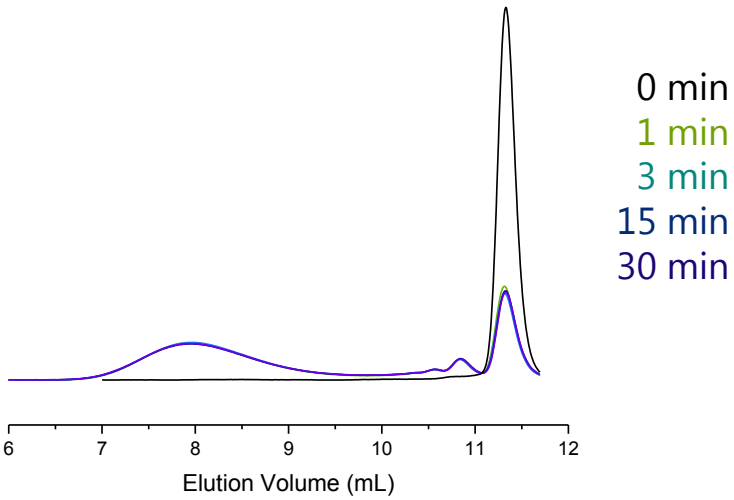

Appendix II, 43: SEC-RI traces (eluent: THF) of crude polymer **4a**^{d} obtained at different reaction times of the polymerizations ([**3a**]$_0$/[MTG]$_0$/[DIPEA]$_0$ = 100:1:1; 1.2 M solution in DMSO at 85 °C) (areas under RI signals are normalized).

10.4 Thermal Analysis

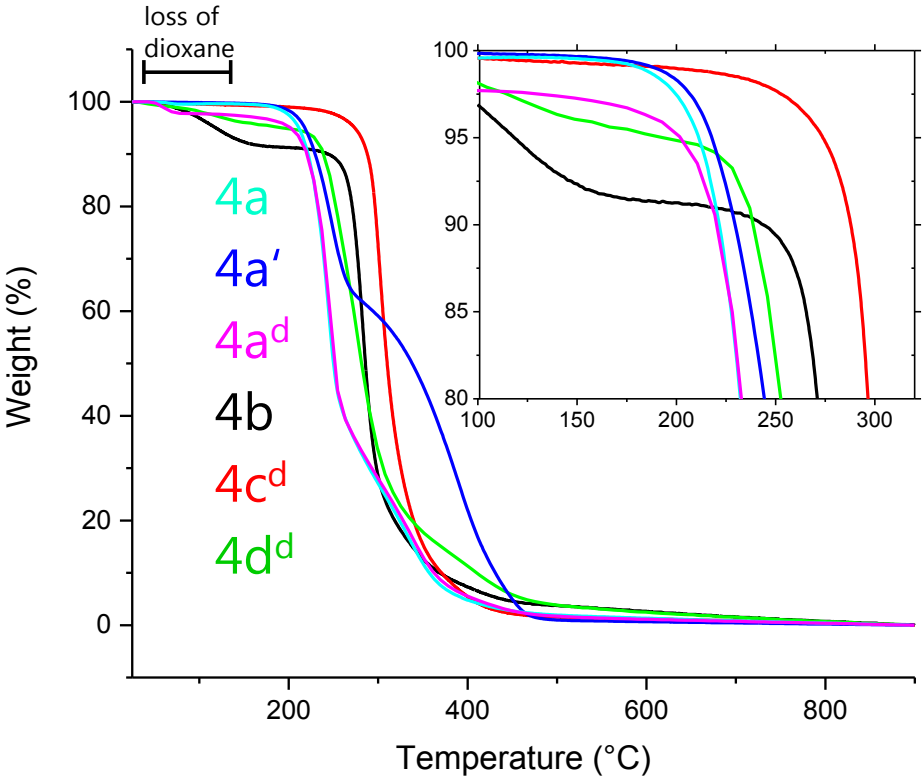

Appendix II, 44: Normalized TGA curves of the polymers **4a**-**4d**, with a magnified inlet of the temperature range from 100-350 °C.

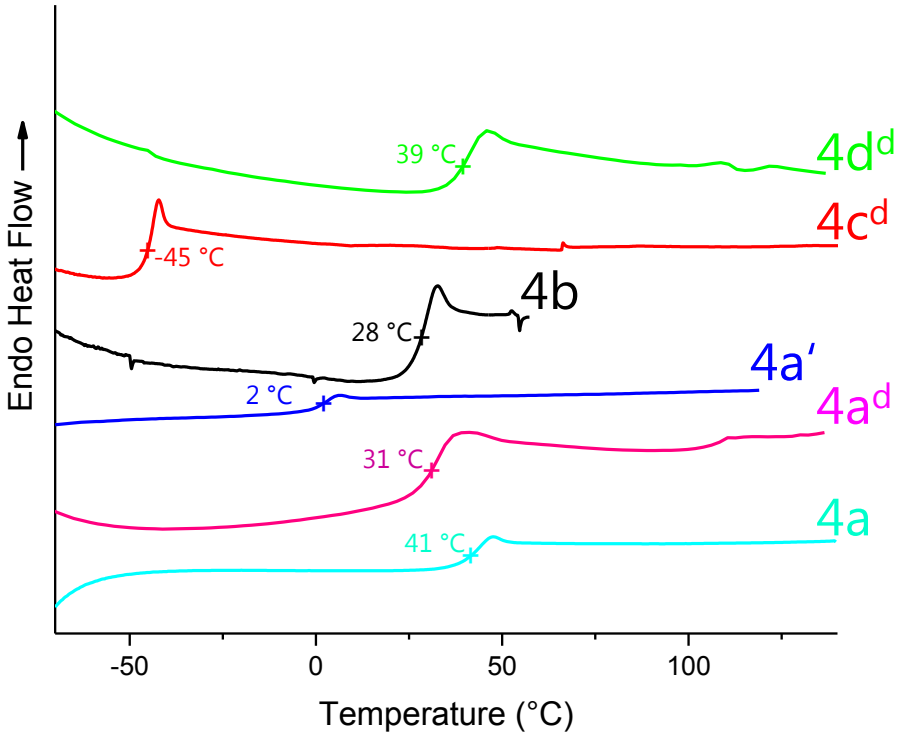

Appendix II, 45: DSC curves of the polymers **4a**-**4d**, showing the corresponding T_g's.

10.5 Static Light Scattering

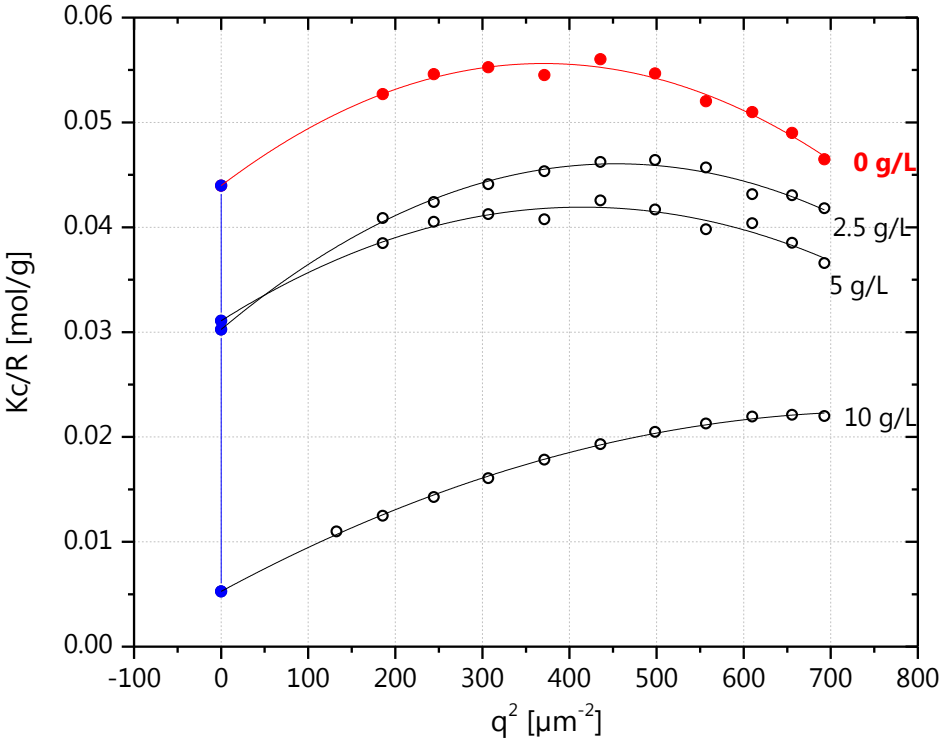

Appendix II, 46: Angle- and concentration-dependent SLS data of polymer **4a** obtained in ethyl acetate at room temperature (dn/dc = 0.128 mL/g).

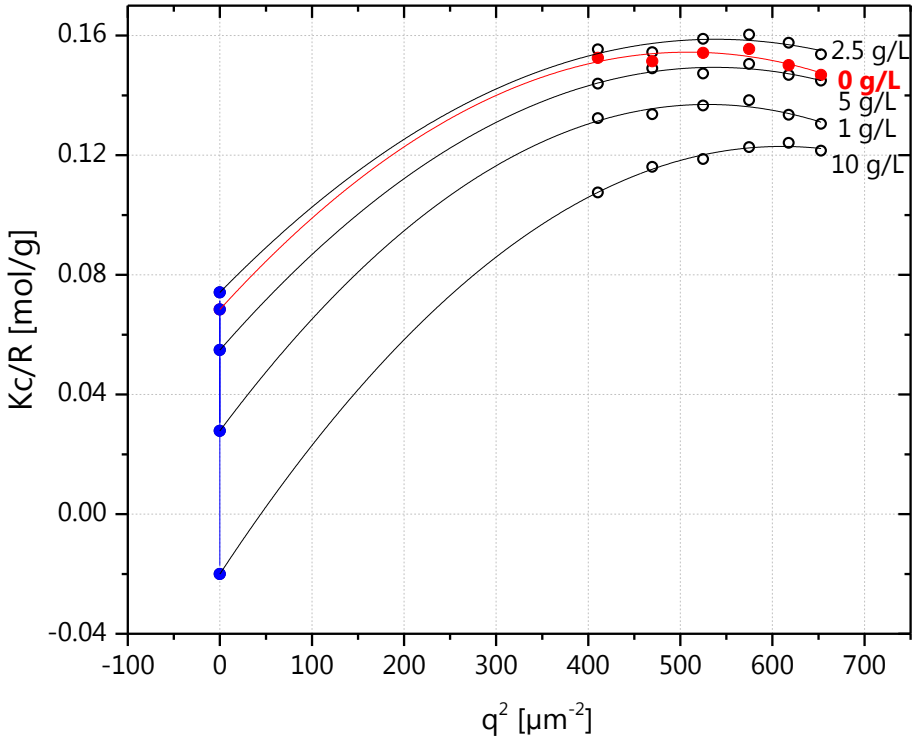

Appendix II, 47: Angle- and concentration-dependent SLS data of polymer **5a** obtained in water at room temperature (dn/dc = 0.184 mL/g).

11 Appendix III: List of Abbreviations

ADMET	acyclic diene metathesis
AIBN	azobisisobutyronitrile
Boc	tert-butyloxycarbonyl
bs	broad singlet
Cbz	Carboxybenzyl
$CDCl_3$	deuterated chloroform
$CHCl_3$	chloroform
CM	cross metathesis
Conv.	conversion
COSY	correlation spectroscopy
C_p	heat capacity
d	doublet
Đ	dispersity
DCM	dichloromethane
ddt	doublet of doublet of triplet
DIPEA	diisopropylethylamine
DLS	dynamic light scattering
DMAc	dimethylacetamide
DMF	*N,N*-dimethylformamide
DMSO	Dimethyl sulfoxide
DMSO-d_6	deuterated dimethyl sulfoxide
DNA	deoxyribonucleic acid
DODT	2-[2-(2-sulfanylethoxy)ethoxy]ethanethiol
DP	degree of polymerization
DSC	differential scanning calorimetry
dt	doublet of triplet
DTE	dithioerythritol
DTT	dithiothreitol
ED-RODiMP	entropy-driven ring-opening disulfide metathesis polymerization
ED-ROMP	entropy-driven ring-opening metathesis polymerization
ED-ROP	entropy-driven ring opening polymerizations
EI	electron ionization
equiv	equivalence
ESI	electronspray ionization
FID	free induction decay
G1	Grubbs' 1st generation catalyst

G2	Grubbs' 2nd generation catalyst
G3	Grubbs' 3rd generation catalyst
GPC	gel permeation chromatography
GVL	γ-Valerolactone
HCl	Hydrochloric acid
HG2	Hoveyda-Grubbs' 2nd generation catalyst
HMBC	heteronuclear multiple-band correlation
HSQC	heteronuclear single-quantum correlation
m	multiplet
MALDI	matrix assisted laser desorption/ionization
M_n	number average molar masses
M_n^{app}	number average apparent molar mass
MTG	methyl thioglycolate
M_w	weight average molar mass
M_n^{app}	weight average apparent molar mass
MWCO	molecular weight cut off
NCA	*N*-carboxyanhydride
NMR	nuclear magnetic resonance
NNGE	negative neighboring group effect
ox.	oxidation
PASA	poly(aspartic acid)
p-Bq	*para*-benzoquinone
PBS	phosphate-buffered saline
PDL	pentadecalactone
PEG	poly(ethylene glycol)
PET	poly(ethylene terephthalate)
PTFE	poly(tetrafluoroethylene)
PVDF	poly(vinylidene difluoride)
q	quartet
RAFT	reversible addition-fragmentation chain transfer
RCM	ring closing metathesis
RI	refractive index
RODiMP	ring-opening disulfide metathesis polymerization
ROM	ring-opening metathesis
ROMP	ring-opening metathesis polymerization
s	singlet
SEC	size exclusion chromatography
SLS	static light scattering
t	triplet
T_c	crystallization temperature
TEA	(triethyl)amine
cryo-TEM	transmission electron cryomicroscopy

Temp	temperature
TFA	trifluoroacetic acid
T_g	glass transition
TGA	thermogravimetric Analysis
THF	tetrahydrofuran
TLC	thin-layer chromatography
T_m	melting temperature
TMS	tetramethylsilane
ToF MS	time-of-flight mass spectrometry
UV-Vis	ultraviolet–visible
γ-PGA	poly-(γ-glutamic acid)

12 Appendix IV: List of Publications and Conference Contibutions

Metathesis polymerization of cystine-based macrocycles
Felix N. Behrendt and Helmut Schlaad, *Polym. Chem.*, **2017**, 8, 366-369

Entropy-Driven Ring-Opening Disulfide Metathesis Polymerization for the Synthesis of Functional Poly(disulfide)s
Felix N. Behrendt and Helmut Schlaad, *Macromol. Rapid Commun.*, **2018**, 39, 1700735

Macromolecular Colloquium, Freiburg, February 2015 (Poster Presentation)
F. N. FÜHRER (Uni Potsdam), C. Secker, H. Schlaad, *Exploring Routes to New Amino Acid-based Polymers*,

Tag der Chemie (TDC), Berlin, July 2017 (Poster Presentation and Presentation)
Felix N. Behrendt and Helmut Schlaad, *Reductively Degradable Cystine Based Polymers and Their Functionalization*

13 Appendix V: Acknowledgements

13.1 Acknowledgement

I would like to use this opportunity to thank the many people who have made it possible for me and supported me to write this thesis, and also those who have accompanied me throughout my career.

First of all, I would like to thank Professor Dr. Helmut Schlaad for his scientific advice and for his warm welcome to his working group. His support even in difficult times and his patience helped me a lot to complete this work. Additionally, I would also like to thank Professor Dr. Markus Antonietti, the Max Planck Society, and the University of Potsdam for making this work possible and/or financing it. I would like to thank Professor Dr. André Laschewsky, my mentor, for his insights into his comprehensive knowledge of polymer chemistry.

I would like to thank Olaf Niemeyer and Angela Krititschka for their support with NMR measurements and for Olaf's East Berlin excursions. Furthermore, I would like to thank Marlies Gräwert and Sascha Prentzel for their help and instructions into SEC, Dirk Schanzenbach and Ahed Abouserie for the support in TGA and DSC measurements, Sylvia Fürstenberg and Ines Starke for ESI-ToF MS measurements and for their patience even with annoying demands, Yasemin Mai-Linde for elementary analyses, and Sebastian Noack and Anna Bogomolova for the help with light scattering experiments. Special thanks go once again to Sacha Prentzel for his help with all laboratory concerns.

Additionally, I would like to thank the entire working group: Ines Bastian, Sascha Prentzel, Charlotte Vacogne, Aleksandar Matic, Tapas Debsharma, Andreas Hess, Nils Lüdecke, Shuangyan Hu, Matilde Concilio, Sebastian Noack, Ina Dambowsky, Afroditi Doriti, Scott Kilbride, Boonya Thongrom, Andreas Schwagerus, Anna Bogomolova, Jingyang Yu, Sarah Brosnan, Christian Secker. My start into the life of

a doctoral student would certainly not have been so easy without the support of Sarah Brosnan and Christian Secker and would have been much more boring without the diverse discussions in the REWE Group. I would like to say to Sebastian Noack and Charlotte Vacogne: G0.01 is the best office you can imagine. And, Charlotte, thank you for all the help and your patience.

At this point, I would also like to thank Felix Schwarz and Felix Limberg for the great time together during our studies and the many hours of learning together.

I would like to thank my chemistry teacher, Mr. Rühs, for teaching me the joy of this fascinating science. With this, he laid the foundation for my interest in chemistry.

Of course I would also like to thank my family, Anton Bunge, Rick Bunge, Tom Behrendt, Max Behrendt and Jan Brinkman, Eva and Reinhardt Bunge as well as Klaus Behrendt and Karin Deininger, and Sylva Körber, Konrad Klockmeier, Johannes Ellendorff and Mark Kohnert, as well as my brother David Führer.

Special thanks to my parents, Barbara and Thomas Führer, who invested a lot of time, money, patience, and love in my support during my studies.

Last but not least I would like to thank my wife Vera and my children Sofia and Lars. You have accompanied me throughout this time and have gone through the ups and downs of my time as a doctoral student with me. You are a firm anchor for me, which helps me never to lose focus and perspective.

Thank you!!!

Felix Behrendt

13.2 Danksagung

Ich möchte diese Gelegenheit dafür nutzen, den vielen Leuten zu danken, die es mir ermöglicht und mich unterstütz haben, diese Arbeit zu schreiben, und auch bei denen die mich während meines Werdeganges begleitet haben.

Zuerst möchte ich mich bei Professor Dr. Helmut Schlaad, für seine wissenschaftliche Anleitung und für die herzliche Aufnahme in seine Arbeitsgruppe bedanken. Seine Unterstützung auch in schwierigen Zeiten und seine Geduld haben mir sehr geholfen diese Arbeit abzuschließen. Mein besonderer Dank gilt auch Professor Dr. Markus Antonietti, der Max-Planck-Gesellschaft und der Uni Potsdam dafür, dass sie mir die Anfertigung dieser Arbeit ermöglicht bzw. finanziert haben. Bei Professor Dr. André Laschewsky, meinem Mentor, möchte ich mich für die Einblicke in sein umfassendes Wissen der Polymerchemie bedanken.

Olaf Niemeyer und Angela Krititschka möchte ich für ihre Unterstützung mit NMR Messungen und für Olafs Ostberlin Exkurse danken. Des Weiteren gebührt mein Dank Marlies Gräwert und Sascha Prentzel für ihre Hilfe und Einweisungen in die GPC; Dirk Schanzenbach und Ahed Abouserie für die Unterstützung bei TGA bzw. DSC Messungen, Sylvia Fürstenberg und Ines Starke für ESI-ToF MS Messungen und für ihre Geduld auch bei nervigen Nachfragen, Yasemin Mai-Linde für elementar Analysen, sowie Sebastian Noack und Anna Bogomolova für die Hilfe mit der Lichtstreuung. Ein besonderer Dank gilt an dieser Stelle noch einmal Sacha Prentzel für seine Hilfe mit allen Laborbelangen.

Ein Dank auch an die gesamte Arbeitsgruppe: Ines Bastian, Sascha Prentzel, Charlotte Vacogne, Aleksandar Matic, Tapas Debsharma, Andreas Hess, Nils Lüdecke, Shuangyan Hu, Matilde Concilio, Sebastian Noack, Ina Dambowsky, Afroditi Doriti, Scott Kilbride, Boonya Thongrom, Andreas Schwagerus, Anna Bogomolova, Jingyang Yu, Sarah M. Brosnan, Christian Secker. Mein Start in das Leben eines Doktoranden wäre ohne die Unterstützung von Sarah Brosnan und Christian Secker mit Sicherheit nicht so einfach gewesen und ohne die vielseitigen Diskussionen in der REWE-Gruppe viel langweiliger. Zu Sebastian Noack und

Charlotte Vacogne möchte ich sagen: G0.01 ist das beste Büro das man sich vorstellen kann. Und Charlotte, danke für deine vielen Hilfen und deine Geduld.

An dieser Stelle möchte ich auch Felix Schwarz und Felix Limberg für die großartige gemeinsame Zeit während des Studiums und die vielen gemeinsamen Lernstunden danken.

Meinem Chemie LK Lehrer, Herrn Rühs möchte ich dafür danken, dass er mir die Freude an dieser faszinierenden Wissenschaft näher gebracht hat. Er hat damit den Grundstein für mein Interesse an der Chemie gelegt.

Natürlich geht mein Dank auch an meine Familie, an Anton Bunge, Rick Bunge, Tom Behrendt, Max Behrendt und Jan Brinkman, an Eva und Reinhardt Bunge sowie Klaus Behrendt und Karin Deininger, und an Sylva Körber, Konrad Klockmeier, Johannes Ellendorff und an Mark Kohnert, sowie an meinen Bruder David Führer.

Ein besonderer Dank gebührt meinen Eltern, Barbara und Thomas Führer, die viel Zeit, Geld, Geduld und Liebe in meine Unterstützung, während meines Studiums investiert haben.

Zu guter Letzt gilt mein größter Dank meiner Frau Vera und meinen Kinder Sofia und Lars. Ihr habt mich während dieser ganzen Zeit begleitet und seit mit mir durch die Höhen und Tiefen meiner Zeit als Doktorand gegangen. Ihr seid für mich ein fester Anker, der mir hilft, nie den Fokus und die Perspektive zu verlieren.

Danke!!!

Felix Behrendt